INFORMATION TO USERS

This manuscript has been reproduced from the microfilm master. UMI films the text directly from the original or copy submitted. Thus, some thesis and dissertation copies are in typewriter face, while others may be from any type of computer printer.

The quality of this reproduction is dependent upon the quality of the copy submitted. Broken or indistinct print, colored or poor quality illustrations and photographs, print bleedthrough, substandard margins, and improper alignment can adversely affect reproduction.

In the unlikely event that the author did not send UMI a complete manuscript and there are missing pages, these will be noted. Also, if unauthorized copyright material had to be removed, a note will indicate the deletion.

Oversize materials (e.g., maps, drawings, charts) are reproduced by sectioning the original, beginning at the upper left-hand corner and continuing from left to right in equal sections with small overlaps.

ProQuest Information and Learning
300 North Zeeb Road, Ann Arbor, MI 48106-1346 USA
800-521-0600

TRANSFER MATRIX APPROACH TO THE STATISTICAL MECHANICS OF SINGLE POLYMER MOLECULES

by

Lucian Livadaru

SUBMITTED IN PARTIAL FULFILMENT OF THE
REQUIREMENTS FOR THE DEGREE OF
DOCTOR OF PHILOSOPHY
AT
DALHOUSIE UNIVERSITY
HALIFAX, NOVA SCOTIA, CANADA
SEPTEMBER 2002

DALHOUSIE UNIVERSITY

FACULTY OF GRADUATE STUDIES

The undersigned hereby certify that they have read and recommend to the Faculty of Graduate Studies for acceptance a thesis entitled "Transfer Matrix Approach to the Statistical Mechanics of Single Polymer Molecules" by Lucian Livadaru in partial fulfilment for the degree of Doctor of Philosophy.

Dated: September 6, 2002

External Examiner:

Research Supervisor:

Examining Committee:

DALHOUSIE UNIVERSITY

Date: September 2002

Author: **Lucian Livadaru**

Title: **Transfer Matrix Approach to the Statistical Mechanics of Single Polymer Molecules**

Department: **Physics**

Degree: **Ph.D.** Convocation: **October** Year: **2002**

Permission is herewith granted to Dalhousie University to circulate and have copies for non-commercial purposes, at its discretion, the above title upon the request of individuals or institutions.

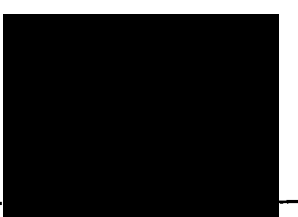

Signature of Author

DEDICATION

This work is dedicated to my wife, Roseanna, and to my parents, Aurica and Emil.

CONTENTS

LIST OF TABLES

LIST OF FIGURES

Abstract

In this work, we demonstrate, implement and critically assess the capabilities and the limitations of the *Transfer Matrix* (TM) method to the statistical mechanics of single polymer molecules within their classical models. We first show how the TM can be employed with the help of computers, to provide highly accurate results for the configurational statistics of polymers in $\theta-$conditions. We proceed gradually from simple to complex polymer models, analyzing their statistical properties as we vary the model parameters.

In the order of their complexity, the polymer models approached in this work are: (i) the freely jointed chain (FJC); (ii) the freely rotating chain (FRC); (iii) the rotational isomeric state (RIS) model with and without energy parameters; (iv) the continuous rotational potential model (for n-alkanes); (v) an interacting chain model (ICM) with virtual bonds for poly(ethylene glycol)(PEG).

The Statistical Mechanics of polymer chains is carried out in both the Helmholtz and Gibbs ensembles, depending on the quantities of interest. In the Helmholtz ensemble the polymer's Green function is generally a function of both the spatial coordinates and orientations of chain bonds. In the Gibbs ensemble its arguments are the bond orientations with respect to an applied external force. This renders the latter ensemble more feasible for an accurate study of the mechanical properties of the mentioned models.

We adapt the TM method to study statistical and thermodynamical properties of various models, including: chain end distribution functions, characteristic ratios, mean square radius of gyration, Kuhn length, static structure factor, pair correlation function, force-extension curves, Helmholtz and Gibbs free energies.

For all cases, the TM calculations yielded accurate results for all these quantities. Wherever possible, we compared our findings to other results, theoretical or experimental in literature. A great deal of effort was focused on precise determination of the stretching response for each model for a wide range of applied external forces. A remarkable finding on the functional form of the stretching curve is the similar behavior that the FRC and the continuous rotational potential model present to the FJC model in the large-force regime, in contrast to the RIS and the ICM for PEG, which display drastic differences. We found that the latter two models, while reliable for the study of unperturbed chains, do not realistically represent polymers under the action of a strong external force. In that situation, a larger set of rotational states must be included for an accurate description.

The influence of the chain length and model parameters, where applicable, on the spatial configuration of polymer chains is investigated in great detail. In the complex stages of the modeling we analyze the effects of the energy parameters incorporated in the models. We use this information to extract the Kuhn and persistence lengths and make a comparison to the Gaussian chain distribution.

List of Symbols

a : Kuhn length

$A_N(\mathbf{R}, T)$: Helmholtz free energy

b : bond length

$\mathbf{b}_i$: bond vector of monomer i

$\langle \cos \psi_{ij} \rangle$: statistical average of the angular correlation between the bonds i and j

$\mathbf{C}$: connectivity operator for a polymer model

C_N : characteristic ratio of a polymer chain

EG : ethylene glycol

E_b : potential energy associated with the bond stretching

E_γ : potential energy associated with the bond angle bending

E_φ : potential energy associated with the variation of the rotational angle

E_α : self-energy of a bond in rotational state α

$\mathbf{f}$: external stretching force

FJC : freely jointed chain

FRC : freely rotating chain

$F_N(\mathbf{f}, T)$: Gibbs free energy

$g(r)$: radial distribution function (or the pair correlation function)

$g_N^{(n)}(\mathbf{r}^n)$: the n-particle distribution function

$g_\theta, g_\psi, g_r, g_z$: functions entering the expression of the connectivity operator

G : polymer's Green function for a generic problem

$G_i^{(f)}$: Green function for the angular distribution of monomer i with respect to the direction of the external force $\mathbf{f}$

$G_i^{(r)}$: Green function for the radial distance distribution of monomer i

$G_i^{(z)}$: Green function for the vector z–component

distribution of monomer i

i, j : order number of monomers or bonds

ICM : interacting chain model

$\mathbf{k}$: scattered vector
(or the transferred momentum vector)

k : wave number
(the magnitude of the scattered vector)

k_B : Boltzmann constant

L : contour length of a polymer

l_P : persistence length of a polymer

l_{geom} : geometrical factor entering the expression
of the contour length of a polymer

N : number of chain bonds

PEG : poly(ethylene glycol)

$p_i^{(f)}(\Gamma)$: probability for bond i to occupy state Γ

R : end-to-end distance of a chain

RIS : rotational isomeric state

R_z : z–component of the end-to-end vector

r_{ij} : distance between monomers i and j

$\langle R^2 \rangle_0$: unperturbed mean square end-to-end
distance

$\langle R_g^2 \rangle$: mean square radius of gyration

$S(k)$: static structure factor

$\mathbf{s}_i$: i-th subunit vector

S_N : entropy of a polymer chain with N bonds

T : temperature

TM : transfer matrix

$\mathbf{t}_i$: rotational matrix of bond i

$\mathbf{T}^{(f)}$: transfer matrix for the angular distribution with
respect to the direction of the external force $\mathbf{f}$

$\mathbf{T}^{(r)}$: transfer matrix for radial distance distribution

$\mathbf{T}^{(z)}$: transfer matrix for the z–component vector distribution

U_N : total potential energy of the polymer chain

$V_{\alpha\beta}$: nearest neighbor interactions between
two bonds in rotational states α and β

WLC : worm-like chain

$W_N(\mathbf{R})$: end-to-end vector distribution function

$W_N^{(r)}(R)$: end-to-end distance distribution function

$W_N^{(x)}(R_x), W_N^{(y)}(R_y), W_N^{(z)}(R_z)$: end-to-end vector x, y, z–component
distribution function, respectively

z_i : bond partition function of bond i

$Z_N(\mathbf{R}, T)$: canonical configurational partition function

α_i, β_{i+1} : rotational state of bonds $i, i+1$

$\beta = 1/k_B T$: inverse of temperature

$\Delta_N(\mathbf{f}, T)$: Gibbs free energy

γ : bond angle

φ_i : rotational (dihedral) angle of bond i

θ_i : orientation of the bond i with respect
to a specified direction

ψ : angular coordinate serving as argument
of the transfer matrix

$\rho_N^{(n)}(\mathbf{r}^n)$: n-particle density

ACKNOWLEDGMENTS

I would like to gratefully acknowledge the financial support offered by Dalhousie University by a Killam Scholarship. Special thanks to Dr. H.J. Kreuzer for guiding me through this work and to Dr. R.R. Netz for useful collaboration. Also, I would like to thank Dr. C. Bracher for proofreading this manuscript.

CHAPTER 1

INTRODUCTION

The statistical physics of polymers has gained considerable interest in the last few decades. Some of the reasons for this are closely related to the realization that the biological systems at molecular scale can be described in terms of the properties of a particular class of polymer molecules, namely, biopolymers. Moreover, the recent advances in the technology of natural and synthetic polymeric materials has shown wide applicability and usefulness of this field.

An important branch of this subject, the configurational statistical physics is concerned with the study the molecular properties deriving from the spatial arrangements and motion of atoms within the polymers. Although it is based on the classical statistical mechanics, this field is enriched with new ideas and techniques of modern physics. Historically[1], the development of this field originated shortly after H. Staudinger proved the chain-like structure of polymers, in 1922. Kuhn, Mark and Guth in their pioneering work on high elasticity of polymer networks set the conceptual basis for the contemporary understanding of physical properties of polymer materials. The next developments are associated with the work done by Flory[2] and Volkenstein[3] in the 1950's, and more recently by Edwards[4], de Gennes and Lifshitz[5].

The motivational aspects behind theoretical investigations in this field are manyfold. The conformational behavior of polymers are known to be responsible for many properties of polymeric materials, such as rubber elasticity, morphological properties, glass-transition temperatures. A particularly interesting and vast class is the represented by the biological phenomena involving biopolymers. One cannot hope to understand the structure and functions of such biological systems without an insight in the conformational properties of macromolecules at a representative scale.

Another great incentive to the study of single polymer properties is the recent capability of direct comparison between the theoretical and experimental results for particular systems. With the advent of Atomic Force Microscope techniques, single

molecule stretching experiments brought a wealth of data. For instance, in the experiment performed by Oesterhelt et al.[6], thiol and butoxy terminated poly(ethylene glycol) (PEG) molecules were placed in hexadecane. The molecules were allowed to adsorb on a gold surface, after which an AFM tip was employed for stretching. Once adsorption of a PEG molecule on the tip occurred, the latter was moved away from the grafting surface in a direction perpendicular to it. The resistive force as a function of chain extension was recorded for several chain lengths. It was verified that the obtained curves are fully reversible by recording the trace backwards (tip moving toward the grafting surface) and retrieving identical results. When normalized by their contour length, all curves were found to superimpose. This is in agreement with our findings on the long chain limit behavior. A rigorous statistical mechanical analysis of the polymer-cantilever system is made by Kreuzer et al.[14].

Recently, the increasing interest in problems of polymer physics has been accompanied by an import of powerful techniques from other topics of the Physics of Condensed Matter. Among these, the Transfer Matrix (TM) method stands out due to its wide applicability and adaptability as a computational method. The feature that makes this technique particularly suitable for studying polymer chains is their linear connectivity. Owing to this characteristic, the macromolecule can in many situations be treated as a system with nearest neighbor interactions, which enables an elegant treatment of polymer problems. In this work, we will demonstrate, implement and critically assess the capabilities and the limitations of the TM technique to the statistical mechanics of single polymer molecules within their classical models.

As mentioned before, a polymer molecule is a chain-like entity consisting of atoms linked by covalent bonds. Given a large set of atoms of specified nature, one can imagine the vast number of possibilities in which the links could be realized—we call this the polymer's *primary structure*—a fact that justifies an attempt or need to classify polymers. At first glance, out of the whole variety, one can distinguish those that have a linear backbone without any added branches. These are known as *linear polymers*. Among them, we can further differentiate the ones that have a periodical structure (repeating sequence of atoms) along the backbone —*homopolymers*—and others, whose structure varies in an arbitrary way—*heteropolymers*. Other primary structures like *ring polymers* (a chain whose contour is a closed cycle), *star-like* (chain sections that meet in a common centre), *comb-like* (linear chain sections attached to

a common central segment) and *randomly branched* will not be the subject of this dissertation.

With the advent of polymer physics, a variety of polymer models have been established in the literature, the usefulness and propitiousness of which vary from a physical situation to another. A crucial question when dealing with a specific polymer problem therefore is "how reliable is our model?". Thus, it is clearly of considerable importance that the formulation of such a model is accompanied by its statistical treatment and, subsequently, comparison to experimental results, if available.

The simplest polymer models also seem to be the most widely known and successful ones, due to their amenability to analytical treatment. Among these we mention:

- the Gaussian chain (GC)
- the worm-like chain (WLC)
- the freely jointed chain (FJC)
- the freely rotating chain (FRC)
- the rotational isomeric state (RIS) model

In their basic formulation, all of these models are "phantom" chains in that their path is allowed to intersect itself without any restrictions—there are no long range interactions whatsoever with other monomers or molecules of the solvent. Mathematically, they are distinguished by the form of the connectivity operator, characterizing the links between adjacent repeat units in the chain.

The Gaussian chain, worm-like chain and freely jointed chain have enjoyed the most extensive attention in the literature, because of their accessibility to analytical calculations. Especially for the GC, the mathematical apparatus is well established and its exact treatment can be carried out to a great extent. Simply stated, the GC is a chain with a Gaussian (normal) probability distribution for the bond length or, the distance between two adjacent monomers, while the angular distribution of a link is uniform. A good review of results on the GC can be found in reference [1]. The more sophisticated WLC[11, 32] is defined as a continuous model obtained from a FRC in the limit in which its bond length and bond angle tend to zero, while the contour length and the persistence length remain fixed.

A detailed description of the last three models in the above list will be given in the following chapters of this work. The other two models in that list, GC and WLC, will appear wherever reference to them is deemed relevant. Remarkably, even for some simple models, exact treatment is non-trivial. For example, the analytical treatment of FRC and RIS does not go beyond calculating a few statistical quantities, like the end-to-end distance, radius of gyration and other closely related quantities *in the absence of any external field.*

The main concern of this work is to analyze the role of the internal architecture and short-ranged interactions in the configurational statistical mechanics of single polymer chains. For this purpose, we adapt the transfer matrix method (or the Green function of polymer chains) to determine the statistical quantities associated with polymer chains. We cover a diversity of polymer models found in the literature, from simple to complex, and implement our method in an appropriate way for each of them. We will analyze the role of the structural and energy parameters entering the various models.

One of the main assumptions throughout this work will be that the polymer chains are found in the so-called $\theta-$condition. This entails the fact that the excluded volume interactions and the action of the solvent molecules mutually cancel out. We will not approach here the case of charged polymers, since the electrostatic interaction is long-ranged and therefore impossible to handle in a transfer matrix approach. Moreover, this also enables us to treat the polymer as a Markov chain, a concept that will be clarified in the beginning of the next chapter. In the centre of our investigation will be neutral linear polymer molecules in their various models having specific geometrical structures and potential energy functions.

A principal advantage of the TM method is the possibility to study polymer chains of arbitrary lengths, anywhere between very short and very long, thus seizing the effects of chain lengths on the statistical properties. This is usually not possible by analytical methods, when only the asymptotic limit of infinitely long chains is accessible.

Chapter *3* will be dedicated to the study of the FJC model. This model was extensively studied by analytical methods, therefore very few new results can be added. Its purpose will be twofold: it will serve both as the simplest example and as a reliability test of the transfer matrix method. Only the Helmholtz ensemble will

be employed. We will critically assess the potential and precision of our method. In Chapter *4* we approach the FRC, a model that presents a further complication — a fixed bond angle. This model was studied analytically only to a certain extent and we conjecture that the TM method can bring valuable new insight. Therefore, we do extensive calculations in both Helmholtz and Gibbs ensembles in order to obtain chain end distribution functions, characteristic ratios, mean square radius of gyration, and force-extension curves for a large array of chain lengths and bond angles.

The next logical step in single polymer modelling would be to introduce the effects of rotational potentials associated with the variation of the dihedral angles. This task is undertaken in the fifth and sixth chapters as case studies of two concrete types of polymer: n-alkanes and poly(ethylene glycol), respectively. Chapter *5* is dedicated for the study of n-alkanes and we proceed gradually by studying in this order the RIS model with: (*i*) no energy parameters, (*ii*) self energies only, (*iii*) self energies and nearest neighbor interactions. For all cases we analyze the role of the parameters on the statistical properties such as the characteristic ratio, the radius of gyration, the temperature coefficients, the force-extension curve and the persistence length of the molecule. Next, we attempt to incorporate the continuum of the rotational potential by increasing the number of rotational states with their appropriate weights. Due to the great computational resources required for the implementation of the TM method for this case, the feasibility is limited to mainly calculations in the Gibbs ensemble. Nonetheless, this enables good quantitative and qualitative findings on this type of molecule.

Finally in Chapter *6* we approach a more challenging case study — poly(ethylene glycol). This molecule is built from a monomer comprising three covalent bonds with two different lengths and exhibits strong intrachain interactions, with larger range than those aforementioned models. Recently there have been important ab initio studies on short molecules of this type, a fact that enables us to utilize quantum mechanical results as input. Again we will focus on the statistical mechanics in the Gibbs ensemble for this molecule, particularly on the force-extension curves and related quantities.

To further clarity and ease of reading we will define below a number of frequently used terms in this work.

- *monomer* – the basic structural repeat unit of a polymer chain;
- *N-mer* – polymer chain with N monomers;
- *chain bond* – the covalent bond that joints two consecutive monomers;
- *chain subunit* – a sequence of one or more monomers of a polymer chosen for convenience of statistical study;
- *spatial configuration* of a chain – the collection of all points in space where the chain monomers are located;
- *conformer or conformation*– the sequence of states occupied by all bonds along the chain (e.g. rotational states);
- *ideal chain* – polymer chain whose monomers have no interaction with molecules in its environment or with other monomers in the chain.
- *intrachain interactions* – interactions between monomers of a single chain.

1.1 The Geometrical Structure and the Potential Energy of a Polymer Molecule

A linear polymer consists of a sequence of atoms (or group of atoms) — the chain's monomers — each of which is bonded by covalent bonds to two others. The only exception from this rule are the two end monomers, which are bonded to only one other monomer each. The connection between two consecutive monomers is geometrically described by a *bond vector*, $\mathbf{b}$. For a linear polymer with $(N+1)$ monomers there are N bond vectors: $\mathbf{b}_1, \mathbf{b}_2, ..., \mathbf{b}_N$. Due to the directional nature of the covalent bonds, the angle formed by two consecutive bond vectors — the *bond angle*, γ — is restricted to a limited range, around 70^o in most cases. In Figure 1.1 for a sequence of four bonds, we indicated the intervening bond angles by γ_{12}, γ_{23} and γ_{34}. Finally, the other geometrical parameters relevant to the chain structure are the *dihedral angles*, φ, defined as the angle formed by the planes of consecutive pairs of bond vectors (e.g. $(\mathbf{b}_1, \mathbf{b}_2)$ and $(\mathbf{b}_2, \mathbf{b}_3)$, or the planes containing the atoms 012 and the plane containing 123 in Figure 1.1).

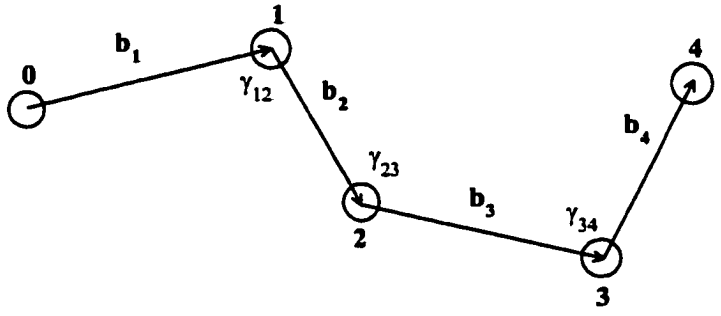

Figure 1.1: Schematic representation of a sequence of four consecutive bond vectors.

If we are concerned with the ground state of a polymer molecule, the bond length, the bond angles and the dihedral angles associated with a given bond vector generally depend on the chemical structure of its adjacent monomers, the contour length, and the location of that bond within the molecule. For a particular molecule, these parameters are determined experimentally or by quantum chemistry methods. In the fortunate case when these parameters are available, they can serve as input for statistical mechanical analysis of that molecule. However, in order to make long chains amenable to study, we can assume that they are only dependent on the type of monomers involved in their construction.

With each of these degrees of freedom certain potentials are associated, more or less realistic, in order to mimic the intramolecular energy landscape. Near its equilibrium position, b_0, the potential energy curve associated with bond stretching is well approximated by a parabola

$$E_b(b) = \frac{k_b}{2}(b - b_0)^2, \tag{1.1}$$

in other words, a Hooke's law behavior. Similarly, the potential describing the bond angle bending is accurately represented about its minimum, γ_0, by

$$E_\gamma(\gamma) = \frac{k_\gamma}{2}(\gamma - \gamma_0)^2. \tag{1.2}$$

Here, k_b is the elastic constant of stretching the bond vector and k_γ is the elastic constant of bending the bond angles.

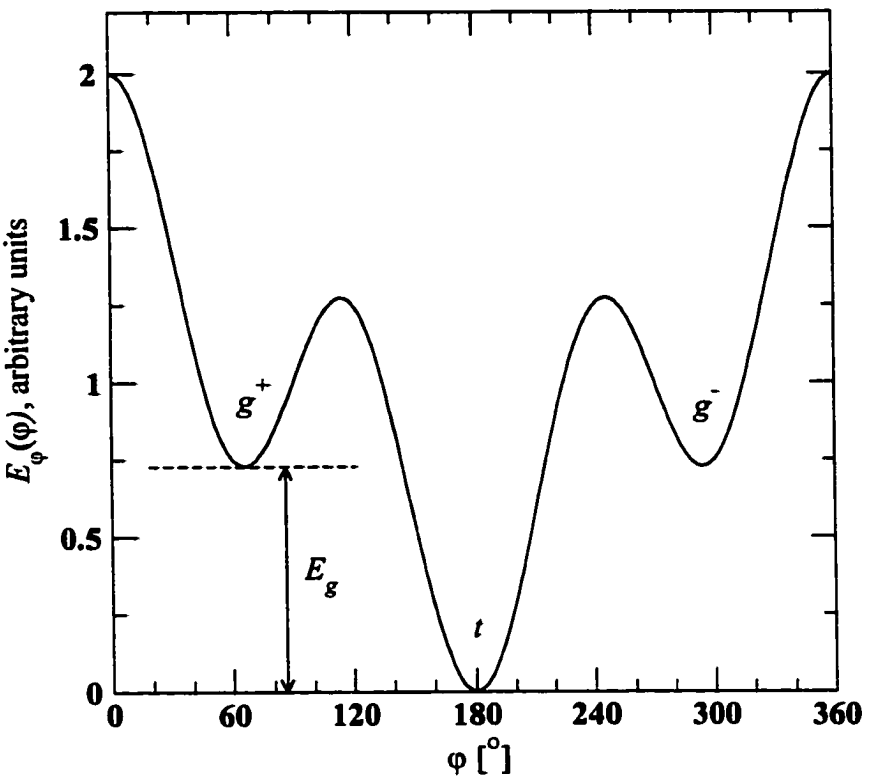

Figure 1.2: Typical shape of a three-fold rotational potential $E_\varphi(\varphi)$, given by eq. 1.3 with the parameters arbitrarily chosen $E_1 = E_3 = 2$.

The strong directional character of the covalent bonds confers great stiffness to the bond stretching and bond angle bending, to the effect that these degrees of freedom can in many situations be safely ignored. On the other hand, the potential energy curve associated with the variation of the dihedral angles—the *rotational potential*, or sometimes called the *torsional potential*—is the "softest" among the elastic potentials and therefore plays the most important role in the configurational statistics of the polymer coil. Usually, it has a shape with three minima labeled, *trans (t), gauche plus (g^+), gauche minus (g^-)* like in Figure 1.2.

The precise determination of the actual shape of the rotation potential is the subject of quantum chemistry, but often the two leading Fourier components are sufficient:

$$E_\varphi(\varphi) = \frac{E_1}{2}(1+\cos\varphi) + \frac{E_3}{2}(1+\cos 3\varphi) \tag{1.3}$$

The accuracy of the approximations for the potentials above will not be extensively discussed in this dissertation. In our study they enter as an input and it is important to make use of reasonable approximations and appropriate values for the parameters, many of which are encountered in the specialized literature. Herein, we give priority to the objective of analyzing the role of the most relevant parameters involved in the statistical mechanical properties of the polymer.

If in a chain the rotational potentials described above are independent of each other, then the total potential energy of that chain can be written as a sum of bond energies and, consequently, the chain partition function can be expressed as a product over all bond partition functions, which greatly simplifies the statistical mechanical treatment of the chain. In general, however, this does not hold true. The rotational potentials may depend on the rotational angles of nearest neighboring bonds, as well as of second neighbors or even bonds further along the chain. This dependence is due to the interactions between atoms comprising the monomers — belonging either to the backbone of the molecule or to the pendant groups. For such complex cases, the potential energy associated with a chain segment will be a function of the set of rotational angles belonging or adjacent to that segment. When interactions are present the chain partition function cannot be factored out into bond partition functions, thus posing a considerable complication to the statistical treatment. In all models studied in this work, we will neglect interactions beyond second nearest neighbors.

A great simplification for the configurational statistics of a polymer chain is introduced by the *rotational isomeric state* (RIS) approximation[2, 3]. This procedure incorporates fixed bond lengths and bond angles and it allows only for a small number of dihedral states for each bond, representing the rotational potential curve by a few sample points — its minima, i.e. the points marked t, g^+, g^- in Figure 1.2. This yields an accurate representation of the configurational statistics of a chain only if the potential barriers between the rotational minima are large with respect to k_BT. In other cases, nonetheless, it can serve as a good mathematical tool for dealing with single polymer problems.

All the potential energy functions described in the above have a common characteristic: they are short-ranged. A single polymer chain in solution experiences interactions with the molecules of the solvent and with other monomers of the chain. The latter is known in literature as the *excluded volume interaction*, or simply the volume interaction. Simply put, this is the restriction that two or more chain monomers cannot occupy the same volume element of space. The "path" assumed by the chain cannot intersect itself, or come close, within an arbitrary distance, to itself. Therefore a monomer-monomer repulsion is present, regardless of the distance along the backbone between two monomers. By including the volume interaction and the interactions with the solvent one takes a step beyond the ideal chain in constructing a successful model for real polymers.

Without considering the quantitative aspects of the problem, in the general case of neutral polymer solutions, the solvent is generally classified to fall in one of there distinct types:

- *good solvent:* the attraction between monomer and solvent molecules and the volume interaction act to create an effective repulsion between chain monomers; the coil is swollen from its ideal size;

- $\theta-$ *solvent*: the monomer-solvent interaction and the volume interaction mutually cancel their effect; to a good approximation, the polymer can be treated as an ideal chain;

- *poor solvent:* the repulsion between monomer and solvent molecules and the volume interaction act to create an effective attraction between chain monomers; as a result, the coil shrinks.

The presence of volume interaction poses additional difficulties in calculating the statistical properties of a polymer coil, since then one encounters all the complications of a many-body problem. However, there are many situations when one can neglect this type of interaction. From the perspective of this work, it will suffice to consider that the polymer molecule is always found in a $\theta-$solvent (or, equivalently, $\theta-$conditions), thus disregarding the excluded volume effects.

1.2 Statistical Characterization of Polymer Configuration

Owing to their large number of degrees of freedom that grows exponentially with the length of the molecule, polymer chains must be treated as statistical systems. In the following we will present a series of characteristics, or physical quantities of specific interest in the study of polymers. Let us assume that the molecule under consideration has N bonds (and therefore $N+1$ monomers) characterized by the bond vectors $\mathbf{b}_i$ $(i = 1, 2, ..., N)$ of length b; for now we ignore the details of the internal structure of the chain. Thus these considerations apply to all models of polymers. Throughout this section, angular brackets $\langle ... \rangle$ designate statistical averages.

The unperturbed mean square end-to-end distance of the polymer coil is given by[2]

$$\begin{aligned} \langle R^2 \rangle_0 &= \left\langle \left(\sum_{i=1,N} \mathbf{b}_i \right)^2 \right\rangle = \sum_{i=1,N} \langle \mathbf{b}_i^2 \rangle + 2 \sum_{1 \le i < j \le N} \langle \mathbf{b}_i \mathbf{b}_j \rangle \\ &= Nb^2 + 2b^2 \sum_{1 \le i < j \le N} \langle \cos \psi_{ij} \rangle , \end{aligned} \tag{1.4}$$

where ψ_{ij} is the angle between the bond vectors $\mathbf{b}_i$ and $\mathbf{b}_j$. The statistical quantity $\langle \cos \psi_{ij} \rangle$ is a measure of the correlations between the orientations of the two bond vectors and it is generally determined by the internal structure of the chain. For a linear homogenous chain it will depend only on the difference $|i - j|$. Moreover, assuming that the bond angles of any two monomers are statistically independent, we can write

$$\langle \cos \psi_{ij} \rangle = \langle \cos \psi_{ik} \rangle \langle \cos \psi_{kj} \rangle , \text{ for any } i < k < j. \tag{1.5}$$

This suggests that the correlation of bond orientations will decay exponentially according to

$$\langle \cos \psi_{ij} \rangle = \exp \left(-\frac{|i - j|}{l_P} \right) , \tag{1.6}$$

where by definition l_P is the *persistence length* of the polymer. The modulus of bending elasticity of the chain is related to the persistence length by[1]

$$\varkappa = k_B T l_P. \tag{1.7}$$

The *characteristic ratio* C_N of a polymer is defined as

$$C_N = \frac{\langle R^2 \rangle_0}{Nb^2}. \tag{1.8}$$

If the bonds are variable in length, we can re-define the characteristic ratio as

$$C_N = \frac{\langle R^2 \rangle_0}{N\overline{b^2}}, \tag{1.9}$$

where $\overline{b^2}$ is the mean square bond length of the polymer.

In his pioneering work (1936) Kuhn showed that there is a connection between the statistical structure of any given linear polymer and the FJC model. Namely, the average square end-to-end distance of a long polymer chain with the characteristic ratio C_N can be identified with the one of a FJC with the appropriate bond length, say a, and a corresponding bond number, N_K

$$\langle R^2 \rangle_0 = C_N N b^2 = N_K a^2 = La. \tag{1.10}$$

The quantity a is known as the *effective (or Kuhn) length* of the chain. Here, L is the contour length of the polymer and equals the length of the maximally stretched chain and it generally has the expression

$$L = Nbl_{geom}, \tag{1.11}$$

where l_{geom} is a factor depending only on the geometrical structure of the chain and is proportional to the length of the projection of a bond on the contour line, when the chain is in the completely stretched configuration. For instance, for the FJC this factor is 1, while for the FRC it equals $\cos\frac{\gamma}{2}$, with γ as the bond angle. Generally speaking, the Kuhn length is approximately twice the persistence length, owing to the fact that from any point of the chain, the bond orientation persists in the two directions along the chain's contour. With eq. 1.10, 1.11 we can re-express the

characteristic ratio for long chains as

$$C_N = \frac{La}{Nb^2} = \frac{a}{b} l_{geom}. \tag{1.12}$$

For an understanding of the chain's spatial extent we need to look at the *mean square radius of gyration*, $\langle R_g^2 \rangle$, defined as

$$\langle R_g^2 \rangle = (N+1)^{-1} \left\langle \sum_{i=0,N} (\mathbf{r}_i - \mathbf{r}_{cm})^2 \right\rangle, \tag{1.13}$$

where $\mathbf{r}_{cm}$ is the position of the centre of mass of the entire chain

$$\mathbf{r}_{cm} = (N+1)^{-1} \sum_{i=0,N} \mathbf{r}_i. \tag{1.14}$$

Owing to a theorem by Lagrange, $\langle R_g^2 \rangle$ can be expressed in a manner that involves only the distances between the different monomers of the chain denoted by $r_{ij} = |\mathbf{r}_j - \mathbf{r}_i|$

$$\langle R_g^2 \rangle = (N+1)^{-2} \left\langle \sum_{0 \le i < j \le N} r_{ij}^2 \right\rangle. \tag{1.15}$$

Remarkably[2], all the random models of polymers in the limit of very long chains are characterized by a simple relation between the mean square radius of gyration and the average square end-to-end distance: $\langle R_g^2 \rangle \to \frac{\langle R^2 \rangle_0}{6}$ as $N \to \infty$. This can be analytically demonstrated for simple models like the FJC, GC and the FRC.

A well known result for the stretching of the polymer in the small-force limit $\frac{fb}{k_B T} \ll 1$ states that the relative extension is proportional to the force as well as to the Kuhn length of the chain

$$\frac{R_z}{L} \cong \frac{fa}{3k_B T}. \tag{1.16}$$

This fact is directly derived from Kuhn's finding that a long polymer chain can be modelled by a corresponding FJC with an appropriate bond length, a.

For a more complete understanding of the spatial configuration of a polymer coil, one has to define the *end-to-end vector distribution*, $W_N(\mathbf{R})$, that is the probability

density that the vectorial separation between the ends of a chain with N bonds is within the interval $[\mathbf{R}, \mathbf{R}+\mathbf{dR}]$. Assuming that the components of the chain end vector are statistically independent, which is well justified for molecules long with respect to their persistence length, we have

$$W_N(\mathbf{R}) = W_N^{(x)}(R_x) W_N^{(y)}(R_y) W_N^{(z)}(R_z), \tag{1.17}$$

where $W_N^{(x)}(R_x)$ is the probability distribution function for the $x-$component of chain end, and similarly for y and z. Indeed, this property is satisfied by Gaussian-type functions which are expected to be good approximations of $W_N^{(x)}, W_N^{(y)}, W_N^{(z)}$ and W_N for long chains.

Alternatively, one can focus on the *end-to-end distance distribution* $W_N^{r}(R)$, defined as the probability density for the distance between the chain ends to be located in the interval $[R, R+dR]$. Note that for an isotropic system we have

$$W_N^{(r)}(R) \propto R^2 W_N(\mathbf{R}). \tag{1.18}$$

These quantities are also related for an ideal coil with isotropic distribution by the identity[25]

$$W_N^{(z)}(R_z) = \int_0^\infty \mathrm{d}R \frac{R W_N^{(r)}(\sqrt{R^2+R_z^2})}{2(R^2+R_z^2)}. \tag{1.19}$$

The end distribution functions defined above are in fact, up to a constant factor, identical to the *canonical configurational integral* of the chain expressed as

$$Z_N(\mathbf{R}, T) = \sum_{\{\Omega_i\}} \mathrm{e}^{-\beta U_N(\{\Omega_i\})} \delta[\mathbf{r}(\{\Omega_i\}) - \mathbf{R}], \tag{1.20}$$

where $\{\Omega_i\}$ designates a chain conformer, $|\mathbf{r}(\{\Omega_i\})|$ is the length of that conformer, $U_N(\{\Omega_i\})$ is its potential energy and $\beta = 1/k_B T$. The *Helmholtz free energy* of the chain is

$$A_N(\mathbf{R}, T) = A_0(T) - k_B T \ln Z_N(\mathbf{R}, T), \tag{1.21}$$

where $A_0(T)$ is a function of temperature only. If the Helmholtz free energy is known for a system, then the various thermodynamic relations of that system are obtained as partial derivatives, such as the mechanical equation of state

$$\langle \mathbf{f} \rangle_{\mathbf{R}} = -\nabla_{\mathbf{R}} A_N(\mathbf{R}, T) \tag{1.22}$$

and the entropy

$$S_N(\mathbf{R}, T) = -\left(\frac{\partial A_N(\mathbf{R}, T)}{\partial T}\right)_{\mathbf{R}}. \tag{1.23}$$

When the chain is subjected to a fixed external force, the appropriate ensemble is the Gibbs, or isothermal-isobaric one. The *Gibbs partition function* of the chain is the Laplace transform of $Z_N(\mathbf{R}, T)$ with respect to $\mathbf{R}$

$$\Delta_N(\mathbf{f}, T) = \int \mathrm{d}\mathbf{R} e^{\beta \mathbf{f} \cdot \mathbf{R}} Z_N(\mathbf{R}, T), \tag{1.24}$$

and the *Gibbs free energy*

$$F_N(\mathbf{f}, T) = -kT \ln \Delta_N(\mathbf{f}, T), \tag{1.25}$$

can be used to calculate the average length

$$\langle \mathbf{R} \rangle_{\mathbf{f}} = \nabla_{\mathbf{f}} F_N(\mathbf{f}, T) \tag{1.26}$$

$$= \frac{\int \mathbf{R} e^{\beta \mathbf{f} \cdot \mathbf{R}} Z_N(\mathbf{R}, T) \mathrm{d}\mathbf{R}}{\int e^{\beta \mathbf{f} \cdot \mathbf{R}} Z_N(\mathbf{R}, T) \mathrm{d}\mathbf{R}}, \tag{1.27}$$

while the entropy is given by

$$S_N(\mathbf{f}, T) = -\left(\frac{\partial F_N(\mathbf{f}, T)}{\partial T}\right)_{\mathbf{f}}. \tag{1.28}$$

Note that the Helmholtz and Gibbs ensembles for a "small system"[8], like a polymer of finite length N, are not equivalent; the two force-extension curves represented by the two relations, eq. 1.22 and eq. 1.26, will not be the inverse of one another. However, as the size of the chain is increased, $N \to \infty$, they will converge, the system becoming a thermodynamic system.

A more detailed understanding of the spatial structure of a polymer chain can be achieved through the study of the statistical quantities known as *n–particle densities*[9]. In the canonical ensemble, they are defined as

$$\rho_N^{(n)}(\mathbf{r}^n) = \frac{1}{Q_N}\int\int \mathbf{dr}^{(N-n)}\mathbf{dp}^N \exp\left[-\mathcal{H}_N(\mathbf{r}^N,\mathbf{p}^N)/k_BT\right] \quad (1.29a)$$

$$= \frac{1}{Z_N}\int \mathbf{dr}^{(N-n)} \exp\left[-U_N(\mathbf{r}^N)/k_BT\right], \quad (1.29b)$$

where $\mathcal{H}_N$ is the Hamiltonian, Q_N is the canonical partition function, U_N is the total potential energy and Z_N is the configurational part of the canonical partition function of the system. Closely related to this, one can define the *n–particle distribution functions*

$$g_N^{(n)}(\mathbf{r}^n) = \frac{\rho_N^{(n)}(\mathbf{r}^n)}{\prod\limits_{i=1,n}\rho_N^{(1)}(\mathbf{r}_i)}. \quad (1.30)$$

If the system is homogeneous $\rho_N^{(1)}(\mathbf{r}_i) = \rho_0$, a constant, and the above becomes

$$g_N^{(n)}(\mathbf{r}^n) = \frac{\rho_N^{(n)}(\mathbf{r}^n)}{\rho_0^n}. \quad (1.31)$$

Of a particular interest for a homogeneous and isotropic system in which particles interact through pairwise additive forces is the 2-particle distribution function, $g(r)$, also named the *radial distribution function* (or sometimes the *pair correlation function*)

$$g(r) \equiv g(|\mathbf{r}_1 - \mathbf{r}_2|) = \frac{\rho_N^{(2)}(\mathbf{r}_1,\mathbf{r}_2)}{\rho_0^2}, \quad (1.32)$$

where we decided to ignore the other scripts from this notation and $r = |\mathbf{r}_1 - \mathbf{r}_2|$. An interesting property of $g(r)$ for a liquid medium is that it approaches unity as $r \to \infty$, signifying the complete loss of order at large distances. It also can be expressed as

$$g(\mathbf{r},\mathbf{r}') = \langle\rho(\mathbf{r})\rho(\mathbf{r}')\rangle, \quad (1.33)$$

where we introduced the local particle density at point $\mathbf{r}$

$$\rho(\mathbf{r}) = \sum_{i=0.N} \delta(\mathbf{r} - \mathbf{r}_i). \tag{1.34}$$

Another relevant quantity for the structure of the polymer coil is the *static structure factor* defined as

$$S(\mathbf{k}) = (N+1)^{-1} \left\langle \left| \sum_{i=0,N} \exp(i\mathbf{k} \cdot \mathbf{r}_i) \right|^2 \right\rangle \tag{1.35a}$$

$$= (N+1)^{-1} \left\langle \sum_{i,j=0,N} \exp[i\mathbf{k} \cdot (\mathbf{r}_i - \mathbf{r}_j)] \right\rangle, \tag{1.35b}$$

which for a homogeneous chain is proportional to the intensity of the radiation with the wavelength λ scattered at the angle θ and $\mathbf{k}$ is the transferred momentum vector having the magnitude (the wave number)

$$k = |\mathbf{k}| = \frac{4\pi}{\lambda} \sin \frac{\theta}{2}. \tag{1.36}$$

For a homogeneous and isotropic system (e.g. a free polymer coil) the structure factor is a function of the wave number only and can be re-expressed as

$$S(k) = (N+1)^{-1} \sum_{i,j=0,N} \left\langle \frac{\sin(kr_{ij})}{kr_{ij}} \right\rangle. \tag{1.37}$$

The static structure factor is the Fourier transform of the radial distribution function

$$S(\mathbf{k}) = 1 + (N+1)^{-1} \iint \mathbf{dr}\mathbf{dr}' \rho_N^{(2)}(\mathbf{r}, \mathbf{r}') \exp\left[-i\mathbf{k} \cdot (\mathbf{r} - \mathbf{r}')\right], \tag{1.38}$$

which for a homogeneous system is

$$S(\mathbf{k}) = 1 + \rho_0 \int \mathbf{dr} \exp(-i\mathbf{k} \cdot \mathbf{r}) g(\mathbf{r}), \tag{1.39}$$

and if the system is isotropic, too, this becomes

$$S(k) = 1 + 4\pi\rho_0 \int r^2 g(r) \frac{\sin(kr)}{kr} \mathrm{d}r, \tag{1.40}$$

which recovers the identity in 1.37. If the structure factor for a system is known, the radial distribution function can be calculated as its inverse Fourier transform

$$g(\mathbf{r}) = \frac{1}{(2\pi)^3 \rho_0} \int \mathbf{dk} \exp(i\mathbf{k} \cdot \mathbf{r}) \left[S(\mathbf{k}) - 1\right] \tag{1.41}$$

We deem that the theoretical concepts presented in the above are of major importance for the theoretical polymer physics. They constitute very valuable information wherever there is an attempt to investigate phenomena that involve macromolecules. Besides the need of gathering, classifying and correlating the equilibrium properties of such large molecules and systems of molecules, there is the possibility of direct verification of the statistical mechanical analysis of small systems to experimental data.

The above concepts represent not only tools in understanding the conformational behavior of polymers, but also a starting point in studying other higher levels of organization of soft matter, such as the secondary, tertiary and quaternary structure of proteins. Other applications of high interest are: the helix-coil transition in biological or synthetic polymers; the penetration of a cellular membrane by a single polymer molecule; the properties of long adsorbed chains at interfaces; the role of the degree of polymerization in the properties of polymeric materials etc.

It becomes apparent from the above why one of the objectives of this work is to pursue the precise determination of the properties introduced in this chapter. In order to proceed toward that objective, we have to identify and implement an appropriate method to the variety of polymer models aforementioned. This will be done in the chapters to follow.

CHAPTER 2

THE TRANSFER MATRIX METHOD

The Statistical Mechanics of such complex systems as polymer chains has been tackled by a variety of techniques of which the *transfer matrix* (TM) method is the most elegant and powerful. It was originally developed by Kramers and Wannier to solve the Ising model of a ferromagnet[60] and has been implemented in polymer science by Birshtein and Ptitsyn[61, 62], Nagai[63], Lifson[64] and others. A good review of the transfer matrix method for calculating the partition function and averages of 3-state polymer chains in the absence of external fields is given in the classical work of Flory[2] as well as by Boyd and Phillips[7]. Although there have been attempts to develop the TM method for polymers subject to an external force field, to our knowledge none has been satisfactory. A successful implementation will be presented in this thesis.

The applicability of the transfer matrix technique to the study of single polymer chains is subject to certain conditions with respect to the nature of their structure. A convenient way to express these conditions is in terms of Markov chains. A *k-fold Markov chain (or process)*[9, 11], in its most general definition, is a sequence of systems (or events), each of which can occupy a particular set of states, and which satisfies the following condition: the probability of finding a system in a certain state at location s depends only on the states occupied by the systems at a *limited* number of locations $(s-1), (s-2), ..., (s-k)$, where s is the counting variable of that sequence. If the system at any given location is independent of the states at all the preceding locations, we have a simple Markov process. In our case the systems in sequence are just the chain's monomers or bonds, whichever is convenient, while the order of the associated Markov process is dictated by the extent of short ranged interactions within that chain.

2.1 The Polymer's Green Function

We consider the general case of a polymer chain with N subunits. Let $i = 1, 2, ..., N$ be the order index of subunits along the chain. For each i, we comprise all the independent coordinates relevant to the state of that subunit in the notation Γ_i (e.g. the position and orientation with respect to a reference frame). For any $i < j$, we denote by $G(j, \Gamma_j; i, \Gamma_i)$ the conditional probability that subunit j is in the state Γ_j, given that subunit i is in the state Γ_i. This quantity is known in polymer physics as the *Green function of the polymer chain (or the chain's propagator).* For example, for a Gaussian coil, in the absence of any external fields, the Green function associated with the spatial location, $\mathbf{R}$, is given by

$$G(j, \mathbf{R}_j; i, \mathbf{R}_i) = G(j-i, \mathbf{R}_j - \mathbf{R}_i) = \left(\frac{2\pi(j-i)b^2}{3}\right)^{-3/2} \exp\left[-\frac{3\,|\mathbf{R}_j - \mathbf{R}_i|^2}{2(j-i)b^2}\right]. \quad (2.1)$$

The partition function for all possible conformations of the chain is

$$Z_N = \int d\Gamma_1 d\Gamma_N G(1, \Gamma_1; N, \Gamma_N) \quad (2.2)$$

Following the definition of Green functions, for any $i < k < j$

$$G(j, \Gamma_j; i, \Gamma_i) = \int d\Gamma_k d\Gamma_{k-1} G(j, \Gamma_j; k, \Gamma_k) \mathbf{T}(\Gamma_k, \Gamma_{k-1}) G(k-1, \Gamma_{k-1}; i, \Gamma_i). \quad (2.3)$$

Here, $\mathbf{T}(\Gamma_i, \Gamma_{i+1})$ is the Green function of a dimer, also called the *transfer operator.* This property of Green functions enables us to calculate by a recursive procedure the Green function of any subunit $(i+1)$, in terms of the one of subunit i

$$G(i+1, \Gamma_{i+1}; 1, \Gamma_1) = \int d\Gamma_i G(i, \Gamma_i; 1, \Gamma_1) \mathbf{T}(\Gamma_i, \Gamma_{i+1}). \quad (2.4)$$

Together with initial conditions, the above equation determines G uniquely for any i and j.

In the particular case when the state Γ_i is represented by discrete coordinates, $\mathbf{T}(\Gamma_i, \Gamma_{i+1})$ will be represented by a matrix — the *transfer matrix.* Indeed, in the

following chapters we will discretize the coordinates to allow for a numerical solution by matrix manipulations. Henceforth, we will use exclusively the denomination of $\mathbf{T}$ as the transfer matrix.

For an ideal chain, the transfer matrix is determined just by the geometrical structure of the chain, mathematically expressed by the connectivity matrix, $\mathbf{C}(\Gamma_i, \Gamma_{i+1})$. This matrix reflects only the geometrical constraints associated with the bond lengths, bond angles and dihedral angles. If we also consider intramolecular interactions and the presence of an external field, then the transfer matrix will include the connectivity matrix and the Boltzmann factor due to these fields

$$\mathbf{T}(\Gamma_i, \Gamma_{i+1}) = \mathbf{C}(\Gamma_i, \Gamma_{i+1}) \exp\left(-\frac{U(\Gamma_{i+1})}{k_B T}\right), \tag{2.5}$$

where U is the total field potential that subunit $(i+1)$ experiences when in state Γ_{i+1}.

For convenience, we introduce the notations

$$G_i(\Gamma_i) = \int \mathrm{d}\Gamma_1 G(1, \Gamma_1; i, \Gamma_i), \tag{2.6}$$

$$\tilde{G}_i(\Gamma_i) = \int \mathrm{d}\Gamma_N G(i, \Gamma_i; N, \Gamma_N). \tag{2.7}$$

The statistical average of an arbitrary physical quantity, $F(\Gamma_i)$, that depends on the state of subunit i is calculated with the help of the Green function

$$\langle F(\Gamma_i) \rangle = \frac{1}{Z_N} \int \mathrm{d}\Gamma_i \int \mathrm{d}\Gamma_{i+1} F(\Gamma_i)\, G_i(\Gamma_i) \mathbf{T}(\Gamma_i, \Gamma_{i+1}) \tilde{G}_{i+1}(\Gamma_{i+1}). \tag{2.8}$$

Similarly, if a quantity depends on the state of two subunits, $F(\Gamma_i, \Gamma_j)$, with $(i+1) < j$, we have

$$\begin{aligned} \langle F(\Gamma_i, \Gamma_j) \rangle \;=\; & \frac{1}{Z_N} \int \mathrm{d}\Gamma_i \int \mathrm{d}\Gamma_{i+1} \int \mathrm{d}\Gamma_{j-1} \int \mathrm{d}\Gamma_j F(\Gamma_i, \Gamma_j)\, G_i(\Gamma_i) \\ & \times \mathbf{T}(\Gamma_i, \Gamma_{i+1}) G(i+1, \Gamma_{i+1}; j-1, \Gamma_{j-1}) \mathbf{T}(\Gamma_{j-1}, \Gamma_j) \tilde{G}_j(\Gamma_j). \end{aligned} \tag{2.9}$$

2.2 Transfer Matrix for the Gibbs Ensemble

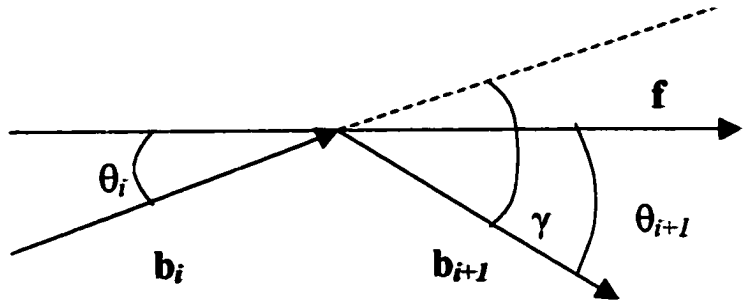

Figure 2.1: Vector geometry of a sequence of two subunits of a chain subjected to an external stretching force **f**.

Depending on the quantities of interest, we can employ the TM formalism to study the properties of a polymer chain in the (i) Gibbs ensemble or (ii) Helmholtz ensemble. Again, we must emphasize the fact that these two ensemble are not equivalent except in the limit of very long chains. To match the experimental situations, one must carefully identify the environmental variables, e.g. a fixed external pulling force, and choose the appropriate ensemble.

Henceforth, we will designate the *chain subunit vector* i, $1 < i < N$, as the vector joining the ends of the sequence of bond vectors belonging to monomer i. In the case where the monomer is comprised on only one bond, the subunit i is just the bond vector $\mathbf{b}_i$. Henceforth we will use the notation $\mathbf{b}_i$ for the chain subunit, regardless of how many bonds it contains.

In the situation in which the chain is acted upon by an external stretching force, f, at its ends, we can employ the Gibbs ensemble to calculate its average properties. The arguments of the Green function of subunit i, denoted in this case by $G_i^{(f)}(\Gamma)$ for "force" as the environmental variable, need to be adapted to encompass the relevant coordinates for this problem. Γ will necessarily include the angle θ formed by the direction of the subunit with the external force and the length of that subunit b (if variable with Γ) (see Figure 2.1).

Assuming that the stretching force is the sole external influence on the molecule, the transfer matrix becomes

$$\mathbf{T}^{(f)}(\Gamma_i, \Gamma_{i+1}) = \mathbf{C}(\Gamma_i, \Gamma_{i+1}) e^{f b_{i+1} \cos\theta_{i+1}/k_B T}, \tag{2.10}$$

and the integral equation 2.4 now reads

$$G_{i+1}^{(f)}(\Gamma_{i+1}) = e^{f b_{i+1} \cos\theta_{i+1}/k_B T} \int d\Gamma_i G_i^{(f)}(\Gamma_i) \mathbf{C}(\Gamma_i, \Gamma_{i+1}). \tag{2.11}$$

The *Gibbs partition function* of the polymer chain is calculated from the Green function by

$$\Delta(N, f, T) = \int d\Gamma_N G_N^{(f)}(\Gamma_N). \tag{2.12}$$

The *mechanical equation of state* or the *force-extension curve* for the polymer chain

$$\langle R_z \rangle = k_B T \frac{\partial}{\partial f} \ln \Delta(N, f, T), \tag{2.13}$$

where $\langle R_z \rangle$ is the average chain extension along the direction of force. The force-extension relation can also be determined from knowledge of the radial distribution function, for a chain with isotropic distribution as

$$\langle R_z \rangle = \frac{\int_0^\infty dR \int_{-1}^1 d(\cos\theta) W_N^{(r)}(R) R \cos\theta \exp(f R \cos\theta/k_B T)}{\int_0^\infty dR \int_{-1}^1 d(\cos\theta) W_N^{(r)}(R) \exp(f R \cos\theta/k_B T)} \tag{2.14}$$

$$= \frac{k_B T}{f} \frac{\int_0^\infty d\xi W_N^{(r)}(\xi k_B T/f) \xi [ch(\xi)/\xi - sh(\xi)/\xi^2]}{\int_0^\infty d\xi W_N^{(r)}(\xi k_B T/f) sh(\xi)/\xi}, \tag{2.15}$$

where $\xi = fR/k_B T$.

Alternatively, one can calculate the chain extension for an infinitely long molecule using the N-independent Green function, $G_{N^\bullet}^{(f)}(\Gamma)$, obtained for N larger than a threshold value, N^*. The latter can be chosen large enough so that the shape of $G_N^{(f)}(\Gamma)$ is practically the same for all $N > N^*$ (as one can expect for a diffusion-type process). In this situation, the force-extension curve can be calculated according to

$$\left\langle \frac{R_z}{N} \right\rangle_{N^\bullet} = \langle b \cos\theta \rangle = \frac{\int d\Gamma \int d\Gamma' b \cos\theta G_{N^\bullet}^{(f)}(\Gamma) G_{N^\bullet}^{(f)}(\Gamma') \mathbf{T}^{(f)}(\Gamma, \Gamma')}{\int d\Gamma \int d\Gamma' G_{N^\bullet}^{(f)}(\Gamma) G_{N^\bullet}^{(f)}(\Gamma') \mathbf{T}^{(f)}(\Gamma, \Gamma')}. \tag{2.16}$$

Given a desired accuracy for the force-extension curve, for any given chain model, we can estimate the value of the chain length for which the Green function becomes practically independent of N, as we will see in subsequent chapters.

We can also calculate the *probability that chain subunit i assumes a given state* Γ under an external force f according to eq. 2.8

$$p_i^{(f)}(\Gamma) = \frac{1}{\Delta(N,f,T)} \int d\Gamma' \int d\Gamma'' G_i^{(f)}(\Gamma') \tilde{G}_{N-i}^{(f)}(\Gamma'') \mathbf{T}^{(f)}(\Gamma',\Gamma'') \delta(\Gamma - \Gamma'), \quad (2.17)$$

and *the average fraction of chain units found in state* Γ will be given by

$$p^{(f)}(\Gamma) = \frac{1}{N} \sum_{i=1}^{N} p_i^{(f)}(\Gamma). \quad (2.18)$$

The probability for a pair of subunits to occur in the states Γ and Γ' is obtained by particularizing eq. 2.9 to read

$$\begin{aligned} p_i^{(f)}(\Gamma,\Gamma') \;=\; & \frac{1}{\Delta(N,f,T)} \int d\Gamma_i \int d\Gamma_{N-i} G_i^{(f)}(\Gamma_i) \tilde{G}_{N-i}^{(f)}(\Gamma_{N-i}) \\ & \times \mathbf{T}^{(f)}(\Gamma_i,\Gamma_{N-i}) \delta(\Gamma_i - \Gamma) \delta(\Gamma_{N-i} - \Gamma'). \end{aligned} \quad (2.19)$$

2.3 Transfer Matrix for the Helmholtz Ensemble

To calculate the end vector distribution function of a chain in θ—condition, we can employ new coordinates as arguments of the Green function in eq. 2.4. In proceeding with this task, we will distinguish and discuss two possible choices for the orthogonal coordinate system used for computation:

(*i*) a frame with the origin at one of the chain ends and arbitrary but fixed direction of axes; this frame is appropriate for studying the z–component probability distribution of the chain.

(*ii*) a frame with the origin at one of the chain ends and one of its axes in the same direction as the end-to-end vector; this frame is advantageous in calculating the end-to-end distance (or radial) distribution of the chain.

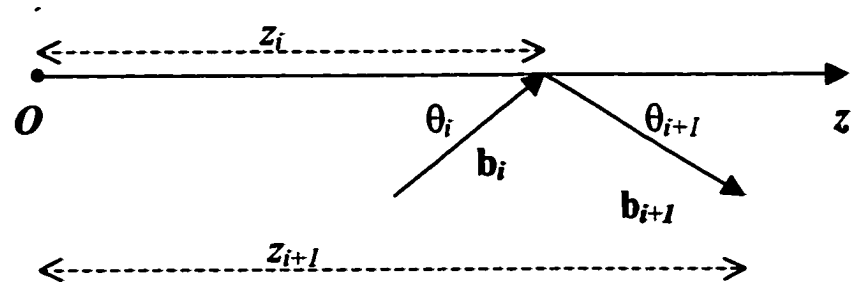

Figure 2.2: Geometry of a sequence of two subunits with their z–coordinates and relevant angles.

Note that while the first choice is a unique frame for all the configurations of the chain, the second one will change with the chain configuration. If we want to calculate the z–component probability distribution we should carry out computations in the frame (i) and identify the necessary coordinates. They include the position z_i, of the i-th bond along the z–axis and the angle θ_i formed by the bond vector $\mathbf{b}_i$ with the positive direction of this axis (see Figure 2.2). Thus we must replace Γ_i in eq. 2.4 by the set $\{z_i, \theta_i\}$ and designate the Green function for this case by $G_N^{(z)}(z_i, \theta_i)$, while the transfer matrix, $\mathbf{T}^{(z)}(\Gamma_i, \Gamma_{i+1}) = \mathbf{T}^{(z)}(z_i, \theta_i; z_{i+1}, \theta_{i+1})$, should equal the probability distribution that subunit $(i+1)$ is at z_{i+1} with an orientation θ_{i+1}, given that subunit i is at z_i with an orientation θ_i.

Alternatively, if we want to calculate the end distance distribution function (frame (ii)), we must replace the z–coordinate by the radial coordinate, $r_i \equiv |\mathbf{r}_i|$ (Figure 2.3) and the angle θ_i designates the angle formed by the bond vector $\mathbf{b}_i$ with $\mathbf{r}_i$. Consequently, the Green function is denoted by $G_N^{(r)}(r_i, \theta_i)$ and its argument are $\Gamma_i = \{r_i, \theta_i\}$.

Once we have calculated $G_N^{(z)}(R_z, \theta)$, we can readily find the Helmholtz partition function $Z_z(N, T, R_z)$, Helmholtz free energy $A_z(N, T, R_z)$ and the average contractile force in the chain $\langle f_z \rangle$ by the following relations

$$Z_z(N, T, R_z) = \int_0^\pi \mathrm{d}\theta G_N^{(z)}(R_z, \theta), \tag{2.20}$$

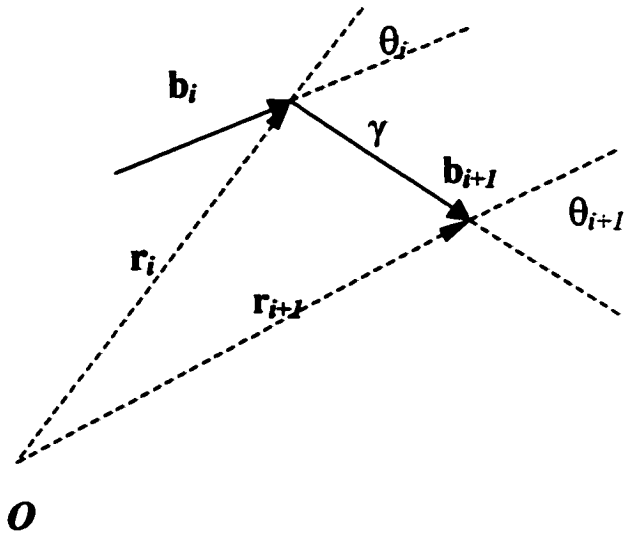

Figure 2.3: Geometry of a sequence of two subunits with their radial coordinates and corresponding orientations.

$$A_z(N,T,R_z) = -k_BT \ln Z_z(N,T,R_z), \tag{2.21}$$

$$\langle f_z \rangle = \left(\frac{\partial A_z}{\partial R_z}\right)_T. \tag{2.22}$$

Alternatively, if we study the chain in the reference frame (ii)

$$Z_r(N,T,R) = \int_0^\pi \mathrm{d}\theta G_N^{(r)}(R,\theta), \tag{2.23}$$

$$A_r(N,T,R) = -k_BT \ln Z_r(N,T,R), \tag{2.24}$$

$$\langle f_r \rangle = \left(\frac{\partial A_r}{\partial R}\right)_T. \tag{2.25}$$

Let us also denote the end-to-end distance distribution, which is obtained by normalizing the Helmholtz partition function, by $W_N^{(r)}(R)$ and the chain end z–

component distribution function by $W_N^{(z)}(R_z)$, in other words,

$$W_N^{(r)}(R) = \frac{Z_r(N,T,R)}{\int_0^\infty \mathrm{d}R Z_r(N,T,R)}, \tag{2.26}$$

and

$$W_N^{(z)}(R_z) = \frac{Z_z(N,T,R_z)}{\int_0^\infty \mathrm{d}R_z Z_z(N,T,R_z)}. \tag{2.27}$$

The relation between these distribution functions is

$$W_N^{(z)}(R_z) = \int_0^\infty \mathrm{d}R 2\pi R \left[\frac{W_N^{(r)}(\sqrt{R^2+R_z^2})}{4\pi(R^2+R_z^2)}\right]. \tag{2.28}$$

Knowledge of the end-to-end distribution functions $W_i^{(r)}(r)$ for any i is particularly useful in calculating other quantities of interest. In the following, we will assume homogeneity along the chain's contour, which guarantees that the monomer-to-monomer distance distribution, $W_{i,j}^{(r)}(r)$ depends on the values of i and j only through the difference $(i-j)$ and is thus identical to $W_{i-j}^{(r)}(r)$. For instance, the pair correlation function of the chain can be calculated directly using

$$g(r) = \frac{1}{N(N+1)} \sum_{\substack{i,j=0,N \\ i\neq j}} \frac{W_{i-j}^{(r)}(r)/r^2}{\int_0^\infty \mathrm{d}r W_{i-j}^{(r)}(r)/r^2}, \tag{2.29}$$

which obviously has the normalization

$$\int_0^\infty \mathrm{d}r g(r) = 1. \tag{2.30}$$

The mean square radius of gyration $\langle R_g^2 \rangle$ can be calculated according to eq. 1.15 by summing terms of the form $\langle r_{ij}^2 \rangle$, which in turn can be calculated by

$$\langle r_{ij}^2 \rangle = \int_0^\infty \mathrm{d}r W_{i-j}^{(r)}(r) r^2. \tag{2.31}$$

Furthermore, the chain's structure factor $S(k)$ in eq. 1.37, can be determined if the

averages under the sum are calculated according to

$$\left\langle \frac{\sin(kr_{ij})}{kr_{ij}} \right\rangle = \int_0^\infty \mathrm{d}r W_{i-j}^{(r)}(r) \frac{\sin(kr)}{kr}. \tag{2.32}$$

2.4 The Role of the Boundary Conditions

The thermodynamics of a single macromolecule can be measured and calculated under different boundary conditions:

(*i*) One can fix the length of the macromolecule and measure the force necessary to maintain this length; this suggests doing the statistical mechanics in the isothermal-isochoric or Helmholtz ensemble, in which the length is a control variable and the average force and its fluctuations are calculated by differentiation.

(*ii*) One can apply a given force and measure the resultant extension of the molecule; this suggests doing the statistical mechanics in the isothermal-isobaric or Gibbs ensemble in which the force is a control variable, and the length and its fluctuations are calculated by differentiation[2].

Because different ensembles in statistical mechanics are only equivalent for thermodynamically large systems, but not for small systems, it is important to formulate the right statistical mechanics for the stretching of a macromolecule. The question to be answered is which of the two thermodynamically conjugate variables, force or length, is held constant and which is the fluctuating response. It has recently been shown that in stretching a single polymer molecule with an Atomic Force Microscope (AFM), both situations can be realized by changing the force constant of the cantilever: for a soft cantilever the Gibbs ensemble is appropriate and for a stiff cantilever one can use the Helmholtz ensemble[14, 13]. Recently a first principles theory was also developed using both Gibbs and Helmholtz ensembles[12].

An additional observation is in place. If in a stretching experiment[6] one end of the macromolecule is attached to a surface and the other end to a cantilever tip, as the force is increased the length and direction of the end-to-end vector $\mathbf{R}$ will change. It is important to discern the overall orientation of the chain with respect to the external force. In general, some force component f_z will act in the direction of $\mathbf{R}$, and the angle between the force and the end-to-end length will vary from experiment to experiment and we must define the appropriate boundary conditions on the ensemble suitable to

the set of constraints to which the chain is subjected. Here, we mention two distinct physical situations requiring different boundary conditions (BC) on the ensemble:

- BC 1: the polymer is stretched by its ends and the end-to-end vector is constrained to be parallel to the direction of the external force. This is the experimental case of PEG stretched by an AFM tip[6], when the chain is grafted to a hard surface and the AFM tip is made to "pick up" the other chain end close to the grafting point and then apply stretching force perpendicular to the grafting surface; under these conditions, equations 2.23-2.25 should be employed.

- BC 2: the polymer is stretched by its ends and the end-to-end vector can form, with appropriate weights, any angle with the direction of the external force; for this case the relations 2.20-2.22 are applicable.

Both boundary conditions are discernible only for short chains and small stretching forces and produce identical results when the chain length exceeds the deflection length, $\lambda = \sqrt{l_P k_B T/f}$, where l_P is the persistence length of the molecule. Henceforth we will mention these distinctions only where they play an essential role in the physical picture.

Generally speaking, one can imagine a variety of boundary conditions for a single molecule. This does not necessarily mean the conditions in which the ends of a molecule are found, but it can refer to any of the chain's monomers or group of monomers. In a given single chain experiment, in order to formulate the appropriate boundary conditions one has to identify the nature of external constrictions (e.g. grafting covalent bonds, impenetrable surfaces) imposed by the molecule's environment and, given the spatial scale for this problem, this is sometimes a non-trivial task.

2.5 Implementation of the TM Method

With the advent of hardware capabilities in computers (speed and memory size), computational theoretical physics in the past decade has experienced a great boost, to the extent that problems that were virtually intractable ten or twenty years ago, can now be tackled with the help of a PC. In fact, the newest PC's are the equivalent of supercomputers in the beginning of the nineties.

The Green function for any of the chain's monomers can be obtained by successive numerical iterations, as given by eq. 2.4. In order to perform this on a computer, we must translate the whole procedure described above into a proper program algorithm. To this end, we convert the continuous coordinates spanned by Γ to discrete ones. For instance, if Γ includes an angular coordinate θ, whose range is $[0, \pi]$, we sample this continuous interval by an array of $M_\theta + 1$ uniformly distributed points (M_θ intervals), which will constitute the only allowed values for θ. Similarly, if Γ includes a radial coordinate r, too, with range $[0, Nb]$ we will divide this range into M_r intervals—corresponding to $M_r + 1$ allowed values of the discrete coordinate r. Assuming that θ and r are the only coordinates included in Γ, the number of allowed values for Γ in this discrete model is $M_\Gamma = M_\theta \times M_r$. The transfer operator $\mathbf{T}(\Gamma_i, \Gamma_{i+1})$ in eq. 2.4 thus becomes a 2-dimensional, $M_\Gamma \times M_\Gamma$ transfer matrix. In the following, we will refer to M_θ, M_r, M_Γ as the *mesh parameters.*

Since we aim to study the properties of continuous models, like the FJC, FRC etc., the role of discreteness of our coordinates (*discretization effects*) on the final results must be critically analyzed. Intuitively speaking, the desired transition from discrete to continuous models can be achieved if the representation of continuous coordinates by discrete ones is fine enough, that is, if the parameter M_Γ is sufficiently large. With the increase in M_Γ one expects the discretization effects to vanish. Anticipating results in the following chapters, we will say here that we performed the entire procedure for increasing values of the mesh parameters and compared the outcomes. We found that the results converge to a unique limit, which can be appropriately called *the continuous limit*. All results obtained for M_Γ larger than a threshold value are virtually identical to each other and therefore to the results obtained with continuous Γ coordinates.

The precision of our calculations, or the degree to which they approach the continuous limit, will increase with larger mesh parameters. But the magnitude of these parameters is practically limited in a numerical procedure by the size of the computer's memory. Therefore, judicious use of the computational resources is required, especially for complex models. As an example, for linear coordinates (e.g. r and z), in order to increase the precision of the calculation, we can adapt the range at each iteration step i, for instance making it proportional to a maximal distance $R_{max} = ib$.

All computations have been performed on a 1GHz *Pentium III* with 512MB

memory and, depending on the complexity of the model, may take from minutes to days of CPU time and can easily occupy the entire memory. For all polymer models considered the computational cost of the method increases linearly with the size of the chain. A *GNU FORTRAN 77 compiler* was used to process all the codes generating the numerical results of our analysis. A sample code for the calculation of the force-extension curve of the FRC model is given in Appendix *A*.

For a given computer system, one can evaluate the limits of feasibility for implementing this method. Roughly speaking, the maximal value of M_Γ will be proportional to the size of the memory. More precisely, a real (double precision) matrix of dimension M_Γ used to store the values of the Green function at all the mesh points cannot occupy more than half the computer's memory. Two such matrices are necessary in order to perform numerically the TM iteration from any given bond to its neighbor. For our system, we found the maximal value of M_Γ to be about 12×10^6.

CHAPTER 3

THE FREELY JOINTED CHAIN

The freely jointed chain is a sequence of segments, mimicking chemical bonds, of the same length b, the ends of each being linked to the end of the neighboring bond to form a chain-like structure (Figure 3.2) .

The probability of a chain bond to have a certain direction with respect to the position of the previous bond is constant over the solid angular interval. In other words, if we look at a sequence of two consecutive bonds of the FJC, like in Figure 3.1, the angular variables θ and ϕ have constant probability densities over their entire range.

If we denote the position vectors of any two consecutive chain links by $\mathbf{r}$, $\mathbf{r}'$ the connectivity operator for the FJC, will be given by

$$\mathbf{C}(|\mathbf{r}-\mathbf{r}'|) = \frac{1}{4\pi b^2}\delta(|\mathbf{r}-\mathbf{r}'|-b), \tag{3.1}$$

with the normalization property

$$\int_0^\infty 4\pi q^2 \mathbf{C}(q)dq = 1, \tag{3.2}$$

where $q = |\mathbf{r}-\mathbf{r}'|$.

The average end-to-end distance of the FJC model is calculated according to eq. 1.4

$$\langle R^2 \rangle = Nb^2, \tag{3.3}$$

since $\langle \cos\psi_{ij} \rangle = 0$ for any $1 \leq i < j \leq N$. Note from the above relation that the characteristic ratio for FRC is exactly 1 for any N. Also, since the contour length of this model is $L = Nb$, using eq. 1.10 and 3.3 one can derive the effective length of this model to be $a = b$.

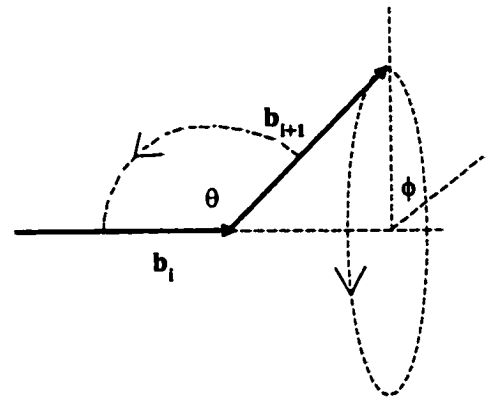

Figure 3.1: Sequence of two bond vectors of the FJC and their associated angular degrees of freedom.

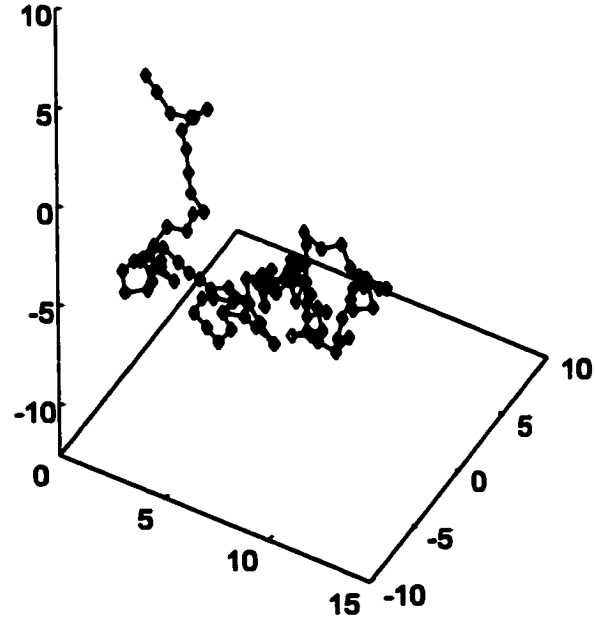

Figure 3.2: A random three-dimensional configuration of a FJC with 100 bonds.

The mean square radius of gyration for this model can be calculated from eq. 1.15, if we use $\langle r_{ij}^2 \rangle = (j-i)b^2$, and yields[2]

$$\langle R_g^2 \rangle = \frac{1}{6}\frac{N+2}{N+1}Nb^2. \tag{3.4}$$

Note that there will be a slight dependence of $\frac{\langle R_g^2 \rangle}{Nb^2}$ on N for small chain lengths, which will rapidly diminish as N increases and in the limit of very long chains one has $\frac{\langle R_g^2 \rangle}{Nb^2} \to \frac{C_N}{6} = \frac{1}{6}$.

The force-extension relation for the FJC is analytically known for all forces, namely the *Langevin function*

$$\frac{R_z}{L} = \coth\left(\frac{fb}{k_BT}\right) - \left(\frac{fb}{k_BT}\right)^{-1}. \tag{3.5}$$

In the large-force regime $\left(\frac{fb}{k_BT} \gg 1\right)$ one can see that $\coth\left(\frac{fb}{k_BT}\right) \to 1$, and the relation becomes

$$\frac{R_z}{L} \cong 1 - \left(\frac{fb}{k_BT}\right)^{-1}. \tag{3.6}$$

The chain end distribution functions for this model were investigated by Lord Rayleigh by means of Fourier decomposition and were found to be of the general form[2]

$$W_N^{(r)}(R) \propto R\int_0^\infty \mathrm{d}q \sin(qR)\left[\frac{\sin(qR)}{qR}\right]^N q, \tag{3.7}$$

which yields, with the help of eq. 1.18, the following expressions[2] of $W_N(\mathbf{R})$ for small chain lengths:

$$W_2(\mathbf{R}) = \frac{1}{8\pi b^2 R}, \tag{3.8}$$

$$W_3(\mathbf{R}) = \begin{cases} 1/8\pi b^3, & \text{for} \quad 0 \le R \le b \\ (3 - R/b)/16\pi b^2 R, & \text{for} \quad b \le R \le 3b \end{cases}, \tag{3.9}$$

$$W_4(\mathbf{R}) = \begin{cases} (8 - 3R/b)/64\pi b^3, & \text{for} \quad 0 \le R \le 2b \\ (4 - R/b)^2/64\pi b^2 R, & \text{for} \quad 2b \le R \le 4b \end{cases}, \tag{3.10}$$

For large N, the radial distribution can be approximated with Gaussian–type functions of the form

$$W_N(\mathbf{R}) = \left(\frac{3}{2\pi N b^2}\right)^{3/2} \exp\left(-\frac{3R^2}{2Nb^2}\right). \tag{3.11}$$

This approximation however is reasonable only for extensions up to values slightly larger than the position of the maximum of $W_N^{(r)}(R)$.

3.1 Transfer Matrix Method for the FJC

Below we will formulate and apply the TM method for the FJC model. We should state that this chapter serves before anything else as a test of TM method, since we can compare our results to the well known analytical findings for this simple model. The transfer operator approach in the Gibbs ensemble is trivial for this model, since there is no correlation whatsoever between the directions of two adjacent bonds. Accordingly, we will only proceed to study the FJC using the transfer operator in the canonical ensemble.

To calculate the end-to-end probability distribution for the FJC, we refer back to the geometry depicted in Figure 2.3. This time, since the orientations of the two adjacent bonds are completely independent, it suffices for us to focus only on the angular coordinates θ and ϕ shown in Figure 3.1, which must be integrated over. Thus, for this problem the only coordinate serving as argument of the Green function $G_i^{(r)}$, is the radial distance, r. Without loss of generalization, we can assume that the radial vector for monomer i is parallel to the bond vector $\mathbf{b}_i$. Then, to calculate the Green function for the monomer $(i+1)$ we perform an iteration according to

$$G_{i+1}^{(r)}(r') = \int \mathrm{d}r G_i^{(r)}(r)\mathbf{T}^{(r)}(r,r'), \tag{3.12}$$

where the transfer matrix in this case is identical to the connectivity matrix

$$T^{(r)}(r,r') = C^{(r)}(r,r') = \int_0^{2\pi} d\phi \int_0^{\pi} d\theta \sin\theta \delta[r' - g_r(r,\theta)], \tag{3.13}$$

and g_r is given by

$$g_r(r,\theta) = \sqrt{r^2 + b^2 + 2rb\cos\theta}. \tag{3.14}$$

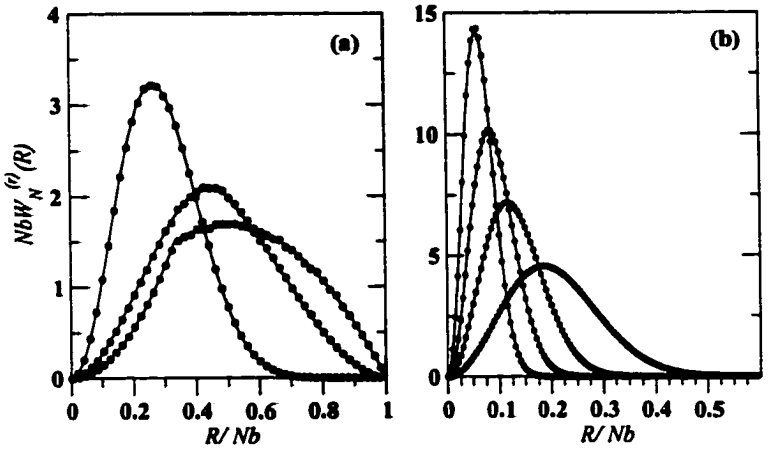

Figure 3.3: The end-to-end distribution function for FJC of lengths $N = 3, 4, 10$ in (a) and $N = 20, 50, 100, 200$ in (b). The curves have increasingly higher maxima with the increase of N. Our computations are plotted as circles, while the solid lines are given by eq. 3.7.

The end-to-end distance distribution function is calculated with this procedure via eq. 2.23 and 2.26. In Figure 3.3 we show as circular symbols the results of our computations for $W_N^{(r)}(R)$ versus the rescaled end-to-end distance R/Nb. From the lowest to highest maxima, the chain lengths are 3, 4, 10 in panel (a), and 20, 50, 100, 200 in (b). Note that we multiplied the distribution function by the number of bonds N in order to make the curves more easily comparable. The accuracy of these calculations is checked by comparing the TM results with the exact results of Rayleigh, eq. 3.7, shown as solid lines. The mesh parameter for the radial coordinate r, is the only variable that dictates the accuracy of our calculations. Here we have used the number of mesh points $M_r = 1000$.

The curves in Figure 3.3 can also be compared to Gaussian-type distributions of the form given in eq. 3.11, which constitutes a good approximation only for relatively long chains. There are important deviations from Gaussian form most noticeably on the "tail" of the curve, which corresponds to the highly extended chain region, where R is larger than approximately twice the most probable distance. As we will see later, this region plays an essential role in the shape of the force-extension curve. To show the deviations from the Gaussian forms we plotted in Figure 3.4, the results for $W_N^{(r)}$ in semilogarithmic axes, for $N = 4, 10$ in panel (a) and $N = 20, 50, 100, 200$ in

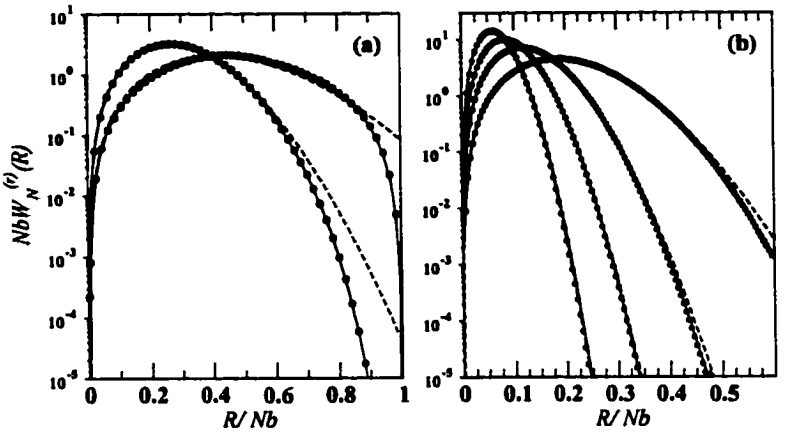

Figure 3.4: End-to-end distribution function plotted in semilogarithmic axes, for $N = 4, 10$ in (a) and same chain lengths as in Figure 3.3 in panel (b). Our computations–circles; the solid lines– exact formula, eq. 3.7; dashed lines–Gaussian curves, eq. 3.11.

(b), together with the corresponding Gaussian curves (dashed lines). As above, the curves can be distinguished by the location of their maxima and the plotting symbols previously used in Figure 3.3. We can see that, in the tail region, for chains up to few tens of bonds, the exact curves differ by order of magnitudes from the Gaussians in eq. 3.11.

Proceeding in a similar manner as above, we can calculate the end-to-end vector $z-$component distribution. For this purpose we refer back to the geometry in Figure 2.2. Based on the observations made in the above subsection regarding the local angles θ and ϕ, we can state that the only argument of the Green function for this problem is z. Thus, we will calculate the Green function $G_i^{(z)}(z)$, for all bonds of the FJC, by repeated application of the formula

$$G_{i+1}^{(z)}(z') = \int \mathrm{d}z G_i^{(z)}(z)\mathbf{T}^{(z)}(z, z'), \tag{3.15}$$

where the transfer matrix in this case is just the connectivity matrix

$$\mathbf{T}^{(z)}(z, z') = \mathbf{C}^{(z)}(z, z') = \int_0^{2\pi} \mathrm{d}\phi \int_0^{\pi} \mathrm{d}\theta \sin\theta \delta[z' - g_z(z, \theta)], \tag{3.16}$$

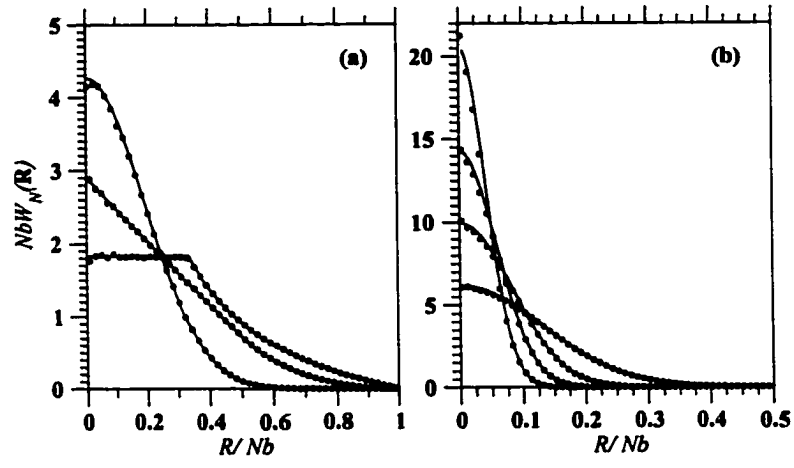

Figure 3.5: End vector distribution function for the FJC with the same chain lengths as in Figure 3.3. Circles–our computations; solid curves–exact result by eq. 3.7

and g_z is given by

$$g_z(z,\theta) = z + b\cos\theta. \tag{3.17}$$

In Figure 3.5 we present the end vector distribution, as calculated from eq. 1.18, for the same chain lengths as in Figure 3.3. Once more, we can see excellent agreement between our computations and the Rayleigh result, eq. 3.7.

Using the calculated distribution function, $W_N^{(r)}(R)$, we next determine the force-extension for the FJC with eq. 2.14, and plot it in Figure 3.6 together with the analytical prediction — the Langevin function in eq. 3.5. If plotted versus the extension rescaled by the contour length, R_z/Nb, this curve has exactly the same shape for any N, and our TM computations (circles) follow the Langevin result very precisely.

Since we already have the distribution functions $W_i^{(r)}(r)$ for any i, the mean square radius of gyration can be calculated using eq. 1.15 and 2.31. In Figure 3.7 we plot the quantity $\langle R_g^2 \rangle / Nb^2$ versus N as calculated by TM (pluses) and the analytical expression in eq. 3.4 (circular symbols). As the chain length increases, this quantity will tend to the limit $\frac{C_N}{6}$ valid for any random polymer model.

Furthermore, by employing the distributions $W_i^{(r)}(r)$ for all i, we can determine the structure factor $S(k)$ for this chain model. For this purpose, we need to refer back to eq. 1.37, where we calculate the averages under the sum by using eq. 2.32.

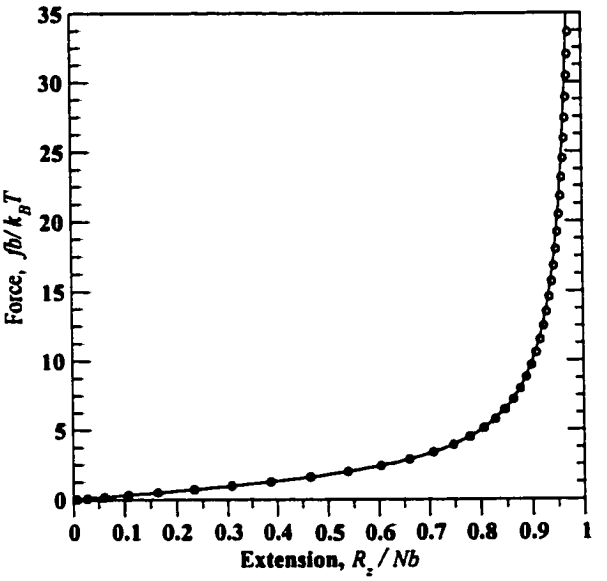

Figure 3.6: Force-extension curve for the FJC. Solid curve–the Langevin relation, eq. 3.5; circular symbols– the transfer matrix result.

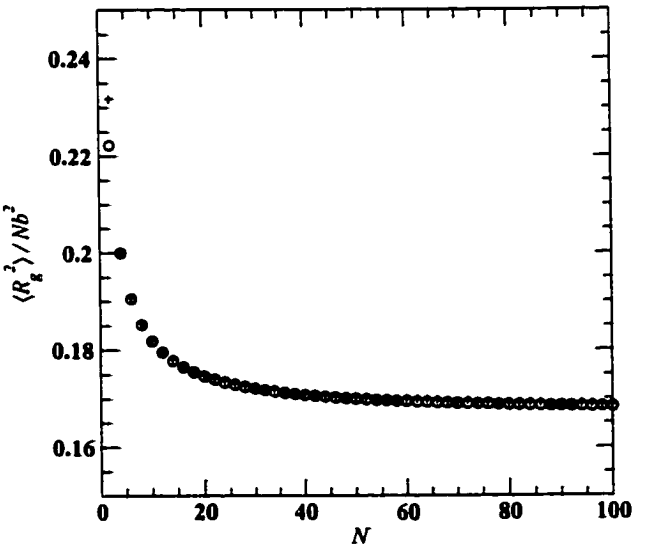

Figure 3.7: Mean square radius of gyration for the FJC versus chain length (pluses– the TM results; circles– the analytical prediction, eq. 3.4).

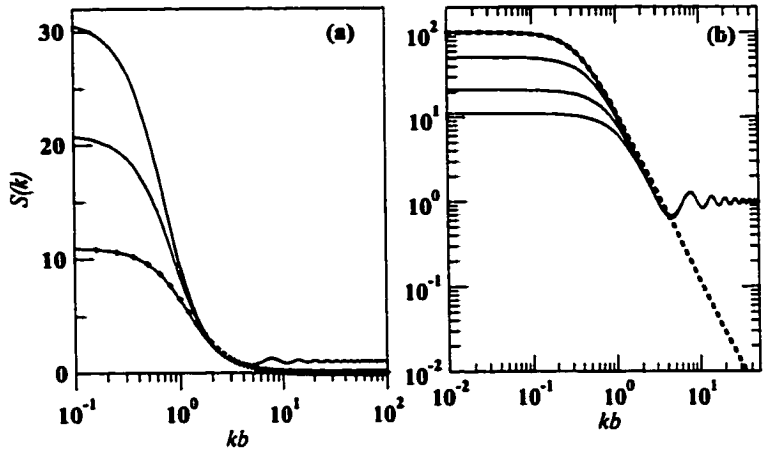

Figure 3.8: Structure factor of the FJC. Panel (a): continuous lines– TM calculations for $N = 10, 20, 30$; pluses– Debye function for N=10. Panel (b): continuous lines– TM calculations for $N = 10, 20, 50, 100$; dotted line– Debye function for $N = 100$.

In Figure 3.8 we present the results of these computations. In panel (a) we show in continuous line, the structure factor for $N = 10, 20, 30$ (from bottom to top) and, as plus symbols, the structure factor for the Gaussian chain model with 10 bonds, given with the help of the Debye function[4]

$$S_N(k) = N f_{Debye}(k^2 \langle R_g^2 \rangle), \tag{3.18}$$

with

$$f_{Debye}(x) = \frac{2}{x^2}\left(x - 1 + \mathrm{e}^{-x}\right). \tag{3.19}$$

In panel (b), we plot in double logarithmic axes $S(k)$ for chains of length $N = 10, 20, 50, 100$ (solid lines) and for the Gaussian chain with 100 bonds (dotted line).

Proceeding in a similar way, we next calculate the pair correlation function for the FJC, using $W_i^{(r)}(r)$ and eq. 2.29. The results are displayed in Figure 3.9. The plots correspond to chain lengths $N = 10, 20, 50, 100$, with maxima from top to bottom. For better visualization of the differences between them, we plotted the curves in both linear axes, panel (a), and semilogarithmic axes, panel (b). All curves display a sharp peak (delta function) at $r/b = 1$, corresponding to the presence of the immediately adjacent monomers situated at distance b.

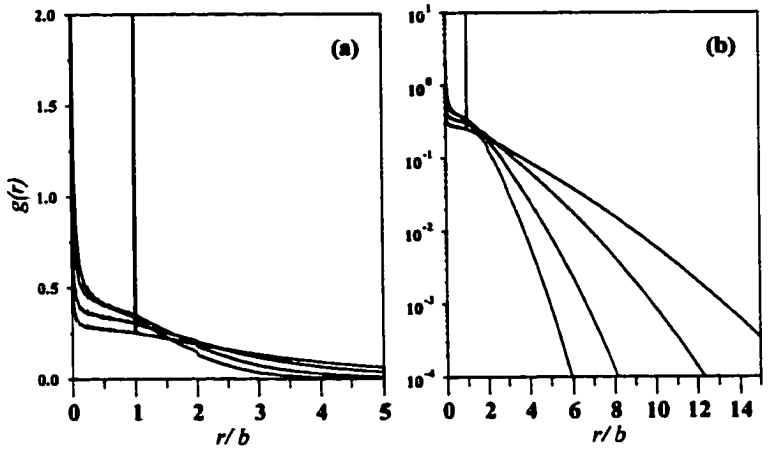

Figure 3.9: Pair correlation function of the FJC in linear (a) and semilogarithmic (b) axes. With maxima from top to bottom curves correspond to chain lengths $N = 10, 20, 50, 100$.

To summarize this chapter: we have used the FJC model to demonstrate the accuracy achievable in the discrete transfer matrix method by comparing our results with the exact solution. The TM technique in the canonical ensemble proved to be extremely accurate, coming in excellent agreement with all the analytical predictions. Instead, we can concentrate our efforts on using the insight gained here to handling more realistic models of polymers, where the behavior is not analytically known. This will be done in the following chapters.

CHAPTER 4

THE FREELY ROTATING CHAIN

The FRC model consists of segments having the same length b while the angle formed by any two segments has a fixed value γ. For the FRC, any bond can freely rotate about the direction of the previous bond maintaining the same angle between the two, as sketched in Figure 4.1. Although a simple model in its geometrical formulation, the statistical mechanical treatment of this model is non-trivial and can be carried out analytically only to a certain extent. The statistical mechanics of the FRC is summarized in the classical book of Flory[2] as well as in the more recent text of Grosberg and Khokhlov[1]. A theoretical study of the FRC using the Green functions method was performed by Kostrowicki and Scheraga[49]. Their work was focused on calculations of the end-to-end distributions for short chains only.

We will employ the TM technique to the study of the FRC with bond angles within a large range of values including very small ones and for a variety of chain lengths. We are interested in the end distribution functions and their comparison with Gaussian forms. We calculate the mechanical equation of state and study in detail the stretching behavior of the FRC emphasizing the effect of the bond angle on the force-extension relation. For small bond angles, we expect to find similarities with the WLC (or the semiflexible) model, which is mathematically obtained as the limit $b \to 0, \gamma \to 0$, with the chain length being held constant. For large bond angles we can speculate that the FRC will resemble more the FJC than the WLC. This will be critically assessed in the following, based on accurate results obtained by the TM method. Most results in this chapter are reproduced from the work coauthored in ref. [25].

Denoting the bond vectors of the chain by $\mathbf{b}_i$, with $i = 1, 2, ..., N$, the connectivity operator for this model can be written as

$$\mathbf{C}(\mathbf{b}_i, \mathbf{b}_{i-1}) = \frac{1}{4\pi}\delta\left(\frac{\mathbf{b}_i \cdot \mathbf{b}_{i-1}}{|\mathbf{b}_i|\,|\mathbf{b}_{i-1}|} - \cos\gamma\right), \tag{4.1}$$

which as one can see, depends only on the angle between the two bond vectors. If φ_i is the dihedral angle between the planes $(\mathbf{b}_i, \mathbf{b}_{i-1})$ and $(\mathbf{b}_{i-1}, \mathbf{b}_{i-2})$ then the probability distribution for φ_i is a constant function over its entire range $[-\pi, \pi]$ for any i.

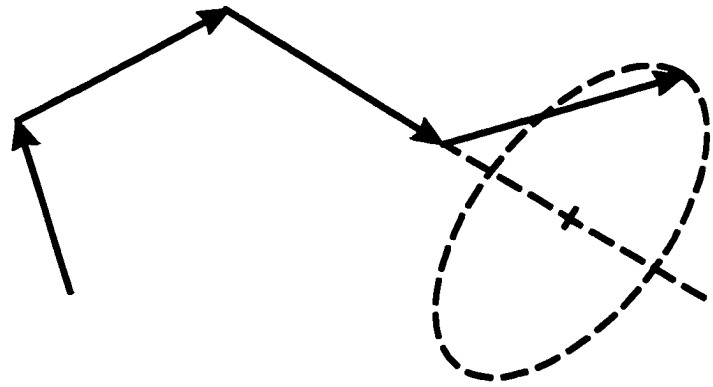

Figure 4.1: Schematical representation of a section of FRC indicating the path of the free rotation for the last bond vector.

The average end-to-end distance in the FRC model[2] is calculated according to eq. 1.4

$$\langle R^2 \rangle = Nb^2 + 2b^2 \sum_{1 \le i < j \le N} \langle \cos \psi_{ij} \rangle , \tag{4.2}$$

and since $\langle \cos \psi_{ij} \rangle = (\cos \gamma)^{j-i}$ for any $1 \le i < j \le N$, the above can be evaluated to give[2]

$$\langle R^2 \rangle = Nb^2 \left(\frac{1 + \cos \gamma}{1 - \cos \gamma} - \frac{2 \cos \gamma}{N} \cdot \frac{1 - (\cos \gamma)^N}{(1 - \cos \gamma)^2} \right) , \tag{4.3}$$

which, in the infinite chain limit $N \to \infty$, becomes

$$\langle R^2 \rangle = Nb^2 \frac{1 + \cos \gamma}{1 - \cos \gamma} . \tag{4.4}$$

The characteristic ratio for FRC in the long chain limit will then be equal to

$$C_N = \frac{1 + \cos \gamma}{1 - \cos \gamma} . \tag{4.5}$$

The effective (or Kuhn) length a is defined by eq. 1.10 as

$$\langle R^2 \rangle = La, \tag{4.6}$$

where L is the contour length of the polymer, which for the this model is given by

$$L = Nb\cos(\gamma/2). \tag{4.7}$$

This yields for the Kuhn length

$$a = b\frac{1+\cos\gamma}{(1-\cos\gamma)\cos(\gamma/2)}. \tag{4.8}$$

The mean square radius of gyration can be derived with the use of eq. 1.15 and 4.3 to yield[2]

$$\begin{aligned}\frac{\langle R_g^2 \rangle}{Nb^2} &= \frac{1}{6}\frac{(N+2)}{(N+1)}\frac{(1+\cos\gamma)}{(1-\cos\gamma)} - \frac{\cos\gamma}{(N+1)(1-\cos\gamma)^2} \\ &+ \frac{2\,(\cos\gamma)^2}{(N+1)^2(1-\cos\gamma)^3} - \frac{2\,(\cos\gamma)^3\,(1-(\cos\gamma)^N)}{N(N+1)^2(1-\cos\gamma)^4}.\end{aligned} \tag{4.9}$$

For $N \rightarrow \infty$ one gets

$$\left(\frac{\langle R_g^2 \rangle}{Nb^2}\right)_{N\rightarrow\infty} = \frac{C_N}{6}, \tag{4.10}$$

as expected for any random polymer model. Finally, the persistence length for the FRC is given by

$$l_P = b\frac{\cos(\gamma/2)}{|\ln(\cos\gamma)|}. \tag{4.11}$$

Since we intend to compare our results with other models such as the worm-like chain, we list here some relevant relations. An interpolation formula for the force response function of the WLC was proposed by Marko and Siggia[38]

$$\frac{fl_P}{k_BT} = \frac{R_z}{L} + \frac{1}{4(1-R_z/L)^2} - \frac{1}{4}, \tag{4.12}$$

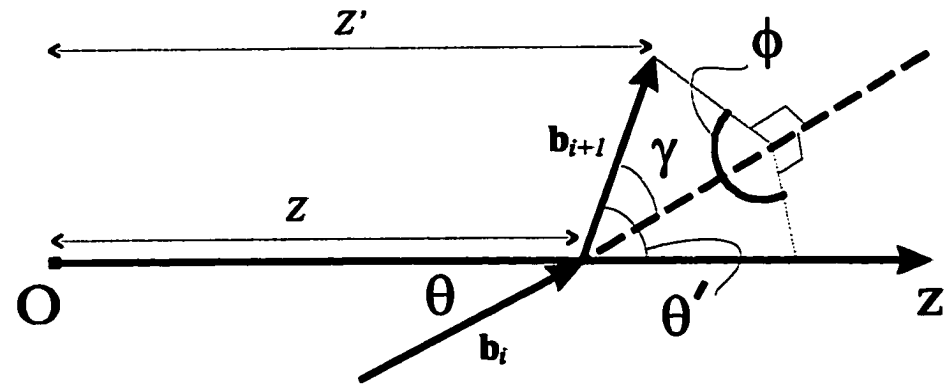

Figure 4.2: Relevant coordinates for the Green function of the end vector z-component for the FRC.

which has a maximum error of 10% in the intermediate force regime, but accurately represents the small and large force regimes. From here we can derive the corresponding large-force relation for the WLC $\left(\frac{fb}{k_BT} \gg 1\right)$

$$\frac{R_z}{L} \cong 1 - \frac{1}{2}\left(\frac{fl_P}{k_BT}\right)^{-1/2}. \tag{4.13}$$

4.1 Transfer Matrix in the Helmholtz Ensemble

As outlined in the 'TM Method' section of this work, there exists a variety of different boundary conditions on the Helmholtz ensemble. For the FRC, we will approach the following two cases: (*i*) for a chain free to rotate about a fixed but arbitrary z–axis, we will calculate the probability distribution of the end-to-end vector z–component; (*ii*) the end-to-end distance probability distribution. Each of these requires a particular formulation of the TM formalism, which constitutes the topic of the following discussion.

4.1.1 Green Function for the End Vector z–component

To calculate the distribution function of the end vector z–component we must use the coordinate pair $\Gamma = \{z, \theta\}$ (see Figure 4.2) and the corresponding transfer matrix for this case is

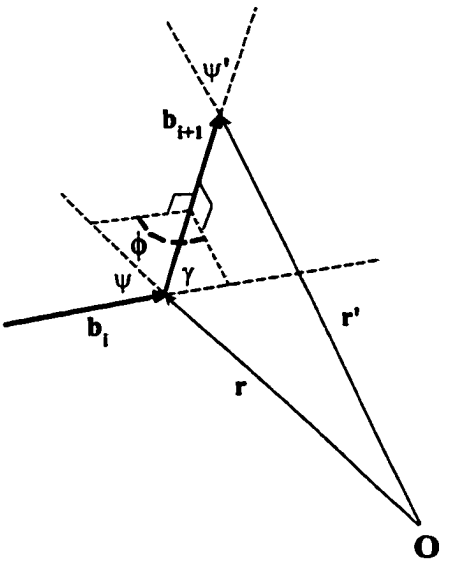

Figure 4.3: Relevant coordinates for the Green function method for calculating the end-to-end distance for the FRC model.

$$\mathbf{T}^{(z)}(z,\theta;z',\theta') = \int_0^{2\pi} d\phi\delta[\theta' - g_\theta(\theta,\phi)]\delta[z' - z - g_z(\theta,\phi)]. \tag{4.14}$$

Here, g_θ characterizes the geometrical restriction exhibited by the orientations of two adjacent chain segments. Following a well-known trigonometric relation, we have

$$g_\theta(\theta,\phi) = \cos^{-1}\left(\cos\theta\cos\gamma + \sin\theta\sin\gamma\cos\phi\right), \tag{4.15}$$

while g_z reads

$$g_z(\theta,\phi) = b(\cos\theta\cos\gamma + \sin\theta\sin\gamma\cos\phi). \tag{4.16}$$

As initial condition, the unnormalized probability for this case is

$$G_1^{(z)}(z,\theta) \propto \delta(z - b\cos\theta)\sin\theta. \tag{4.17}$$

4.1.2 Green Function for the End-to-End Distance

For the "radial" Green function $G_N^{(r)}(r,\psi)$, (see Figure 4.3) the transfer matrix is

$$\mathbf{T}^{(r)}(r,\psi;r',\psi') = \int_0^{2\pi} d\phi\delta[\psi' - g_\psi(r,r')]\delta[r' - g_r(r,\psi,\phi)], \tag{4.18}$$

where g_r is given by

$$g_r(r,\psi,\phi) = \left[r^2 + b^2 + 2rb(\cos\psi\cos\gamma + \sin\psi\sin\gamma\cos\phi)\right]^{1/2}, \tag{4.19}$$

and

$$g_\psi(r,r') = \cos^{-1}\left[\frac{(r')^2 + b^2 - r^2}{2rb}\right]. \tag{4.20}$$

The initial condition is

$$G_2^{(r)}(r,\psi) = \delta[r - 2b\cos\psi]\delta[\psi - \gamma/2]. \tag{4.21}$$

In order to solve the integral equation for the Green's function (2.1) we use a numerical iteration scheme which employs discrete coordinates in direct correspondence with small finite intervals in the continuous coordinates Γ_i. There are N iteration steps for the Green function, corresponding to the number of chain bonds.

4.1.3 Results and Discussion

In Figure 4.4, we display the variation of the radial distribution function $W_N^{(r)}(R)$ calculated by TM, according to eq. 2.23 and 2.26 for selected values of bond angle and chain lengths. The bond angles were chosen $\gamma = 20^o$ in panel (a), $\gamma = 60^o$ in panel (b), $\gamma = 90^o$ in panel (c). In each panel, the curves for chain lengths $N = 10, 25, 50, 100, 200, 400, 800$ can be identified by the location of their maxima with the smallest being at the right extreme and gradually shifting to left. All functions have been multiplied by Nb in order to ease the visual comparison, and have been calculated with mesh parameters $M_\theta = 200$ and $M_r = 400$. We estimate an accuracy of $\pm 2.5\%$ or better for these parameters, except for $N = 400, 800$ where errors may be higher. Note the shift in the location of the maxima, as we increase

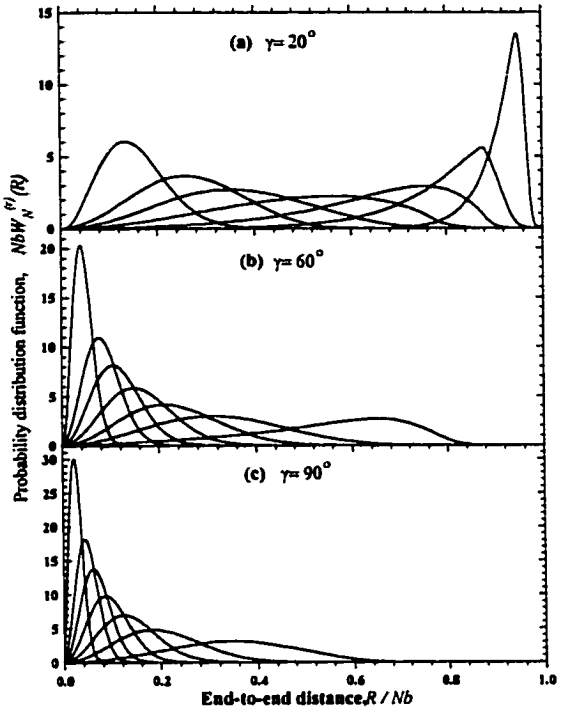

Figure 4.4: End-to-end distance distribution function $NbW_N^{(r)}(R)$, eq.2.26, for selected values of bond angle indicated on each panel and chain length $N = 10, 25, 50, 100, 200, 400, 800$, with location of maxima from right to left in this order.

the chain length, reflecting a loss in the stiffness of the chain. For instance, the chain with $N = 10$ and $\gamma = 20^o$ is extremely stiff, with the radial distribution function being significantly different from zero only for R/Nb between 0.7 and 1, while for $N = 100$, the corresponding curve becomes much wider.

In Figure 4.5 we show an attempt to fit Gaussian-type distribution function derived from eq. 3.11, $W_N^{(r)}(R) \propto R^2 W_N(\mathbf{R})$, to our results for $N = 100$, $\gamma = 20^o, 60^o, 90^o$. The parameter $\langle R^2 \rangle$ was taken according to eq. 4.4. The solid lines are our computed results and the dashed lines correspond to the Gaussian functions. The significance of this procedure is that the FRC can be looked at as a FJC (as first noted by Kuhn) with bond length a and number of bonds $N_{eff} = L/a$. For $\gamma = 20^o$ the deviation from Gaussian form is very pronounced, indicating that the chain is still very stiff, even at this length.

To facilitate a better view at the deviations of $W_N^{(r)}$ from the Gaussian shape we

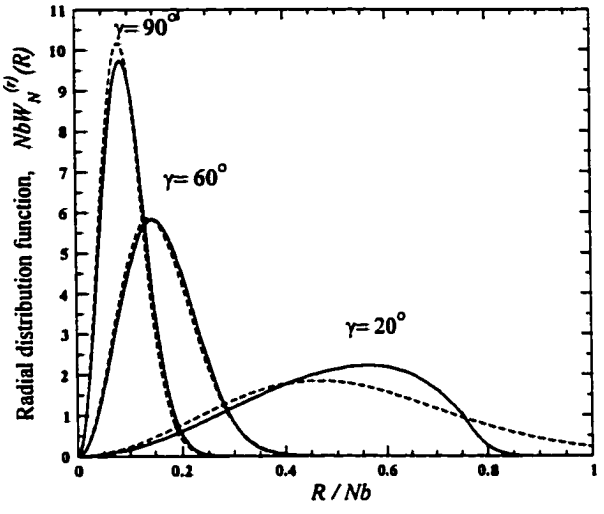

Figure 4.5: Comparison of computed radial distribution functions for $N = 100$ and $\gamma = 20^o, 60^o, 90^o$ with Gaussian-type distribution functions with the parameter $\langle R^2 \rangle$ given by eq.4.4.

plot the curves together in logarithmic axes in Figure 4.6.

Figure 4.7 displays the chain end $z-$component distribution function $W_N^{(z)}(R_z)$ calculated by eq. 2.20 and 2.27 for the indicated values of bond angle and of chain length. The curves correspond to the same chain lengths as in Figure 4.4 with maxima from bottom to top for $N = 10, 25, 50, 100$ in this order. The mesh parameters used here are $M_\theta = 200$ and $M_z = 400$, and we estimate again an accuracy of $\pm 2.5\%$ or better for all curves displayed.

Next we will use these distribution functions to determine other quantities of interest. The characteristic ratio of the FRC is calculated from the end distribution function via eq. 2.31 and compared to the exact expression, eq. 4.3. Good agreement for three values of bond angles $\gamma = 20^o, 60^o, 90^o$ can be seen in Figure 4.8. The small deviations towards large N are mainly due to discretization effects, more specifically to the value of M_r chosen, and are well within the predicted accuracy for this method.

Similarly, we calculated the mean square radius of gyration for the FRC with bond angles $\gamma = 20^o, 60^o, 90^o$ and compared it to the analytical results, eq. 4.9, in Figure 4.9. Again, we obtain good agreement between the two methods.

For the bond angles chosen above, we calculated the structure factor of the FRC

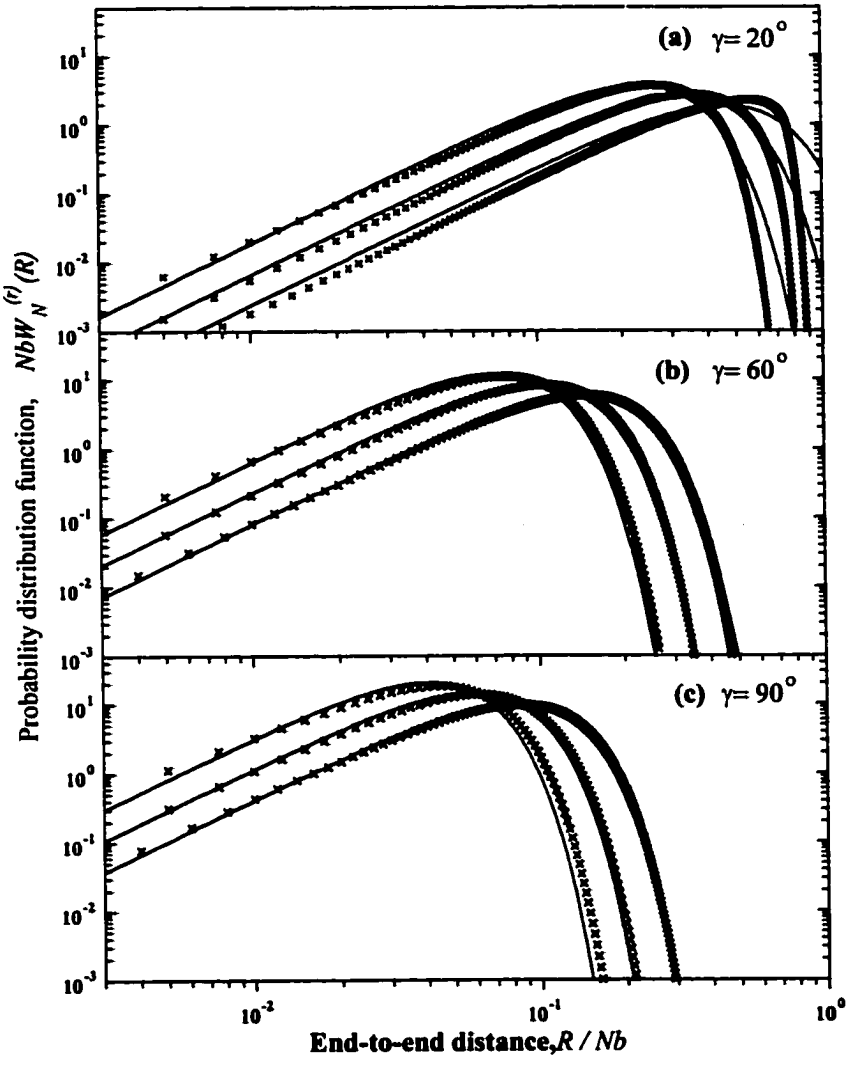

Figure 4.6: Cross symbols: end-to-end distance distribution function $NbW_N^{(r)}(R)$ in double logarithmic axes for selected values of bond angle indicated on each panel and chain length $N = 100, 200, 400$ with location of maxima from right to left in this order. Continuous lines: Gaussian distribution functions derived from eq. 3.11, with the corresponding $\langle R^2 \rangle$ from eq. 4.4.

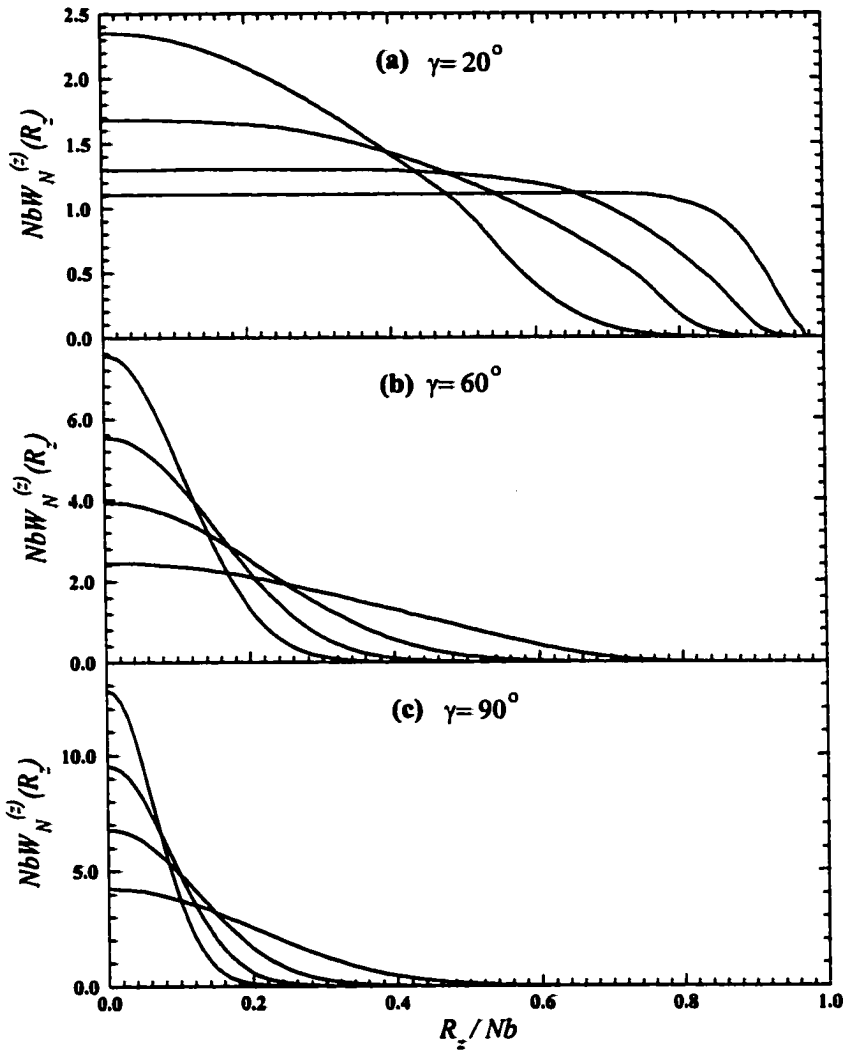

Figure 4.7: Chain end-to-end vector z–component distribution function $W_N^{(z)}(R_z)$ for selected values of bond angle γ and with chain length $N = 10, 20, 50, 100$ (with maxima from bottom to top in this order).

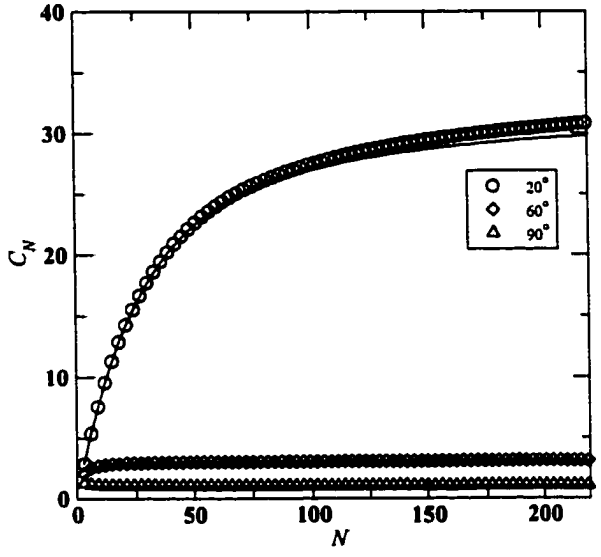

Figure 4.8: Comparison of the TM-calculated mean characteristic ratio versus chain length curves for the FRC with various bond angles indicated in the legend, with the theoretical prediction, eq. 4.3 (solid lines).

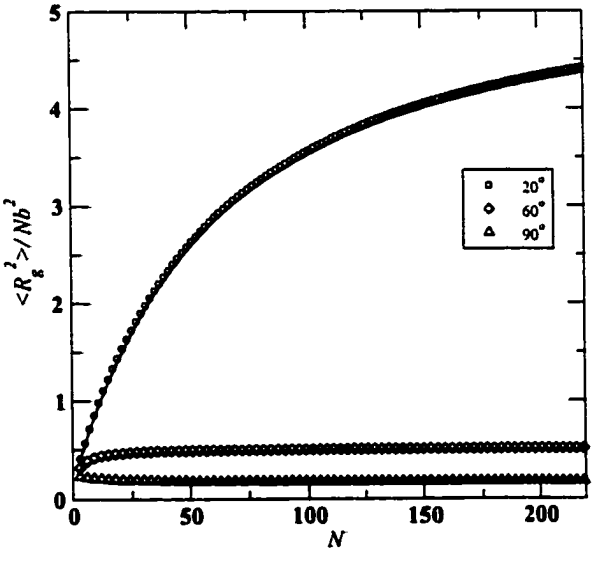

Figure 4.9: Comparison of the TM calculated mean square radius of gyration for the FRC with various bond angles indicated in the legend, with the theoretical prediction of eq.4.9 (solid lines).

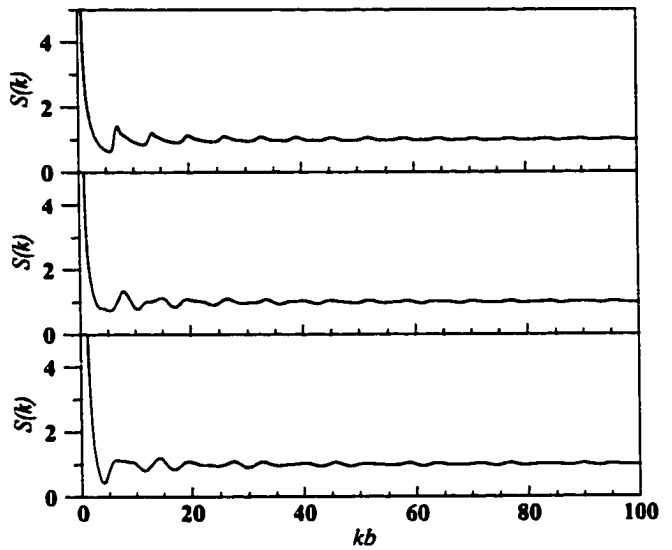

Figure 4.10: Structure factor of the FRC with $N = 10$ and bond angle $\gamma = 20^o$ in (a), $\gamma = 60^o$ in (b) and $\gamma = 90^o$ in (c) calculated by eq.1.37 and 2.32.

with eq. 1.37 and 2.32. The results for $N = 10$ can be seen in Figure 4.10. Note the variation with the bond angle in the shape of the "wavelets" appearing in the three curves. The mesh parameters $M_r = 200, M_\theta = 200$, have been found to be sufficiently large to yield results independent of them. As the bond angle decreases, one expects the peaks to sharpen about their respective locations.

A closer look at the differences between the curves in the long wavelength range is pictured in Figure 4.11, where we compare them with the structure factor of the FJC model, as calculated in the previous chapter. Different features can be seen in this k-range, dependent on the bond angle. The 90^o FRC in particular has very pronounced differences from the others, for instance at about $kb = 4$, as can be seen in the plot.

In Figure 4.12 we show a scaling analysis of the structure factor with the chain length for fixed bond angle, $\gamma = 20^o$. For this purpose, we chose the chain lengths $N = 10, 20, 30$. As expected intuitively, we see that only in the long wavelength or small scattering angle limit are the static structure factors different for the three chain lengths. As the wavelength is decreased, the curves rapidly overlap; there seems to be no difference between the curves for FRC for $kb > 1$. Again, for comparison we

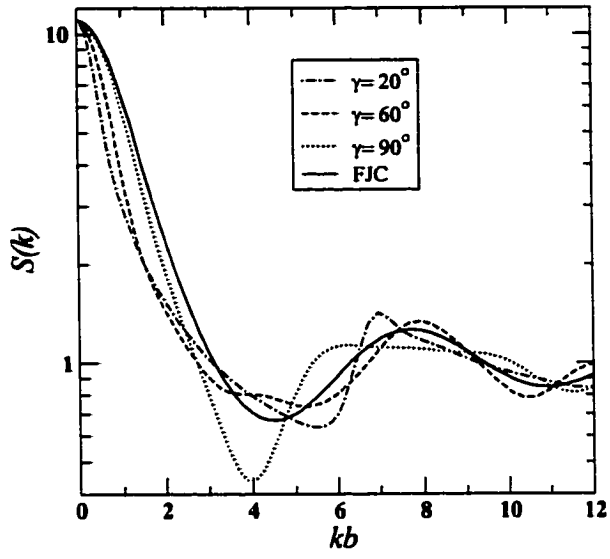

Figure 4.11: Small wavenumber details of the structure factor curves for the FRC with $N = 10$ and bond angles $\gamma = 20°$, $\gamma = 60°$ and $\gamma = 90°$ also compared with the FJC with the same length.

show the corresponding curve for the FJC.

A better view at the large-k region is obtained in Figure 4.13. The differences between the different data sets do not seem to diminish as kb increases (for short wavelengths), but the curves appear to settle down to a damped oscillatory form with a relatively slowly decaying amplitude. The location of the maxima can be approximately determined by the formula characterizing the 'classical' double slit interference pattern: $kb = 2\pi m$, $m = 0, 1, 2, ...$ We should note that the structure factor given in this region (short wavelength) does not describe any real polymer chain, but is rather an artifact of the model. At this scale, the structure of a polymer cannot be studied within a simple model like the FRC, which naively regards the monomer as the immaterial joint between two "phantom" segments.

As the bond angle is decreased, one expects to recover the limit of the rod-like polymer, which for small kb can be well approximated by the formula (see Appendix B)

$$S(k) = N \int_0^1 dx \left[\frac{\sin(Nkbx/2)}{(Nkbx/2)} \right]^2 . \tag{4.22}$$

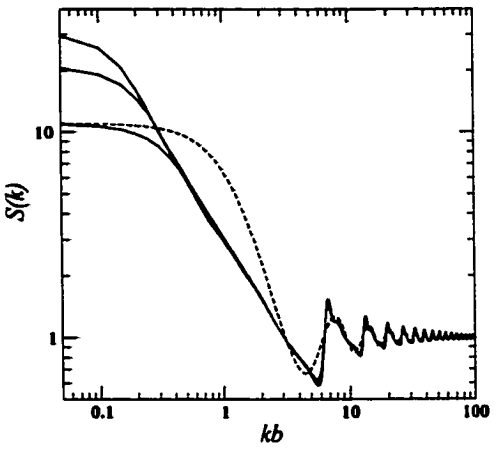

Figure 4.12: Scaling analysis of the structure factor of the FRC with N for fixed bond angle $\gamma = 20^o$, in log-log axes. Curves for $N = 10, 20, 30$ are plotted in continous line with maxima from lowest to highest in the respective order. The curve for the FJC with $N = 10$ is plotted in dashed line.

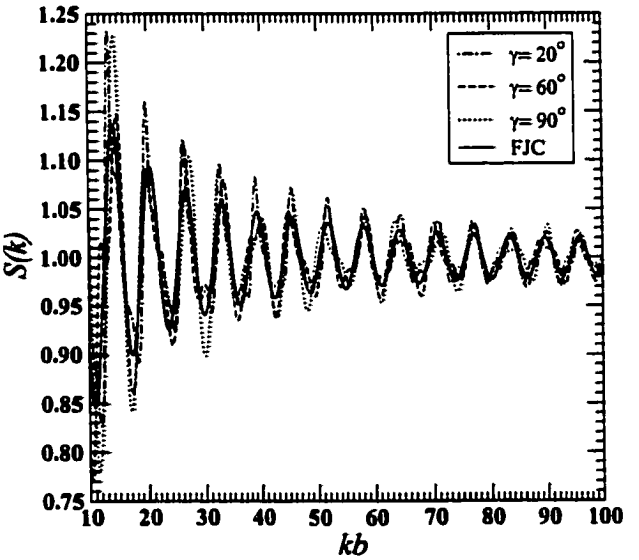

Figure 4.13: Large wavenumber details of the structure factor curves for the FRC with $N = 10$ and bond angles $\gamma = 20^o$, $\gamma = 60^o$ and $\gamma = 90^o$ also compared with the FJC with the same length.

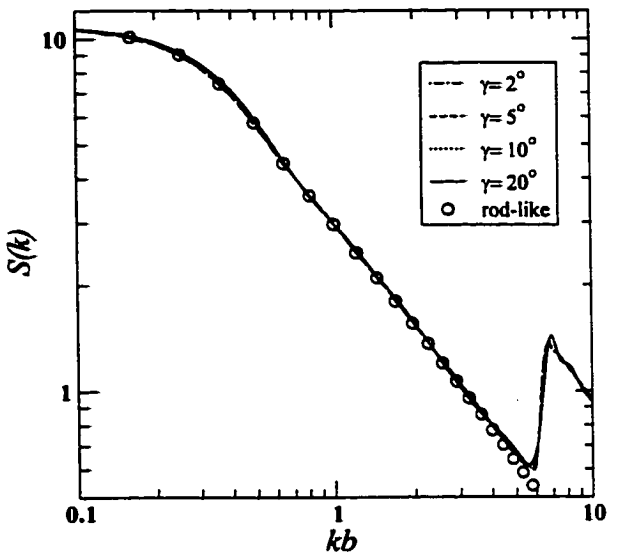

Figure 4.14: Comparison between the structure factor of FRC with bond angles given in the legend and the rod-like polymer, eq.4.22, in the small kb (long wavelength) range.

A comparison between the structure factor of FRC with small bond angles and the above expression is presented in Figure 4.14 and we see indeed excellent agreement up to the region where the oscillatory behavior begins to manifest.

4.2 Transfer Matrix for the FRC in the Gibbs Ensemble

In computing the Green function of the chain stretched by its ends by a constant external force $\mathbf{f}$ (Gibbs ensemble), we must account for a single coordinate, namely the angle, θ, formed by a bond vector with the direction of the external force (thus $\Gamma = \theta$). Since there are no interactions, the integral equation for the Green function in the Gibbs ensemble reads

$$G_{i+1}^{(f)}(\theta) = e^{fb\cos(\theta)/k_BT} \int d\theta' G_i^{(f)}(\theta') \mathbf{T}^{(f)}(\theta, \theta') \tag{4.23}$$

In Figure 4.15, we depict the relevant geometrical configuration of two chain segments for this situation. The transfer matrix in this case is

$$\mathbf{T}^{(f)}(\theta, \theta') = \int_0^{2\pi} d\phi \delta[\theta' - g_\theta(\theta, \phi)], \tag{4.24}$$

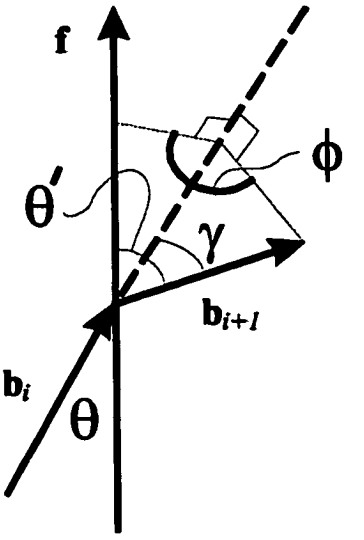

Figure 4.15: Relevant coordinates for a sequence of two adjacent bonds vectors of FRC with respect to an external force **f**.

where the ϕ is the dihedral angle between the planes $(\mathbf{f}, \mathbf{b}_i)$ and $(\mathbf{b}_i, \mathbf{b}_{i+1})$ and the function g_θ characterizes the geometrical restriction of the consecutive chain segments and is given by eq. 4.15. The initial condition for this problem is

$$G_1^{(f)}(\theta) \propto \exp\left(\frac{fb\cos\theta}{k_B T}\right)\sin\theta. \tag{4.25}$$

4.2.1 Results and Discussion

Since the stretching behavior of the FRC is of major interest, being a first step to the theoretical study of real polymer stretching, we have focused in great detail on the Gibbs ensemble for this model. In order to optimize our computation method, we performed the entire procedure for various parameters M_θ, M_r and compared the results. In all cases, we found that results converge practically to the continuous limit for values of the mesh parameters no higher than a few hundreds.

The variation of the probability distribution function of the orientation of the last chain bond, $G_N^{(f)}(\theta)$, with respect to the direction of the external force under increasing forces is shown in Figure 4.16 for chains with $N = 100$ and $\gamma = 20^o, 60^o, 90^o$ respectively in panels (a), (b), (c). All curves are normalized to an undergraph area

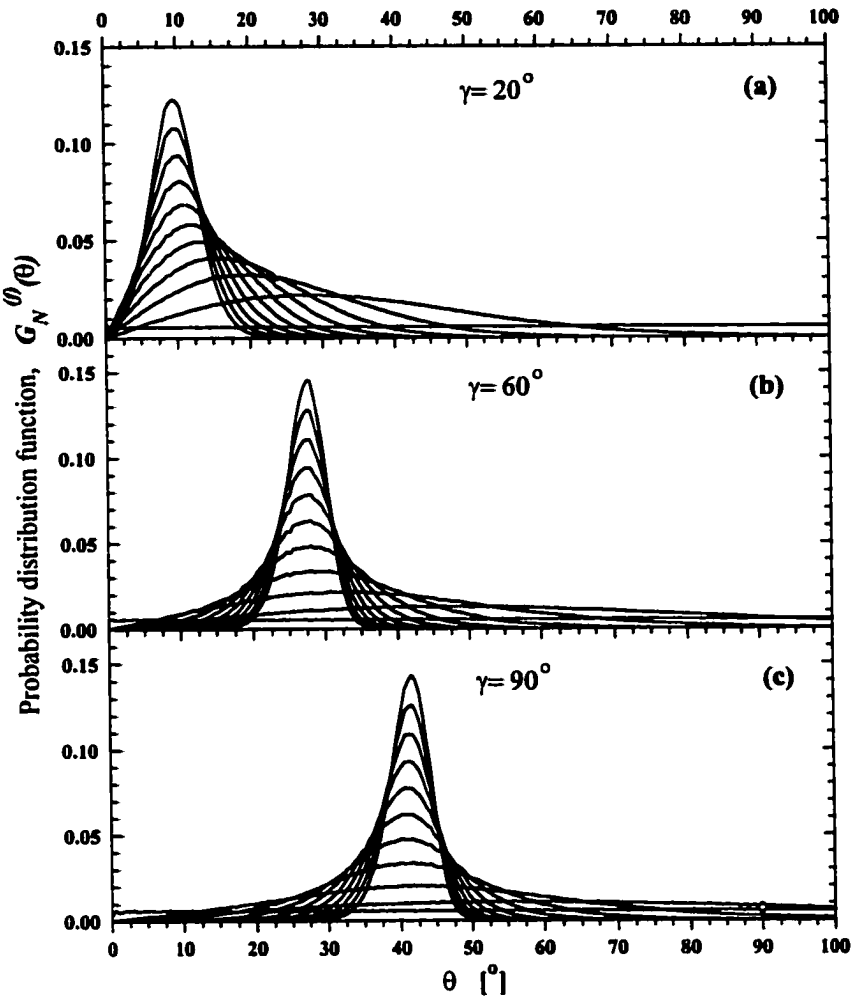

Figure 4.16: The probability distribution function of the orientation of the end chain bond with respect to the direction of the external force for chains with $N = 100$ and (a) $\gamma = 20^o$, (b) $\gamma = 60^o$, (c) $\gamma = 90^o$. The force values are $fb/k_BT = \{0, 1, 4, 9, 16, 25, 36, 49, 64, 81, 100\}$ corresponding in this order to curves from the flattest to sharpest in each panel. The mesh parameter for all cases is $M_\theta = 500$.

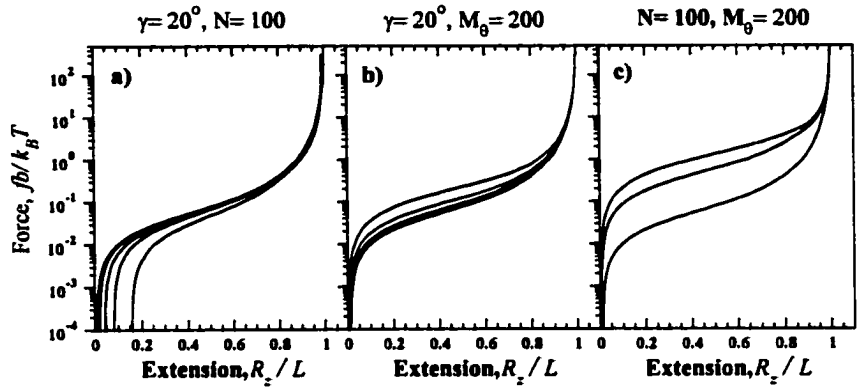

Figure 4.17: (a) Dependence of the force-extension curve on the mesh parameter M_θ, for fixed chain length and bond angle, $N = 100$, $\gamma = 20^o$. From bottom to top curves are for the values $M_\theta = 10, 20, 40, 100, 200$. (b) Dependence of the force-extension curve on the chain length at constant bond angle $\gamma = 20^o$ and mesh parameter $M_\theta = 200$. From top to bottom curves are for the values $N = 10, 25, 50, 100$. (c) Variation of the force-extension curve with the bond angle at constant chain length $N = 100$ and mesh parameter $M_\theta = 200$. From bottom to top curves are for $\gamma = 20^o, 60^o, 90^o$.

of one. The mesh parameter is fixed to $M_\theta = 500$. The force values have been chosen rather arbitrarily to follow a parabolic form: $fb/k_BT = n^2$, with $n = 0, 1, 2, ..., 10$, corresponding in this order to curves from the flattest to sharpest in each panel. For better visualization of the region of maximum interest, we show only the angular range $[0^o, 100^o]$. Note the almost constant increase in the maxima, accompanied by a decrease in the width of the curves as the force increases. At large forces, a sharp peak forms in $G_N(\theta_N)$, with the θ_N value close to $\gamma/2$ — the most probable orientation as is intuitively expected for strongly stretched chains. This value however is only asymptotically approached.

In Figure 4.17 we present a scaling analysis of the force-extension relation with respect to all the model parameters γ, N and the number of angular mesh points M_θ. In panel (a), we show the results of a scaling analysis of the force-extension curve with the mesh parameter M_θ, for fixed chain length $N = 100$, and bond angle, $\gamma = 20^o$. From bottom to top curves are for the values $M_\theta = 10, 20, 40, 100, 200$. For better visualization of the differences between the curves at small forces, we chose a logarithmic axis for the force. This is also a means of determining the accuracy of our method for a given number of mesh points. The curves practically overlap for

values of M_θ greater than 200, a trend that can be noticed already in the closeness of the curves with $M_\theta = 100$ and $M_\theta = 200$. In panel (b), we can see the variation of the stretching curve with the chain length. From top to bottom curves are for the values $N = 10, 25, 50, 100$. The important differences appear for force values ranging from 10^{-3} to 1. Again, the behavior of the force-extension curves is characterized by a limit — all curves tend to overlap for chain lengths larger than 100. Finally, in panel (c), we see the modification of force-extension curves for constant chain length $N = 100$ and mesh parameter $M_\theta = 200$, when the bond angle has various values. From bottom to top curves are for $\gamma = 20^o, 60^o, 90^o$.

We should note that these and all subsequent findings on the force-extension curve have been obtained by using eq. 2.13, which was found to yield the most accurate results.

In Figure 4.18 we present a scaling analysis of the force-extension curve in the form $(1-R_z/L)^{-1}$ versus fb/k_BT plotted in logarithmic axes with the mesh parameter M_θ in the long chain limit. The chain length is $N = 1000$. The force has been varied by about four orders of magnitude, in order to have a comprehensive picture of the behavior. In panel (a) we display the results for large values of bond angle $\gamma = \{30^o,$ $50^o,$ $70^o,$ $90^o\}$ (corresponding to curves from top to bottom in this order), while in panel (b) the curves for small bond angles are shown, $\gamma = 1^o, 5^o, 10^o, 20^o$. Note that the results for $M_\theta = 200$ and $M_\theta = 400$ are almost indistinguishable, which means a high accuracy reached at this point.

We have now enough data to make a comparison between the FRC model and other simple models, such as FJC and WLC. The Langevin function (eq. 3.5) is displayed for comparison in Figure 4.18(a) as a continuous line. Note that in the large-force regime, all the curves in this panel are practically parallel to the Langevin curve, that is their slope is very close to 1. In fact the curve $(1-R_z/L)^{-1} = 2fb/k_BT$, thick dashed line in both panels, gives a very good fit to our large-force results. On the other hand, for small bond angles, we expect the behavior of the FRC to be rather similar to the one of the WLC model. Therefore, we plotted in Figure 4.18(b) straight lines representing the large-force behavior of the latter, given by eq. 4.13, having the same persistence lengths as the FRC with the bond angles appearing here (eq. 4.11).

Figure 4.19 presents the $(1-R_z/L)^{-1}$ versus fb/k_BT curves in a double logarithmic plot for bond angles $\gamma = 1^o$ in (a), $\gamma = 5^o$ in (b), $\gamma = 10^o$ in (c), and $\gamma = 20^o$ in

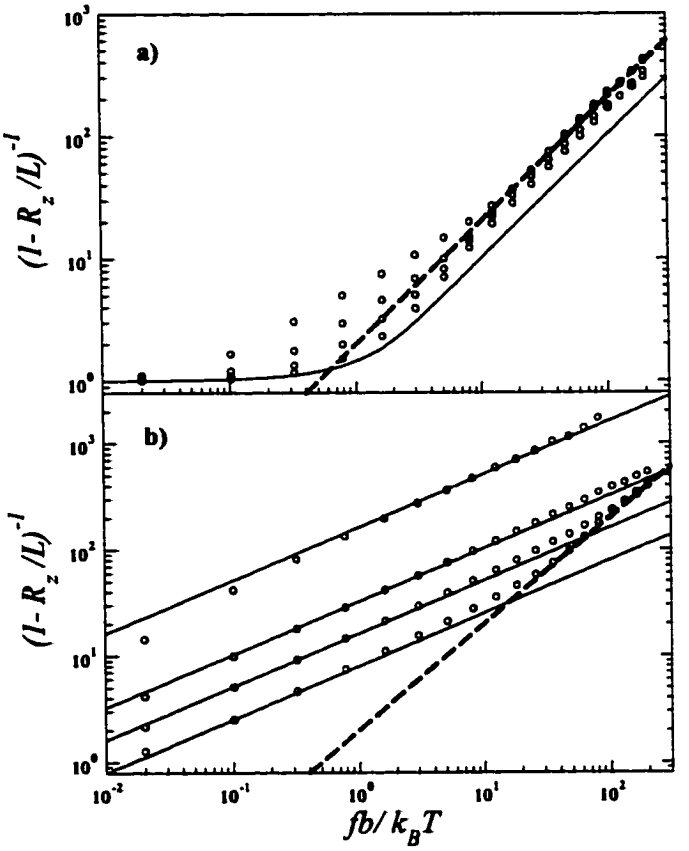

Figure 4.18: (a) Modified form of the force-extension relation in logarithmic axes for large chain length ($N = 1000$) and for large values of bond angle $\gamma = \{30^o, 50^o, 70^o, 90^o\}$ (corresponding to curves from top to bottom in this order). The Langevin function, eq. 3.5, for the FJC is shown for comparison in continuous line, while the curve $(1 - R_z/L)^{-1} = 2fb/k_BT$ is drawn as a thick dashed line. (b) Same as (a), but for small values of bond angle $\gamma = \{1^o, 5^o, 10^o, 20^o\}$ (from top to bottom). For comparison, we show in continuous lines the corresponding analytical result for strong stretching regime of WLC, eq. 4.13 with the persistence length given by eq. 4.11

(d). The chain lengths are $N = 10, 100, 1000, 2000$ and the mesh parameter was set to 1000.

The quantity $(R_z/Nb)(\ fb/k_BT)^{-1}$ as a function of the force for FRC is found to be constant for small forces $\frac{fb}{k_BT} \ll 1$. Figure 4.20 displays our data for various bond angles and for chain lengths 100, 200, 400 and 2000 (from top to bottom). The only important deviation from constant behavior appears for $\gamma = 1^o$. The values for $f = 0$ are obtained by simple linear extrapolation of the nearest two points. The exact same results were obtained by numerically computing the derivative of force-extension curve with respect to f.

Since we know from eq. 1.16 and 4.8 that in the infinite chain limit, $N \to \infty$, the slope of the curve R_z/Nb versus fb/k_BT is $\frac{(1+\cos\gamma)}{3(1-\cos\gamma)}$, it would be relevant to compare this result with the zero-force points extracted from data in Figure 4.20. This is displayed in Figure 4.21. All data sets overlap for bond angles larger than 30^o and coincide also with the theoretical curve (continuous line). These functions strongly diverge when the bond angle is decreased, a trend that can be seen in the figure for the values of γ spanning from 1^o to 30^o. For increasing chain length we recover the predicted curve for $N \to \infty$, plotted as a continuous line. We see that for $N = 2000$ significant deviations from the infinite chain limit appear only for $\gamma < 5^o$.

It is useful to parametrize the stretching behavior of the FRC model in the long chain limit in terms of analytical expressions in the small-force regime ($\frac{fb}{k_BT} < \frac{b}{l_P}$). For comparison we use eq. 1.16 with the corresponding effective length in eq. 4.8. The agreement (see Figure 4.22) is good for all $\gamma > 10^o$ for chain length $N = 1000$. To obtain good agreement for smaller bond angles, one has to go to chains longer by at least an order of magnitude. This appears from the fact that for the limit of long chains to be approached, the contour length has to be much larger that the persistence length, the latter increasing asymptotically as $\gamma \to 0^o$.

Next, we analyze the intermediate force regime, $\frac{b}{l_P} < \frac{fb}{k_BT} < \frac{l_P}{b}$. Figure 4.23 depicts the comparison of our computations with the asymptotic WLC behavior, eq. 4.13. The corresponding persistence lengths for the bond angles appearing here is given by eq. 4.11.

Finally, the large force behavior is shown in Figure 4.24 to be approximately of the form

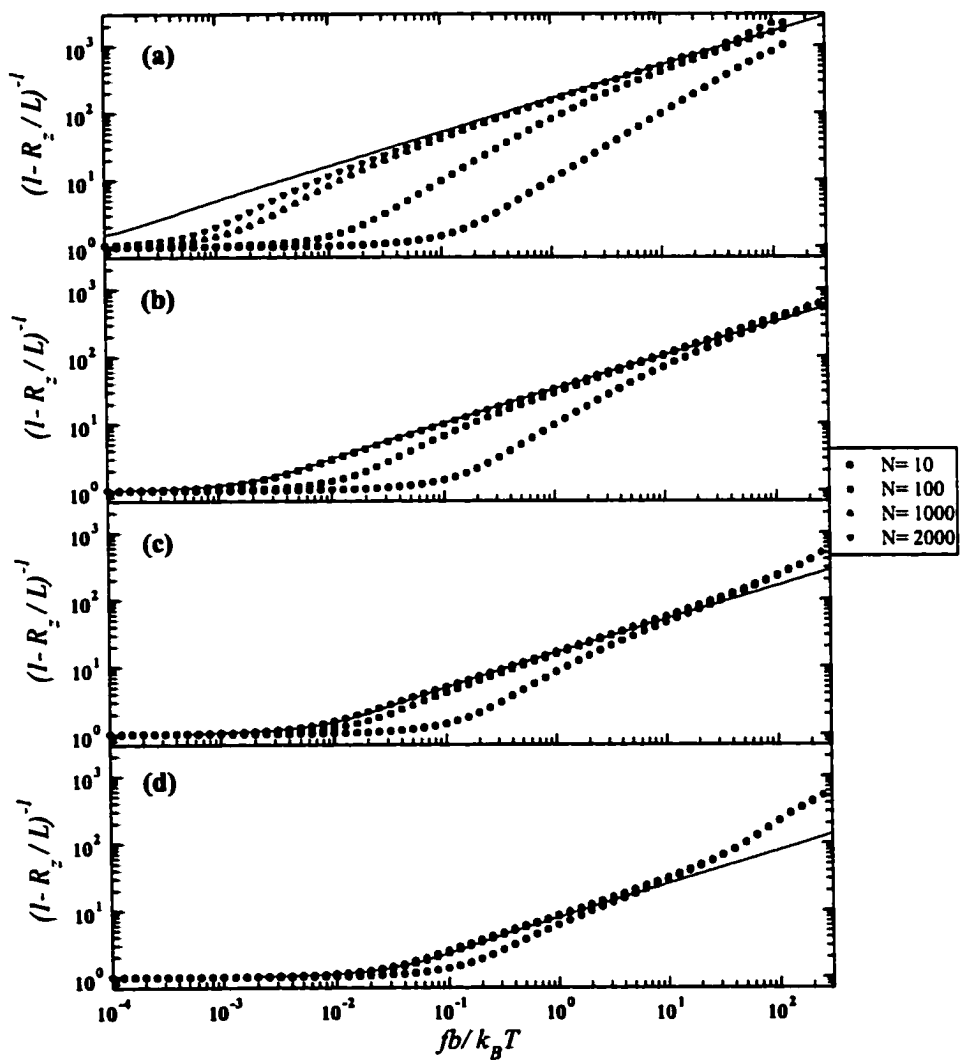

Figure 4.19: Scaling analysis of the force-extension relation with the chain length for small bond angles. The mesh parameter M_θ is maintained to a high value of 1000. The four panels correspond from top to bottom to: (a) $\gamma = 1^o$, (b) $\gamma = 5^o$, (c) $\gamma = 10^o$, (d) $\gamma = 20^o$. Curves for various chain lengths are plotted in different symbols indicated in the legend.

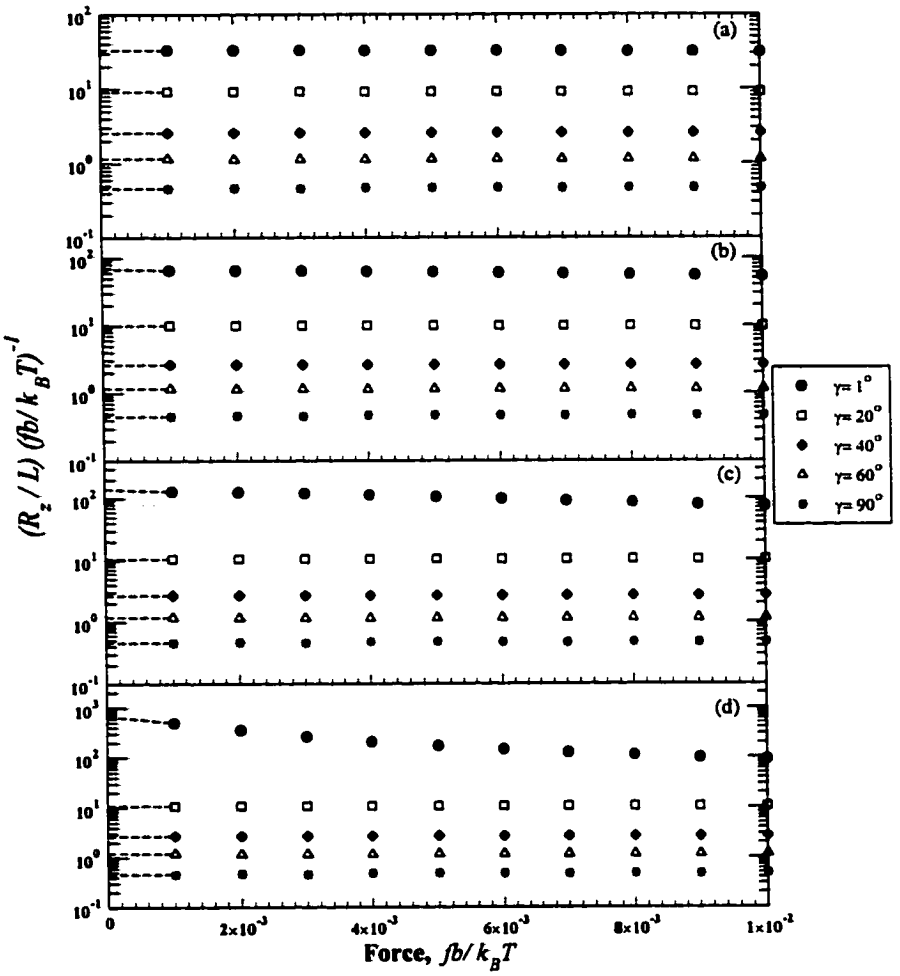

Figure 4.20: Study of the force-extension curves in the small-force regime. The slope of the force-extension curve, $(R_z/Nb)(fb/k_BT)^{-1}$, is plotted as a function of the force. Few representative bond angles have been chosen (indicated in the legend) and the chain length has been increased from top to bottom (a) $N = 100$, (b) $N = 200$, (b) $N = 400$, (d) $N = 2000$. The values of the intercept at zero force is shown in dashed line and is obtained by a linear extrapolation of the nearest two points.

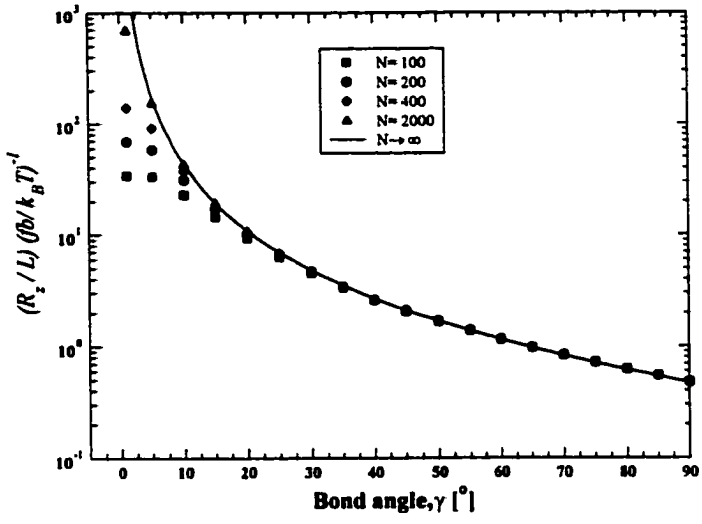

Figure 4.21: Slope of the graph R_z/Nb vs. fb/k_BT in the limit of zero force as a function of bond angle for increasing chain lengths, specified in the legend. The slope values are taken from data displayed in Figure 4.20. The analytical result (continuous line) for N $\rightarrow$ ∞, derived from eq. 1.16 and 4.8, is displayed for comparison.

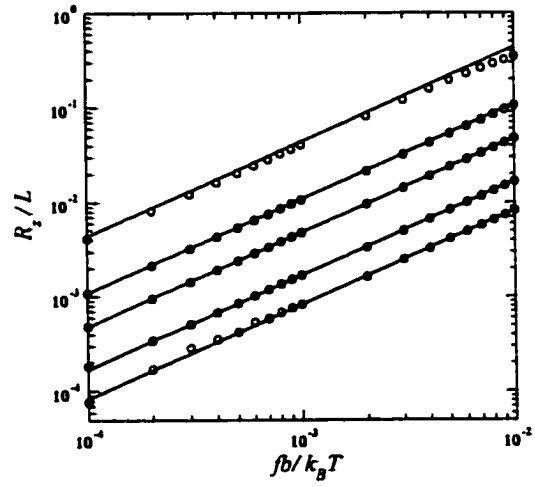

Figure 4.22: Small force fit of the force-extension curve for FRC in the long chain limit ($N = 1000$). The circular symbols represent computation results and the continuous curves are given by eq.1.16 From top to bottom $\gamma = \{10^o, 20^o, 30^o, 50^o, 70^o\}$.

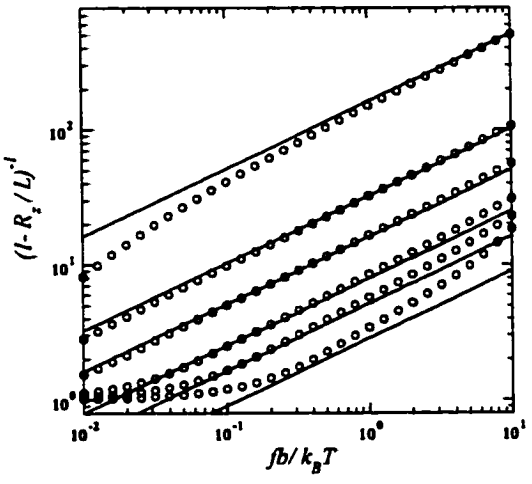

Figure 4.23: Intermediate force fit of the force-extension curve for FRC in the long chain limit ($N = 1000$). The circular symbols represent computation results and the continuous curves are given by eq.4.13. From top to bottom $\gamma = \{1^o, 5^o, 10^o, 20^o, 30^o, 50^o\}$.

$$(1 - R_z/L)^{-1} = 2fb/k_BT. \tag{4.26}$$

To summarize, the stretching of the FRC model can well be described by the following formulae

$$\frac{R_z}{L} \simeq \begin{cases} \frac{fa}{3k_BT} & \text{for } \frac{fb}{k_BT} < \frac{b}{l_P} \\ 1 - \left(\frac{fl_P}{4k_BT}\right)^{-1/2} & \text{for } \frac{b}{l_P} < \frac{fb}{k_BT} < \frac{l_P}{b} \\ 1 - \left(\frac{fl_P}{2k_BT}\right)^{-1} & \text{for } \frac{l_P}{b} < \frac{fb}{k_BT}. \end{cases} \tag{4.27}$$

At this point we are in the position to derive a formula that accurately describes the stretching of the FRC in the long chain limit for any force. In order to retain the small force and large force behavior we fit the force-extension curve by a relation of the form

$$(1 - R_z/L)^{-1} = \left\{[\mathcal{F}_{WLC}(fb/k_BT)]^\beta + [2fb/k_BT)]^\beta\right\}^{1/\beta}, \tag{4.28}$$

where β is a fitting coefficient and $\mathcal{F}_{WLC}(fb/k_BT)$ is the function that characterizes the WLC model, according to eq. 4.12. We find that $\beta = 2$ gives an acceptably good fit for all curves with bond angles between 5^o and 70^o as illustrated in Figure 4.25.

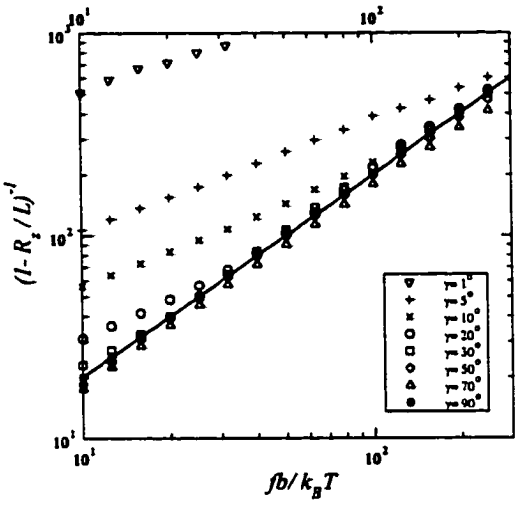

Figure 4.24: Large force fit of the force-extension curve for FRC in the long chain limit ($N = 1000$). The circular symbols represent computation results, while the continuous curve is given by $(1-R_z/L)^{-1} = 2fb/k_BT$. From top to bottom $\gamma = 1^o, 5^o, 10^o, 20^o, 30^o, 50^o, 70^o, 90^o$.

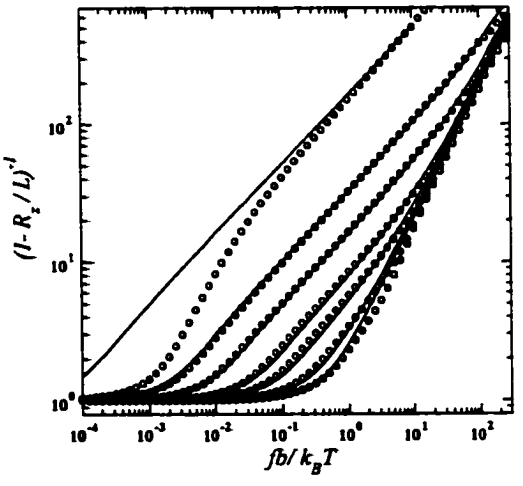

Figure 4.25: Global fit of the force-extension curve for FRC in the long chain limit ($N = 1000$). The circular symbols represent computation results, while the continuous curves are given by formula 4.28 with $\beta = 2$. From top to bottom $\gamma = \{1^o, 5^o, 10^o, 20^o, 30^o, 50^o, 70^o\}$.

4.3 Conclusion

In this chapter we studied the FRC model by transfer matrix techniques in both the Helmholtz and Gibbs ensembles. In the canonical ensemble, we calculated chain end distribution function and the related quantities and compared them to the analytical predictions for the FRC, as well as with other classical models. As expected, chain end distribution functions were found to almost overlap appropriate Gaussian curves for long polymers, but they strongly deviate from the latter for short chains — more so than the FJC model. The role of the bond angle was analyzed in detail.

The stretching of the FRC was investigated by carrying out the statistical mechanics in the Gibbs ensemble. The force-extension curves were calculated with high precision. Under weak forces, the FRC obeys the Gaussian stretching law. As the force is increased a FRC with small bond angle and large N closely resembles the semi-flexible chain model. We base this statement on the results displayed in Figures 4.18 to 4.25.

We found that for even larger forces, the FRC will cross over to a new type of behavior, where the scaling behavior is that of a discrete-chain (DC)[25] characterized by a response similar, but not identical, to the large-force response of the FJC. This can be understood as a result of a force-induced decoupling between adjacent chain segments. This finding should have important consequences from an experimental point of view for fitting the large-force stretching data of polymers. At a force larger than $fb/k_BT \sim l_P/b$, one enters the DC regime, in which the stretching is described by $R_z/L \simeq 1-(cbf/k_BT)^{-1}$ replacing the WLC behavior observed for smaller forces, $R_z/L \simeq 1-(4l_Pf/k_BT)^{-1/2}$. The constant c is sensitive to the details of the molecular structure and, to anticipate the following chapters, to the intrachain interactions. Its determination for a particular model emerges as one of the results of a TM treatment of the type performed herein for the FRC model.

As noted in a recent study[25], the differences in the stretching behavior with respect to the WLC are attributable to the chain fluctuations probing progressively smaller length scales as the force is increased. A typical value for the crossover force is $100pN$, which is in the region of much interest, for instance, in a single chain AFM experiment[6]. This more than justifies proposing a new fitting formula for the stretching of polymer, having as a starting point the exact calculations on the FRC

presented in this chapter.

CHAPTER 5

TRANSFER MATRIX METHOD FOR THE STUDY OF *N*-ALKANES

Up until now, we dealt with relatively simple polymer models, whose energy is independent of the chain conformation. There is no energy difference and no interaction between any chosen pair of chain monomers. This is definitively not the case for real polymer chains. In this chapter we will develop a realistic model that includes relevant geometric and energy details.

The variation of dihedral angles in real polymers is always accompanied by a variation in the potential energy associated with that particular conformer. Often, this rotation potential has the shape depicted in Figure 1.2. While some values of the rotational angles, like the potential minima t, g^+, g^- are favoured, the continuous variation as a function of the dihedral angle should be incorporated for an accurate description. If the situation requires, one should also account for short-ranged interactions between monomers two or more bonds apart along the chain.

As a case study for real polymers, we have chosen n-alkanes as the simplest hydrocarbon chain where we can account the rotational potential energy variation associated with the dihedral angles. The chemical structure is given by the general formula $CH_3\,[-CH_2]_n - CH_3$, with the monomer being $[-CH_2]$. Below we give a few classical considerations on the statistical mechanics of such a system.

5.1 Polymer Chains with Rotational Potentials

As we have mentioned above, a step further towards describing real polymer molecules is made if we associate more or less realistic potentials with the variation of the dihedral angles, $E_i(\varphi_i)$, firstly mentioned in the introductory chapter. Since for most real polymers, each bond has a three-fold rotational potential, we can assume that this potential curve has the shape presented in Figure 1.2, with the appropriate

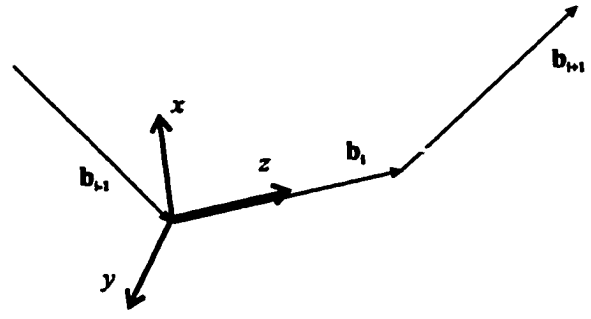

Figure 5.1: Local reference frame for bond i, defined with the help of bond $(i-1)$.

Fourier coefficients. In contrast, the RIS approximation simplistically samples the potential curve by considering only its minima and neglecting the remaining details of the curve. In other words, only three rotational angles, $\varphi_t, \varphi_{g+}, \varphi_{g-}$, are allowed for each chain bond.

If continuous rotational potentials are assumed and there is no interaction between non-bonded monomers, the individual partition function of adjacent bonds will be independent of each other. The probability that the rotational angle φ_i falls within the interval $[\varphi_i, \varphi_i + \mathrm{d}\varphi_i]$, is given by the Boltzmann factor

$$p(\varphi_i)\mathrm{d}\varphi_i = \frac{1}{z_i}\mathrm{e}^{-\beta E_i(\varphi_i)}\mathrm{d}\varphi_i \tag{5.1}$$

where z_i is the bond partition function given by

$$z_i = \int_0^{2\pi} \mathrm{d}\varphi_i \mathrm{e}^{-\beta E_i(\varphi_i)}. \tag{5.2}$$

One can choose[7], as shown in Figure 5.1, a local orthogonal frame for each bond i, with the z-axis along the direction of the bond vector and y-axis in the plane $(\mathbf{b}_i, \mathbf{b}_{i-1})$, such that the y–component of $\mathbf{b}_{i-1}$ is negative. The rotational angle φ_i is the dihedral angle formed by the plane $(\mathbf{b}_{i+1}, \mathbf{b}_i)$ with the plane $(\mathbf{b}_i, \mathbf{b}_{i-1})$ with the positive sign given by the clockwise direction about $\mathbf{b}_i$. Within this convention, the rotational angle corresponding to the *trans* conformation is $\varphi_t = 180^o$, while the *gauche* angles will have values about 70^o and 290^o.

With this choice of coordinates, any bond vector in its own reference frame will

have the components

$$\mathbf{b}_i = \begin{bmatrix} 0 \\ 0 \\ b \end{bmatrix}. \tag{5.3}$$

The rotational matrix associated with the i-th bond vector is defined as

$$\mathbf{t}_i = \begin{bmatrix} \cos\varphi_i & -\sin\varphi_i\cos\gamma & \sin\varphi_i\sin\gamma \\ \sin\varphi_i & \cos\varphi_i\cos\gamma & -\cos\varphi_i\sin\gamma \\ 0 & \sin\gamma & \cos\gamma \end{bmatrix}. \tag{5.4}$$

The components of the i-th bond vector in the frame of the bond $(i-1)$ are related by

$$\begin{bmatrix} (b_i)_{x,i-1} \\ (b_i)_{y,i-1} \\ (b_i)_{z,i-1} \end{bmatrix} = \mathbf{t}_{i-1} \begin{bmatrix} (b_i)_{x,i} \\ (b_i)_{y,i} \\ (b_i)_{z,i} \end{bmatrix}, \tag{5.5}$$

and thus the components of the i-th bond $\mathbf{b}_i$ vector in the frame of the first bond vector are

$$\begin{bmatrix} (b_i)_{x,1} \\ (b_i)_{y,1} \\ (b_i)_{z,1} \end{bmatrix} = \mathbf{t}_1\mathbf{t}_2...\mathbf{t}_{i-1} \begin{bmatrix} (b_i)_{x,i} \\ (b_i)_{y,i} \\ (b_i)_{z,i} \end{bmatrix}. \tag{5.6}$$

Then one can, by successive multiplications and summations of matrices of this type, calculate the end-to-end vector of FRC in any configuration according to

$$\mathbf{r}_N(\varphi_1, \varphi_2, ..., \varphi_N) = \sum_{i=1,N} \mathbf{b}_i = \sum_{i=1,N} \left\{ \mathbf{t}_1\mathbf{t}_2...\mathbf{t}_{i-1} \begin{bmatrix} 0 \\ 0 \\ b \end{bmatrix} \right\}. \tag{5.7}$$

Since we assume that the rotational potentials for adjacent bonds are independent of one another, the configurational energy of the whole chain, $U_N(\varphi_1, \varphi_2, ..., \varphi_N)$, can be separated as the sum of all bond potentials

$$U_N(\varphi_1, \varphi_2, ..., \varphi_N) = \sum_{i=2,N-1} E_i(\varphi_i). \tag{5.8}$$

This implies that the average of a product like the one in eq. 5.6 can be separated as a product of averages

$$\langle \mathbf{t}_1 \mathbf{t}_2 ... \mathbf{t}_{i-1} \rangle = \langle \mathbf{t}_1 \rangle \langle \mathbf{t}_2 \rangle ... \langle \mathbf{t}_{i-1} \rangle , \tag{5.9}$$

where

$$\langle \mathbf{t}_i \rangle = \frac{1}{z_i} \int_0^{2\pi} \mathrm{d}\varphi_i \mathbf{t}_i \mathrm{e}^{-\beta E_i(\varphi_i)} = \begin{bmatrix} \langle \cos\varphi_i \rangle & -\langle \sin\varphi_i \rangle \cos\gamma & \langle \sin\varphi_i \rangle \sin\gamma \\ \langle \sin\varphi_i \rangle & \langle \cos\varphi_i \rangle \cos\gamma & -\langle \cos\varphi_i \rangle \sin\gamma \\ 0 & \sin\gamma & \cos\gamma \end{bmatrix}, \tag{5.10}$$

$$\langle \cos\varphi_i \rangle = \frac{1}{z_i} \int_0^{2\pi} \mathrm{d}\varphi_i \cos\varphi_i \mathrm{e}^{-\beta E_i(\varphi_i)}, \tag{5.11}$$

and

$$\langle \sin\varphi_i \rangle = \frac{1}{z_i} \int_0^{2\pi} \mathrm{d}\varphi_i \sin\varphi_i \mathrm{e}^{-\beta E_i(\varphi_i)}. \tag{5.12}$$

If the potential $E_i(\varphi_i)$ is a symmetrical function with respect to the *trans* angular position (like the one in Figure 1.2), we can further simplify the problem by noting that $\langle \sin\varphi_i \rangle = 0$. In addition, if we assume that all bonds are identical, the characteristic ratio in the infinite chain limit reads[2]

$$C_\infty = \frac{(1+\cos\gamma)(1+\langle\cos\varphi\rangle)}{(1-\cos\gamma)(1-\langle\cos\varphi\rangle)}. \tag{5.13}$$

This relation recovers eq. 4.5 for the FRC, as the particular case when the rotational potential is a constant function and $\langle \cos\varphi \rangle = 0$ (i.e. free rotation). In the more complicated case of an arbitrary shape of the rotational potential, exact calculation of the characteristic ratio and the mean square radius of gyration can be carried out[2] by diagonalization of the matrix $\langle \mathbf{t}_i \rangle$ but the details of this approach will not be discussed here.

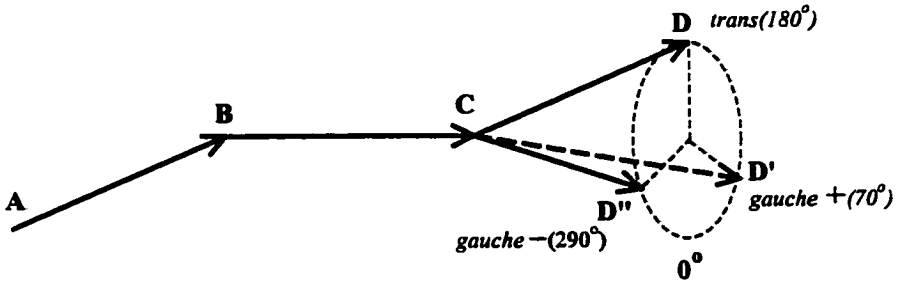

Figure 5.2: The allowed positions of a bond in the RIS model: *trans* (CD), *gauche* $+$ (CD'), *gauche* $-$ (CD'') .

5.2 The RIS Approximation for N-Alkanes

The presence of the intrachain "non-bonded" interactions introduces additional difficulties of dealing with the statistical treatment of polymer chains. In order to overcome these difficulties, some simplifications are required to the problem. A widely accepted scheme of approximations is the Rotational Isomeric State model[3]. It combines a realistic description of the detailed structure of polymer chains with an accurate statistical treatment. In brief, the RIS model assumes a discrete set of rotational angles, three in most cases, ordinarily chosen as the local potential minima, and keeps bond lengths and angles fixed. This approximation accounts for the statistical weights of various bond conformations and for the interactions between neighboring bonds.

In most cases, the rotational potential associated with a bond has three minima, therefore the RIS model will allow three distinct states for that bond. The basic geometrical configuration of a RIS chain is depicted in Figure 5.2. Here we have a sequence of three bonds, among which AB and BC are fixed in the plane of the figure. The last bond is allowed to be only in three positions labeled *trans* (CD), *gauche* $+(CD')$ and *gauche* $-$ (CD''), corresponding to values of dihedral angles $180^o, 70^o$ and 290^o respectively. The *trans* conformation is perfectly aligned in the plane of the figure and is the maximally stretched one, while the *gauche* $+$ and $-$ are out of that plane (behind and above respectively).

In the pioneering work of Lifson[64] and Nagai[63] a statistical theory was developed to study the average dimensions of n-alkanes as well as of other types of linear

polymer. This exact theory is based on the statistical matrix method first proposed by Eyring[31] and has the merit of rigorously taking into account first and second neighbor interactions. Unfortunately, the method is limited to the study of unperturbed chains and cannot be used to obtain quantities like the end-to-end distribution or force-extension curves.

Starting from the statistical weight matrix in the RIS approximation, it is in principle possible to construct various matrices for calculating any statistical properties of polymer coils. Unfortunately, for a polymer chain in an external field this approach becomes impractical. A theory for calculating the distribution of rotational states as a function of extension has been given by Abe and Flory[15] for n-alkane chains with nearest neighbor interactions. However, this method is applicable only for small to moderate degrees of stretching and fails to give insight into the highly stretched polymer regime.

More recent developments in the study the RIS model are mainly based on Monte-Carlo (MC) computer simulations. The RIS Metropolis Monte-Carlo (RMMC) model[65, 66, 67] was used to calculate the conformational and orientational behavior of poly(ethylene terephthalate). The effect of the short-ranged interactions on the end-to-end distance distribution and average fractions of various rotational states and bond orientations were obtained as functions of end-to-end distance. Monte-Carlo simulations on a tetrahedral lattice[68] with short-ranged interactions along the chain and also with volume interactions (solvent effect) were employed to produce end vector distribution functions, Helmholtz free energy and force-extension curves for various solvency and flexibility conditions. A high-coordination lattice model[69] based on the RIS approximation was the base for Monte-Carlo simulations for studying polythiaethylene[70] and polypropylene[71]. This model makes use of statistical weight matrices for dealing with short-ranged interactions while taking the energy and geometrical (bond lengths, angles and rotational angles) parameters from the existing literature in order to calculate characteristic ratios, dipole moments and orientational correlation functions.

A mixed scheme[72], combining the so-called Polymer Reference Interaction Site Model and various approximations for the chain segment correlation function was designed to study the chain structure in polyethylene melts. This work was compared to earlier Monte-Carlo results of Yoon and Flory[73]. A critical analysis of the accuracy

of the RIS approximation and the role of intrachain interactions has been given for polyoxyethylene[75], while for polyoxypropylene, a RIS force-field model is critically discussed by Stepto et al.[76].

While these studies bring valuable insight into the properties of the RIS chains, *an exact statistical mechanical treatment* of many other properties of interest is still needed. In particular, we refer to the quantities presented in the latter part of the introductory chapter, such as: end vector distributions, pair correlation function and force-extension curves. In the context of this work, we conjecture that the TM, as an exact method, can be adapted to determine those characteristics for the RIS model and thus join the panoply of techniques available in literature.

5.2.1 TM for the Helmholtz Ensemble

Proceeding in a similar manner as in the previous chapters, where we studied the FJC and FRC models in the Helmholtz ensemble with the help of the TM method, we will adapt here the same formalism for n-alkanes treated in the RIS approximation. In undertaking such a task, the important complication resides in the fact that the coordinates of any given bond vector depend, through the geometrical restrictions of the rotation and bond angles, not only on those of the immediately preceding bond, but of the one subsequent, too. We therefore need a set of coordinates that will describe this dependence. To facilitate determining those coordinates, the geometry of a segment of four chain bonds is depicted in Figure 5.3.

In order to carry out the statistical treatment of n-alkanes within the RIS model, we need as input numerical values for the geometrical parameters, bonds length b, bond angle γ, dihedral angles $\varphi_t, \varphi_{g+}, \varphi_{g-}$ for respectively *trans*, *gauche* +, *gauche* − conformations, as well as energy parameters E_g, $V_{\alpha\beta}$ $(\alpha, \beta = t, g^+, g^-)$ for our specific chain. The geometrical parameters can be obtained experimentally, by x-ray and electron diffraction[77] on crystalline and gaseous alkanes, respectively, and more recently by quantum chemistry studies on short n-alkane molecules, see for example ref. [55]. The energy parameters, being artifacts associated with the RIS model, are typically chosen to reproduce existing experimental data on this specific chain[2], and are therefore subject to discussion. Since exact knowledge of these parameters is not critical for demonstrating our method, here we have chosen the following widely

accepted set of parameters[2, 7]:

- the geometrical parameters: $b = 1.533\text{Å}, \gamma = 68^o, \varphi_t = 180^o, \varphi_{g+} = -\varphi_{g-} = 67.5^o$;
- the energy parameters: $E_g = 26meV$, $V_{g+g-} = 56meV$ and $V_{tt} = V_{tg} = V_{gg} = 0$.

Note that the above energy parametrization is sometimes called the "pentane effect", due to the fact that in a sequence of alkanes with increasing length, it first appears in pentane. The strong g^+g^- interaction is in fact one between non-bonded monomers situated four bonds apart along the chain, which is exactly the number of bonds in pentane.

5.2.1.1 The Green Function for the End-to-End Distance

If we are to find end-to-end distance distribution for this model, we need to calculate a Green function for this problem, which is the solution of equation 2.4. The transfer matrix is given by

$$\mathbf{T}^{(r)}(\Gamma_i, \Gamma_{i+1}) = \mathbf{C}(\Gamma_i, \Gamma_{i+1}) \exp[(-E_{\alpha_{i+1}} - E_{\beta_{i+1}} - V_{\alpha_{i+1}\beta_i} - V_{\alpha_{i+1}\beta_{i+1}})/k_BT], \quad (5.14)$$

where Γ_i is a collection of coordinates associated with subunit i that correctly reflects the geometrical constraints of the problem. The initial condition is the same as the one given by eq. 4.21. To facilitate identifying these coordinates, we show the vector geometry of a sequence of four chain bonds in Figure 5.3.

We denote the bond vectors of this sequence by $\mathbf{a}_i, \mathbf{b}_i, \mathbf{a}_{i+1}, \mathbf{b}_{i+1}$. Each of these vectors has its ends at the locations of consecutive carbon atoms in the molecule. We will take the chain subunits $\mathbf{s}_i$ encompassing two bond vectors ($\mathbf{s}_i = \mathbf{a}_i + \mathbf{b}_i$, with length $s = 2b\cos(\gamma/2)$) as basis for implementing the TM method. Note that this time, the index i numbers a pair of monomers (and thus runs from 1 to $N/2$) and not only a single monomer. We choose the following coordinate set for this problem: $\Gamma_i = \{r_i, \theta_i, \psi_i, \alpha_i, \beta_i\}$, where:

- r_i is the radial distance from the chain's end considered as origin;

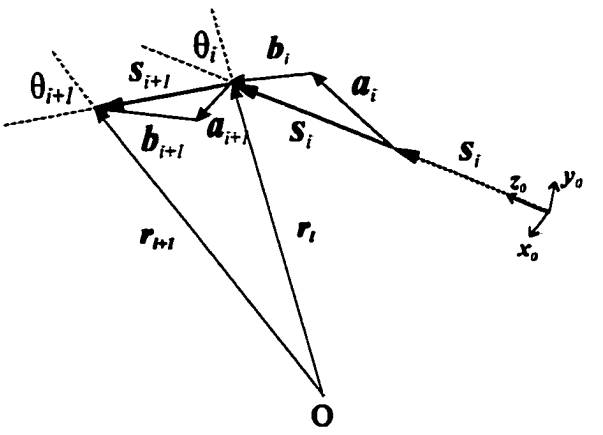

Figure 5.3: Vector geometry of a sequence of four bond vectors of a n-alkane chain and the coordinates necessary to calculate the end-to-end distribution.

- θ_i is the angle formed by the bond vector $\mathbf{s}_i$ with the direction of $\mathbf{r}_i$, with range $[0, \pi]$;
- ψ_i is the dihedral angle formed by the planes $(\mathbf{a}_i, \mathbf{s}_i)$ and $(\mathbf{s}_i, \mathbf{r}_i)$, with range $[-\pi, \pi)$;
- α_i is the rotational state corresponding to bond vector $\mathbf{a}_i$ (i.e. one of the t, g^+, g^- states);
- β_i is the rotational state corresponding to bond vector $\mathbf{b}_i$ (i.e. one of the t, g^+, g^- states);

The choice of these coordinates is not unique, and should be made expeditiously. For example, one could use, instead of ψ_i, the angle formed by the planes $(\mathbf{s}_i, \mathbf{r}_i)$ and $(\mathbf{s}_{i+1}, \mathbf{r}_{i+1})$, but this would only complicate the calculations below.

To compute $\mathbf{C}$, one has to find, from geometrical considerations, the orientation of the $\mathbf{s}_{i+1}$ vector when the orientation of $\mathbf{s}_i$ and the rotation states of the vectors $\mathbf{a}_i, \mathbf{b}_i, \mathbf{a}_{i+1}, \mathbf{b}_{i+1}$ are known. With the choice of the coordinate set above, the connectivity operator becomes

$$\mathbf{C}(\Gamma_i, \Gamma_{i+1}) = \delta[r_{i+1} - g_r(\Gamma_i, \Gamma_{i+1})]\delta[\theta_{i+1} - g_\theta(\Gamma_i, \Gamma_{i+1})]\delta[\psi_{i+1} - g_\psi(\Gamma_i, \Gamma_{i+1})], \quad (5.15)$$

where δ is the Dirac delta function if the coordinates are continuous and the Kronecker symbol if they are discrete. To express the functions g_r, g_θ and g_ψ we can employ the rotation matrices defined in eq. 5.4. To facilitate this, let us denote by $\mathbf{t}(\varphi, \gamma)$ the rotation matrix with dihedral angle φ and bond angle γ. We choose the frame $Ox_0y_0z_0$ in Figure 5.3 as reference for calculating the transfer operator, such that Oz_0 is parallel to $\mathbf{s}_i$ and Ox_0 is perpendicular to the plane $(\mathbf{r}_i, \mathbf{s}_i)$. In order to calculate all the components of $\mathbf{a}_i, \mathbf{b}_i, \mathbf{a}_{i+1}, \mathbf{b}_{i+1}, \mathbf{s}_i, \mathbf{s}_{i+1}$ in this frame, we need the following rotation matrices:

- $\mathbf{t}_0 \equiv \mathbf{t}(\psi_i, \gamma/2)$, corresponding to vector $\mathbf{s}_i$;
- $\mathbf{t}_1 \equiv \mathbf{t}(\pi, \gamma)$, corresponding to vector $\mathbf{a}_i$;
- $\mathbf{t}_2 \equiv \mathbf{t}(\varphi_{\beta_i}, \gamma)$, corresponding to vector $\mathbf{b}_i$;
- $\mathbf{t}_3 \equiv \mathbf{t}(\varphi_{\alpha_{i+1}}, \gamma)$, corresponding to vector $\mathbf{a}_{i+1}$.

Here φ_{α_i} are the dihedral angles characterizing bond i in state α_i. With the help of these matrices we get

$$\mathbf{r}_i = \begin{bmatrix} 0 \\ r_i \sin\theta_i \\ r_i \cos\theta_i \end{bmatrix}, \tag{5.16}$$

$$\mathbf{a}_{i+1} = \mathbf{t}_0\mathbf{t}_1\mathbf{t}_2 \begin{bmatrix} 0 \\ 0 \\ |\mathbf{a}_{i+1}| \end{bmatrix}, \tag{5.17}$$

$$\mathbf{b}_{i+1} = \mathbf{t}_0\mathbf{t}_1\mathbf{t}_2\mathbf{t}_3 \begin{bmatrix} 0 \\ 0 \\ |\mathbf{b}_{i+1}| \end{bmatrix}. \tag{5.18}$$

$$\eta = \cos^{-1}\left(-\frac{\mathbf{r}_i \cdot \mathbf{s}_{i+1}}{|\mathbf{r}_i|\,|\mathbf{s}_{i+1}|}\right) \tag{5.19}$$

As a result we can determine the unknown functions in eq. 5.15

$$g_r(\Gamma_i, \Gamma_{i+1}) = \left(r_i^2 + [2b\cos(\gamma/2)]^2 - 4r_i b\cos(\gamma/2)\cos\eta\right)^{1/2} \tag{5.20}$$

$$g_\theta(\Gamma_i, \Gamma_{i+1}) = \cos^{-1}\left[\frac{\mathbf{s}_{i+1}\cdot\mathbf{r}_{i+1}}{2br_{i+1}\cos(\gamma/2)}\right], \tag{5.21}$$

$$\cos\left[g_\psi(\Gamma_i, \Gamma_{i+1})\right] = \frac{\mathbf{r}_{i+1}\times\mathbf{s}_{i+1}}{|\mathbf{r}_{i+1}\times\mathbf{s}_{i+1}|}\cdot\frac{\mathbf{s}_{i+1}\times\mathbf{a}_{i+1}}{|\mathbf{s}_{i+1}\times\mathbf{a}_{i+1}|}, \tag{5.22}$$

$$\left|\sin\left[g_\psi(\Gamma_i, \Gamma_{i+1})\right]\right| = \left|\frac{\mathbf{r}_{i+1}\times\mathbf{s}_{i+1}}{|\mathbf{r}_{i+1}\times\mathbf{s}_{i+1}|}\times\frac{\mathbf{s}_{i+1}\times\mathbf{a}_{i+1}}{|\mathbf{s}_{i+1}\times\mathbf{a}_{i+1}|}\right|, \tag{5.23}$$

which completely defines the connectivity operator above.

5.2.1.2 Results

In the following, we give a systematic presentation of TM results for the statistical properties of the RIS model for n-alkanes. We will test our findings against other methods in this work and others in the literature and also compare to other models. For all the quantitative results throughout this chapter we maintained the mesh parameters to values sufficiently high such that the discretization effects are negligible, except where otherwise stated. We will unfold our study of n-alkanes by gradually introducing in our model:

1. the geometrical restrictions of bond lengths, bond angles and hindered rotations;
2. the energy difference E_g between the *gauche* and *trans* bond states;
3. the nearest neighbor interactions $V_{\alpha\beta}$.

This approach will allow us to identify the role played by each parameter in the statistical properties of the chain. All results are for temperature $T = 300$ K unless otherwise stated. We begin by testing the results of TM calculations against the ones obtained by other methods. For this purpose we calculated the end-to-end distribution function for the RIS model with all energy parameters being made equal to zero by the TM method and by an exact account of all chain conformers. Thus, we calculated exactly the configurational canonical partition function $Z_N(\mathbf{R}, T)$ in eq. 1.20. For the RIS model there are 3^N conformers, corresponding to the set of all possible combinations of N dihedral angles $\{\varphi_1, \varphi_2, ..., \varphi_N\}$. We can calculate the end-to-end vectors for all the conformers $\mathbf{r}_N(\{\varphi_1, \varphi_2, ..., \varphi_N\})$, via eq. 5.7, and use them to perform the summation in eq. 1.20.

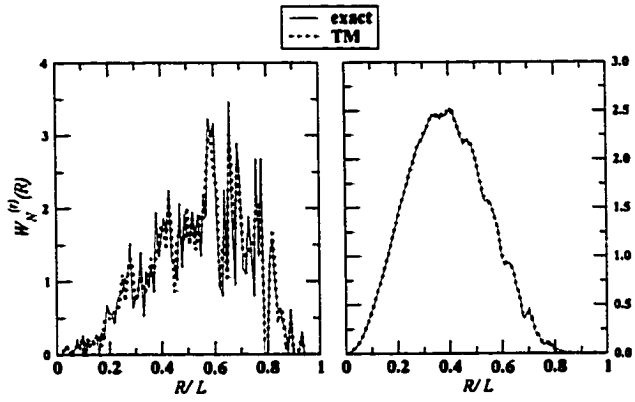

Figure 5.4: End-to-end distribution for n-alkane chains, as RIS model with no energy parameters, with $N = 10$ (left) and $N = 20$ (right) and, as obtained by TM method (squares) and by exact account of all conformers (solid line).

In Figure 5.4 we show the comparison between TM and exact results for $N = 10$ (left) and $N = 20$ (right). The mesh parameters in the TM were $M_\theta = M_\psi = 100$ and $M_r = 100$. Since the results are extremely similar, it is not necessary to go to longer chain lengths to conclude that the TM method yields excellent accuracy. Besides, the exact calculation is only feasible for small chain lengths, it taking a tremendous amount of time. Already for $N = 20$ we are faced with a computation time longer than 2 hours, as opposed to TM, which took only 2 minutes on our computer. The time ratio is expected to get only 'worse' for longer chains.

With this in mind, we can now calculate the end-to-end distribution functions for longer chains, like the ones in Figure 5.5, which are for RIS chains with all energy parameters zero and up to 100 bonds in length. Here we used the same mesh parameters as for the above result. For short chains, N between 10 and 20, we notice a curve with many sharp maxima, spike-like features, which is due to the small number of conformers, 3^N, the chain can assume. As the chain length is increased, the end distribution becomes more or less normal (Gaussian) due to the exponential increase in the number of conformers, and thus the irregularities are smoothed out — a trend that can be well observed in Figure 5.5.

Next we do a scaling analysis of the end-to-end distribution with the chain length, comparing at the same time the three sets of energy parameters mentioned above. As

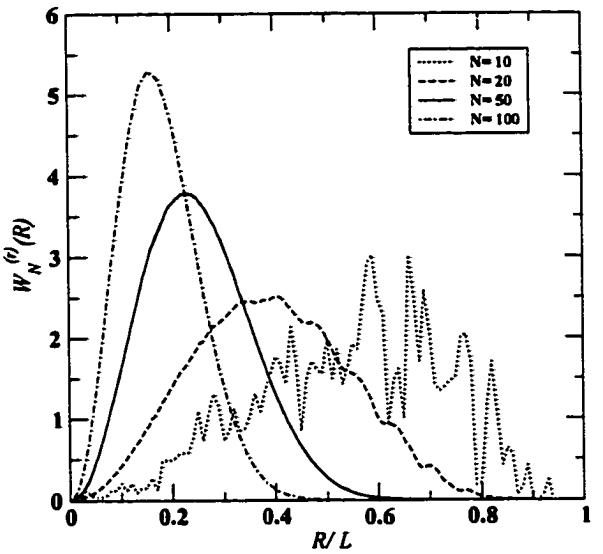

Figure 5.5: End-to-end distributions for n-alkane chains as obtained by TM method within the RIS model with no energy parameters for chain lengths $N = 10, 20, 50, 100$.

we can see in Figure 5.6 incorporation of the *gauche* energy difference and furthermore of the interactions causes this distribution to shift to larger values of R/L. The chain's persistence length increases and the deviations from Gaussian behavior are more pronounced.

Knowledge of the end-to-end distribution functions enables us to calculate, via eq. 2.31 and 1.8, the characteristic ratio of the polymer. Furthermore, we can now analyze the effects of energy parameters on the characteristic ratio. In Figure 5.7 we present plots of the characteristic ratio versus chain length for the three parameter sets and also for the FRC model with the same bond angle as the n-alkanes. The trend is very clear: restricting a bond to only three possible states slightly increases the characteristic ratio of the RIS model from the value corresponding to the FRC. The RIS chain is stiffer than the FRC, given the same bond angle and number of monomers. Following the introduction of different bond energies, the RIS model becomes even stiffer— its characteristic ratio doubles at intermediate chain lengths. This can be phenomenologically explained by the fact the *gauche* states responsible for the 'coiling' of the chain possess a higher self energy and thus become unfavor-

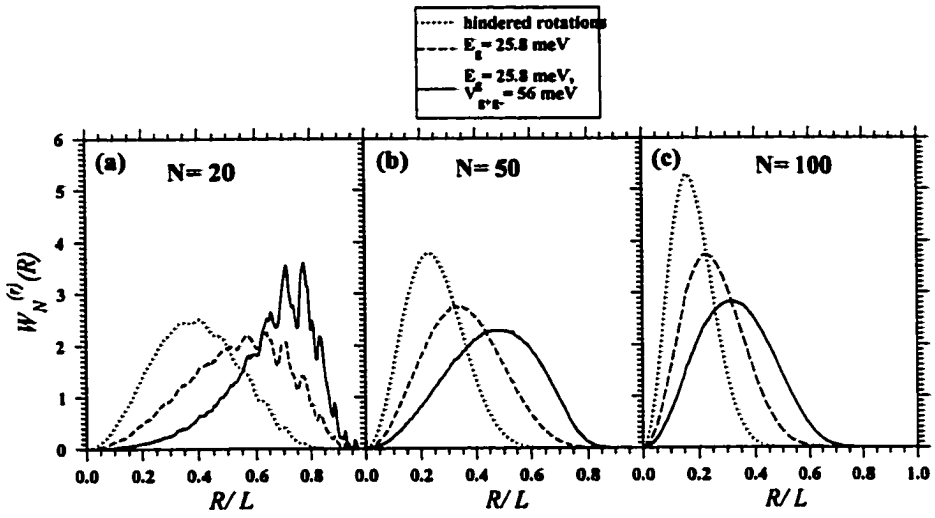

Figure 5.6: Comparison of the end-to-end distribution functions for alkanes within RIS model with various sets of parameters indicated in the legend. Three representative chain lengths (also specified in each panel) were studied.

able. The chain will contain on average more *trans* bonds, which favours its overall stretching.

We note that these calculations have been performed with the mesh parameters $M_\theta = M_\psi = 50$ and $M_r = 400$ for which we estimate a minimal accuracy of $\pm 3\%$. Under these conditions, they require a good deal of computation resources, occupying around 70% of our computer's memory and they are time consuming, taking longer than one day of CPU time. Consequently, obtaining the characteristic ratio in the limit of infinite chains necessitates a careful analysis of the data at hand. Inset in Figure 5.7 we plot the characteristic ratio versus the inverse of the chain length for the same three sets of parameters in order to perform an extrapolation for $N \longrightarrow \infty$. The resulting values are: $C_\infty = 2.58 \pm 0.08$ for hindered rotations, $C_\infty = 5.25 \pm 0.16$ for chain with gauche energy difference only, and $C_\infty = 9.10 \pm 0.27$ for chain with all energy parameters. We also note that between $N = 60$ and 80 the increase of C_N is less than 0.05% per added bond, fact that can also be used to extrapolate the characteristic ratio for longer chains.

Similarly, the mean square radius of gyration for the RIS model can be calculated for any chain length and is presented in Figure 5.8. Here we used the same parameter

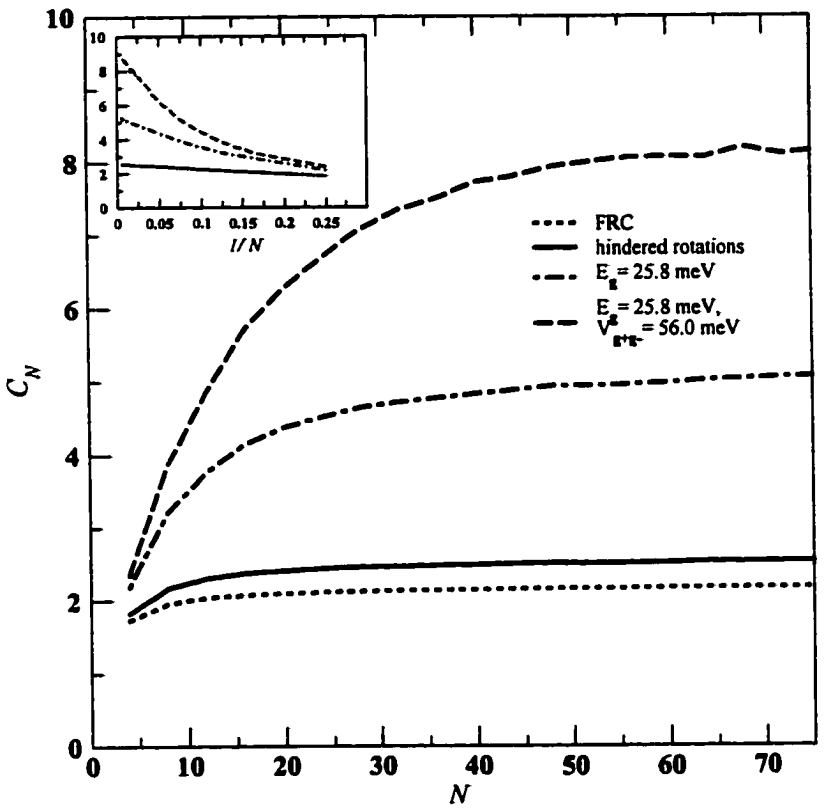

Figure 5.7: The characteristic ratio of n-alkanes for the energy parameters specified in the legend versus the chain length. Also shown for comparison is the characteristic ratio of the FRC with the same bond angle. Inset: the characteristic ratio versus the inverse of the chain length.

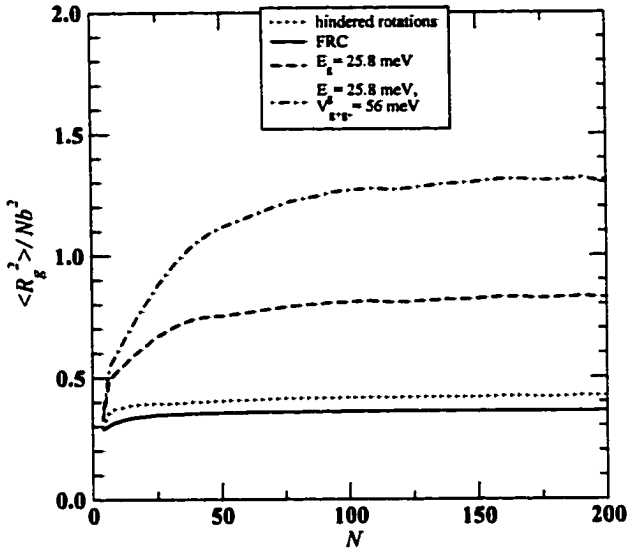

Figure 5.8: The mean square radius of gyration for n-alkanes and the FRC versus chain length for the same cases as in Figure 5.7.

sets as above and compared again to the corresponding FRC. The same findings stated above about the characteristic ratio of the chain, apply for this quantity, too, except that now we must keep in mind that we deal with the distribution of *all bonds* about their common center of mass. Note that, apart from a multiplicative constant, the curves here are very similar in shape and order, to the ones in Figure 5.7.

The temperature coefficient of alkanes was determined experimentally by intrinsic viscosity measurements of this polymer in n-hexadecane, n-octacosane and n-triacontane solvents[27] and also by stress-temperature studies on polymer networks[26]. The consistent value obtained from these experiments is $\left(d \ln \langle R^2 \rangle / dT\right) \times 10^3 = -1.2 \pm 0.2$ at $T = 420K$, in the limit of very long chains. The mean square end-to-end distance for this molecule was also determined from intrinsic viscosities measurements under θ-conditions[28, 29] and they yielded a characteristic ratio of $C_\infty = 6.7 \pm 0.3$.

We performed TM calculations in the canonical ensemble at different temperatures, $T = 200, 300, 400K$, and determined the characteristic ratios and temperature coefficients for alkanes, whose dependence on the chain length is shown in Figures 5.9 and 5.10, respectively. This enables us to compare our results to the experimental ones. At $T = 400K$, we obtain by extrapolation to the infinite chain limit

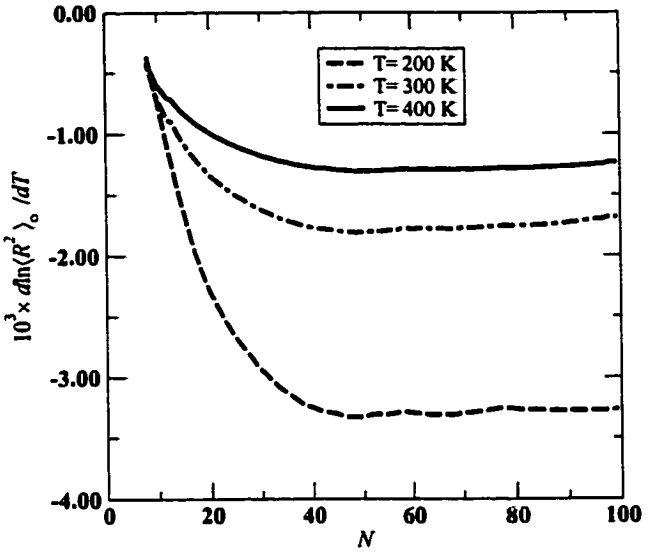

Figure 5.9: Temperature coefficients for n-alkanes versus the chain length at three different temperatures indicated in the legend.

$C_\infty = 7.1 \pm 0.2$ and $(d \ln \langle R^2 \rangle / dT) \times 10^3 = -1.22 \pm 0.10$, in good agreement with the values presented above and also with results found by other theoretical methods[2].

When making the comparison between the TM results and the experiment, an important observation is in place. We recall that one of the essential assumption of our procedure is that of θ-condition. All of our results are valid and accurate if this approximation is justified. However, the quality of the solvent and the temperature, both dictate if the θ-condition is satisfied in a given experimental situation. A chosen solvent satisfies that requirement at only certain values of the temperature. Therefore, it has to be emphasized that the curves for different temperatures in Figures 5.9 and 5.10 are to be taken as reliable only if the polymer is in θ-condition at that temperature, a decision that must be based on the knowledge of the specific experimental situation.

Using the end distribution functions for each monomer we can now compute the static structure factor for alkanes; we display the results for the three parameters sets in Figure 5.11, where we also plot the structure factor for the FRC with identical bond angle as in alkanes. While there are significant deviations from the FRC, the influence of the parameter differences between the three RIS curves seem to fade

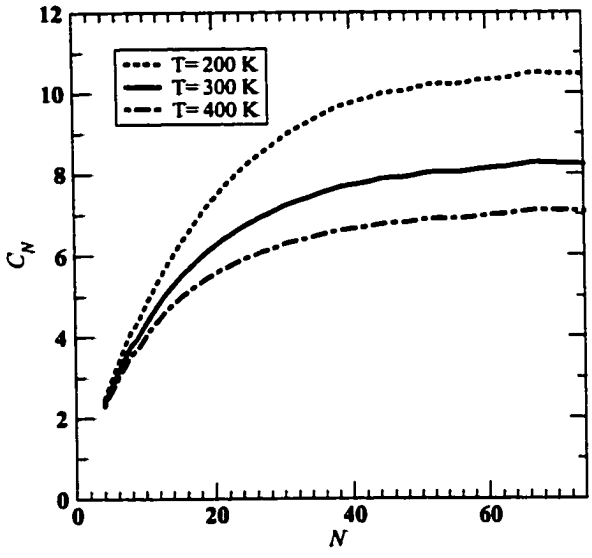

Figure 5.10: Characteristic ratio for n-alkanes versus chain length at various temperatures specified in the legend for each curve.

quickly as k increases.

In Figure 5.12, we present a scaling analysis of the static structure factor with the chain length, for a limited but relevant set of N indicated in the figure for each curve. As for the other models encountered in this work, there seems to be little difference between the three curves for wave numbers larger than 1Å^{-1}, that is in the small wavelength range.

Finally, the radial distribution function for alkanes is computed for the three sets of RIS parameters. In Figure 5.13 we show a compilation of plots of this quantity for short chains $N = 10$ (left panels) and $N = 20$ (right panels). From top to bottom the curves correspond to the three sets of parameters approached throughout this chapter. For all functions displayed, the closest peak to the origin mimics, in a manner characteristic to our numerical procedure with $M_r = 100$, a delta function corresponding to the presence of the first monomer at $r = b$. The second peak corresponds to a second neighbor at $r = 2b\cos\frac{\gamma}{2}$. Beyond this distance $g(r)$ becomes non-singular but the monomers are still very localized, especially for $N = 10$. As we increase the chain length, the first two peaks are normally maintained, but the remaining of the curve becomes smoother as we can notice in Figure 5.14, where

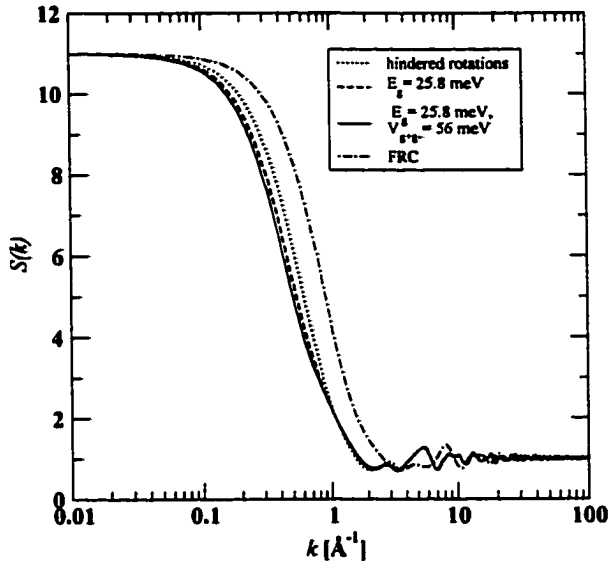

Figure 5.11: The static structure factor of n-alkanes with $N = 10$ and with various parameter sets indicated in the legend for each curve.

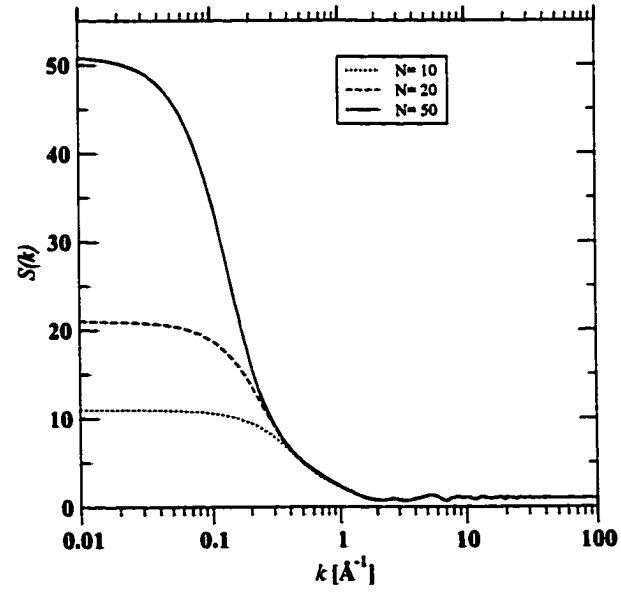

Figure 5.12: Scaling analysis of the structure factor of n-alkanes with the chain length.

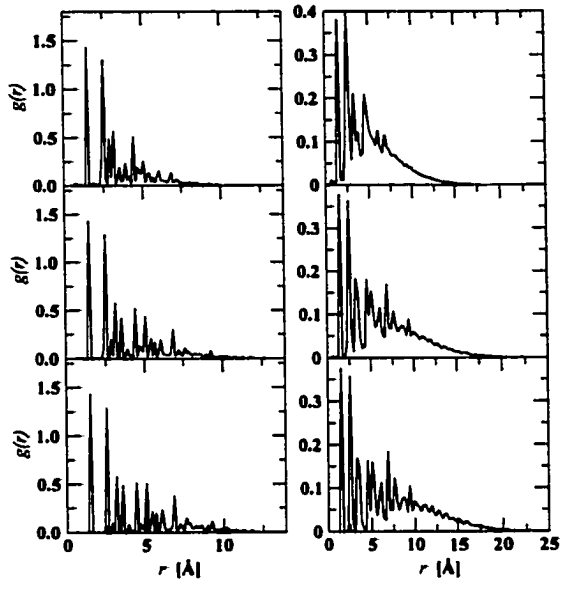

Figure 5.13: Radial distribution function for n-alkanes with $N = 10$ (left three panels) and $N = 20$ (right three panels). From top to bottom the curves correspond to the same three sets of energy parameters as in Figure 5.7.

radial distributions for $N = 50$ are plotted.

5.2.2 Transfer Matrix for the Gibbs Ensemble

To apply the TM method to this problem, we first identify the relevant coordinates depicted in Figure 5.15. The Green function for this problem satisfies the integral equation 2.4, where the transfer matrix is given by

$$\begin{aligned} \mathbf{T}^{(f)}(\Gamma_i, \Gamma_{i+1}) &= \mathbf{C}(\Gamma_i, \Gamma_{i+1}) \exp[(2fb\cos(\gamma/2)\cos\theta_{i+1} \\ &\quad -E_{\alpha_{i+1}} - E_{\beta_{i+1}} - V_{\alpha_{i+1}\beta_i} - V_{\alpha_{i+1}\beta_{i+1}})/k_BT], \end{aligned} \tag{5.24}$$

and the initial condition reads

$$G_1^{(f)}(\Gamma_1) \propto \exp\left(\frac{2fb\cos(\gamma/2)\cos\theta_1 - E_{\alpha_1} - E_{\beta_1} - V_{\alpha_1\beta_1}}{k_BT}\right)\sin\theta_1. \tag{5.25}$$

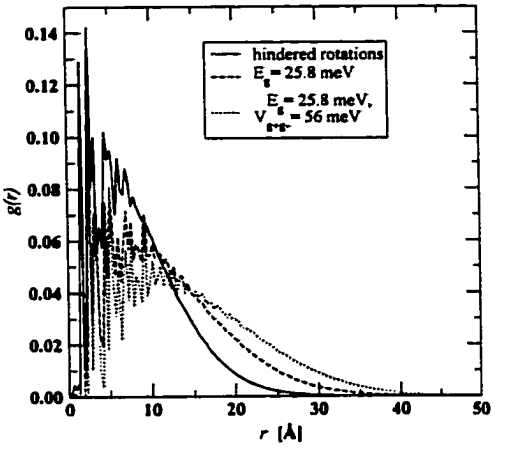

Figure 5.14: Radial distribution function for n-alkanes with $N = 50$ for the three parameter sets indicated in the legend.

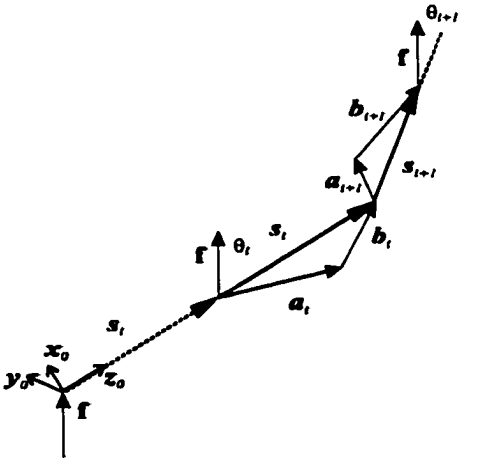

Figure 5.15: Vector geometry of a segment of four chain subunits and the coordinate frame $Ox_0y_0z_0$ in which all vector components are calculated. Oz_0 is parallel to $\mathbf{s}_i$ and Ox_0 in perpendicular to the plane $(\mathbf{f}, \mathbf{s}_i)$.

Similarly to the previous section we denote $\mathbf{a}_i, \mathbf{b}_i, \mathbf{a}_{i+1}, \mathbf{b}_{i+1}$ and $\mathbf{s}_i = \mathbf{a}_i + \mathbf{b}_i$ the relevant vectors for this problem. The most convenient choice for describing the orientation of $\mathbf{s}_i$ is the coordinate set given by $\Gamma_i = \{\theta_i, \psi_i, \alpha_i, \beta_i\}$, which consists of:

- θ_i, the angle formed by the bond vector $\mathbf{s}_i$ with the force $\mathbf{f}$, with range $[0, \pi]$;

- ψ_i the dihedral angle formed by the planes $(\mathbf{a}_i, \mathbf{s}_i)$ and $(\mathbf{s}_i, \mathbf{f})$, with range $[-\pi, \pi)$;
- α_i the rotational state corresponding to bond vector $\mathbf{a}_i$ (i.e. one of the t, g^+, g^- states);
- β_i the rotational state corresponding to bond vector $\mathbf{b}_i$ (i.e. one of the t, g^+, g^- states);

In terms of the coordinates chose above, the connectivity matrix reads

$$\mathbf{C}(\Gamma_i, \Gamma_{i+1}) = \delta[\theta_{i+1} - g_\theta(\Gamma_i, \Gamma_{i+1})]\delta[\psi_{i+1} - g_\psi(\Gamma_i, \Gamma_{i+1})]. \tag{5.26}$$

To get $g_\theta(\Gamma_i, \Gamma_{i+1})$ and $g_\psi(\Gamma_i, \Gamma_{i+1})$ we employ the rotation matrices $\mathbf{t}(\varphi, \gamma)$ corresponding to the dihedral angle φ and bond angle γ. The frame $Ox_0y_0z_0$ in Figure 5.15 is chosen as reference for calculating the transfer operator, with axes Oz_0 parallel to $\mathbf{s}_i$ and Ox_0 perpendicular to $(\mathbf{f}, \mathbf{s}_i)$. Similarly to the previous section, we will calculate the vectors $\mathbf{a}_i, \mathbf{b}_i, \mathbf{a}_{i+1}, \mathbf{b}_{i+1}, \mathbf{s}_i, \mathbf{s}_{i+1}$ in this frame, we need the following rotation matrices:

- $\mathbf{t}_0 \equiv \mathbf{t}(\psi_i, \gamma/2)$, corresponding to vector $\mathbf{s}_i$;
- $\mathbf{t}_1 \equiv \mathbf{t}(\pi, \gamma)$, corresponding to vector $\mathbf{a}_i$;
- $\mathbf{t}_2 \equiv \mathbf{t}(\varphi_{\beta_i}, \gamma)$, corresponding to vector $\mathbf{b}_i$;
- $\mathbf{t}_3 \equiv \mathbf{t}(\varphi_{\alpha_{i+1}}, \gamma)$, corresponding to vector $\mathbf{a}_{i+1}$.

Accordingly, we can write

$$\hat{\mathbf{f}} = \begin{bmatrix} 0 \\ \sin\theta_i \\ \cos\theta_i \end{bmatrix}, \tag{5.27}$$

$$\mathbf{a}_{i+1} = \mathbf{t}_0\mathbf{t}_1\mathbf{t}_2 \begin{bmatrix} 0 \\ 0 \\ |\mathbf{a}_{i+1}| \end{bmatrix}, \tag{5.28}$$

$$\mathbf{b}_{i+1} = \mathbf{t}_0\mathbf{t}_1\mathbf{t}_2\mathbf{t}_3 \begin{bmatrix} 0 \\ 0 \\ |\mathbf{b}_{i+1}| \end{bmatrix}. \tag{5.29}$$

Consequently, we can now express the desired function in eq. 5.26 as

$$g_\theta(\Gamma_i, \Gamma_{i+1}) = \cos^{-1}\left[\frac{\mathbf{s}_{i+1}\cdot\hat{\mathbf{f}}}{|\mathbf{s}_{i+1}|}\right], \tag{5.30}$$

$$\cos\left[g_\psi(\Gamma_i, \Gamma_{i+1})\right] = \frac{\hat{\mathbf{f}}\times\mathbf{s}_{i+1}}{\left|\hat{\mathbf{f}}\times\mathbf{s}_{i+1}\right|}\cdot\frac{\mathbf{s}_{i+1}\times\mathbf{a}_{i+1}}{|\mathbf{s}_{i+1}\times\mathbf{a}_{i+1}|}, \tag{5.31}$$

$$\left|\sin\left[g_\psi(\Gamma_i, \Gamma_{i+1})\right]\right| = \left|\frac{\hat{\mathbf{f}}\times\mathbf{s}_{i+1}}{\left|\hat{\mathbf{f}}\times\mathbf{s}_{i+1}\right|}\times\frac{\mathbf{s}_{i+1}\times\mathbf{a}_{i+1}}{|\mathbf{s}_{i+1}\times\mathbf{a}_{i+1}|}\right|. \tag{5.32}$$

5.2.2.1 Results

We are interested in exploiting the above formalism to derive the force-extension relation and related quantities for this model. Let us start by analyzing the discretization effects in our procedure, which also gives a good measure of the reliability of these results. In Figure 5.16 we show force-extension curves for the RIS model with $N = 10$ calculated with various values of the angular mesh parameter $M_\theta = 10, 20, 40$ (also indicated in the legend). These curves imply that even for the second mesh parameter used we obtain quite accurate results. Henceforth we will maintain a reliable value of M_θ for which the discretization effects are negligible.

It would be interesting to see how the length of the molecule and the energy parameters influence the force-extension relation. Therefore in Figures 5.17-5.19 we present a compilation of such data for various sets of parameters. The short chain behavior, $N = 10$, is illustrated in Figure 5.17, whereas in previous times we chose for the RIS three energy parameter sets. Note that the presence of the interaction does not affect much the shape of the curve.

With the self-energies and interactions incorporated in the model, we increased the chain length from 10 to 200 and graphically compared the corresponding stretching curves in Figure 5.18. Little variation is seen beyond a certain chain length, say $N = 100$, in the RIS model. The long chain limit has been reached, since $L \gg l_P$. Results in this limit are displayed in Figure 5.19 for the three sets (shown in the legend) and chain length $N = 200$.

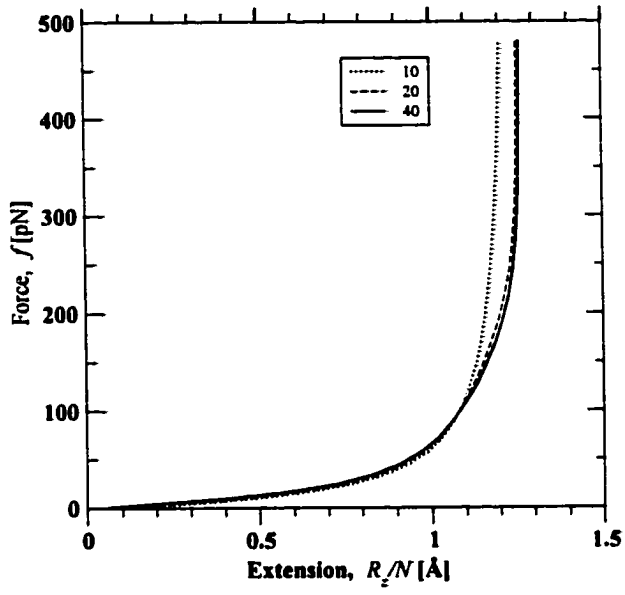

Figure 5.16: Discretization effects in the force-extension curve for the RIS model with $N = 10$. The values of the angular mesh parameters for different curves are indicated in the legend.

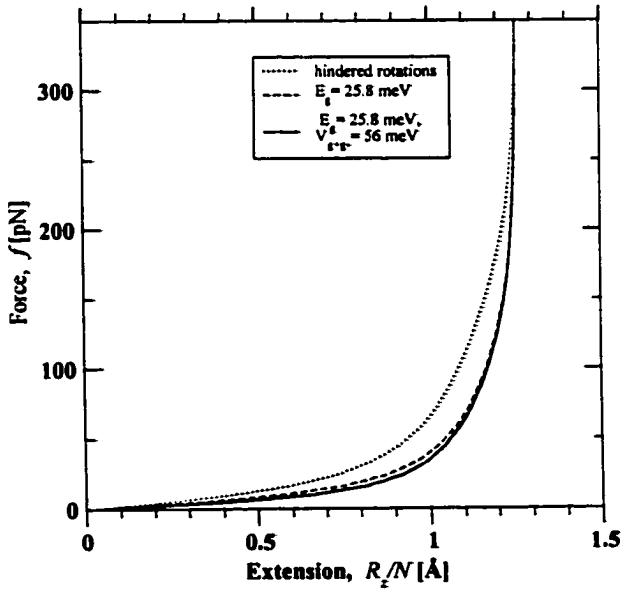

Figure 5.17: Force-extension curves for n-alkanes with $N = 10$ for various sets of parameters shown in the legend.

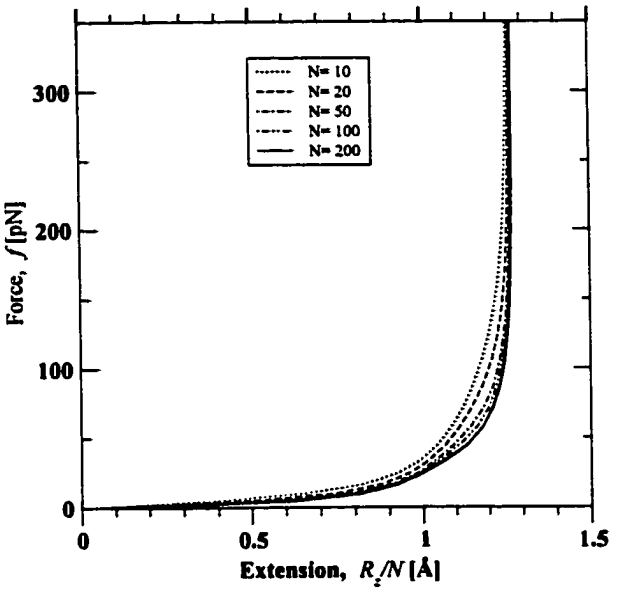

Figure 5.18: Scaling analysis of the force-extension curves for n-alkanes for increasing length. All mesh parameter used here is 50.

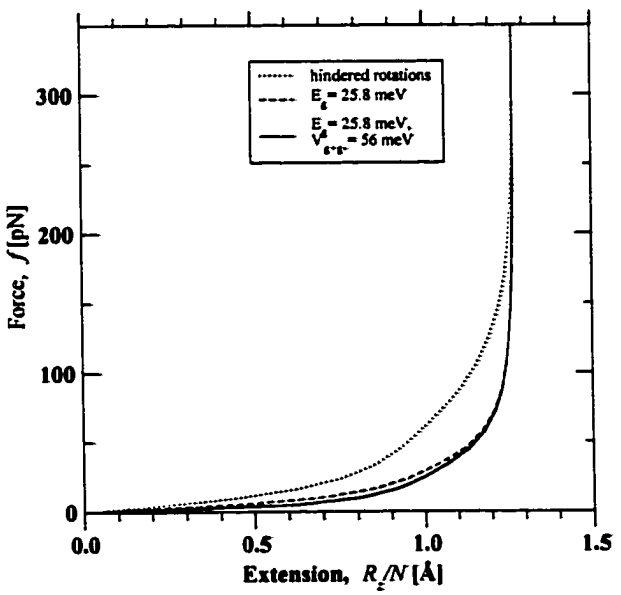

Figure 5.19: Force-extension curves for long n-alkane chains ($N = 200$) for the three sets of parameters shown in the legend.

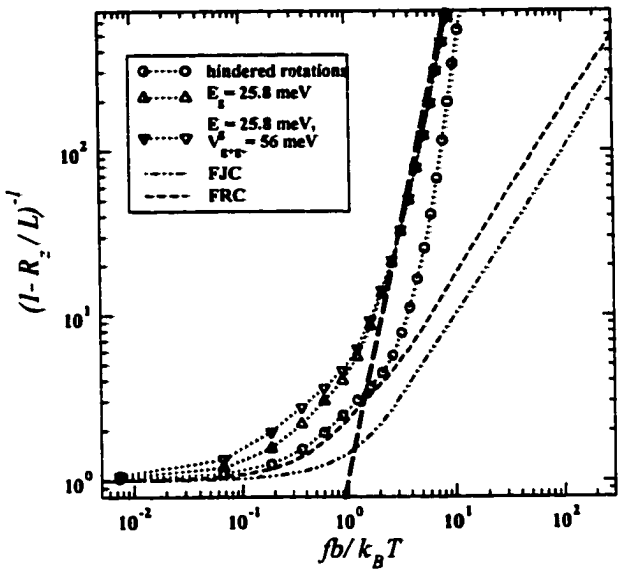

Figure 5.20: Modified form of the force-extension curves for long chains in logarithmic axes. The curves for n-alkanes have been calculated for $N = 200$ and for parameter sets indicated in the figure. For comparison, we show the curves for the FJC and FRC models as well as the curve in eq. 5.33 (thick dashed line).

To compare the large force-behavior of the RIS model with the ones of other models it is convenient to look at a modified form of the force-extension curve: $(1 - R_Z/L)^{-1}$ versus fb/k_BT . In Figure 5.20 we plot these curves in double logarithmic axes for all models encountered so far. We see a strong divergence from one model to another for large forces. To facilitate an analytical description of the large force behavior of the RIS model for n-alkanes, we plotted in this figure a simple power law curve of the form

$$(1 - R_z/L)^{-1} = (fb/k_BT)^3, \tag{5.33}$$

which approximates quite well the behavior of the RIS model for $fb/k_BT > a/b$.

In Figure 5.22 we present the results of fitting Gaussian curves derived from eq. 3.11 to the end distribution function obtained in the previous section for relatively long chains, $N = 100$ and $N = 200$. In each case, the appropriate width of the Gaussian $\langle R^2 \rangle$ was taken from eq. 1.10, with the Kuhn length extracted from the stretching results in the small-force regime displayed in Figure 5.21. In each panel

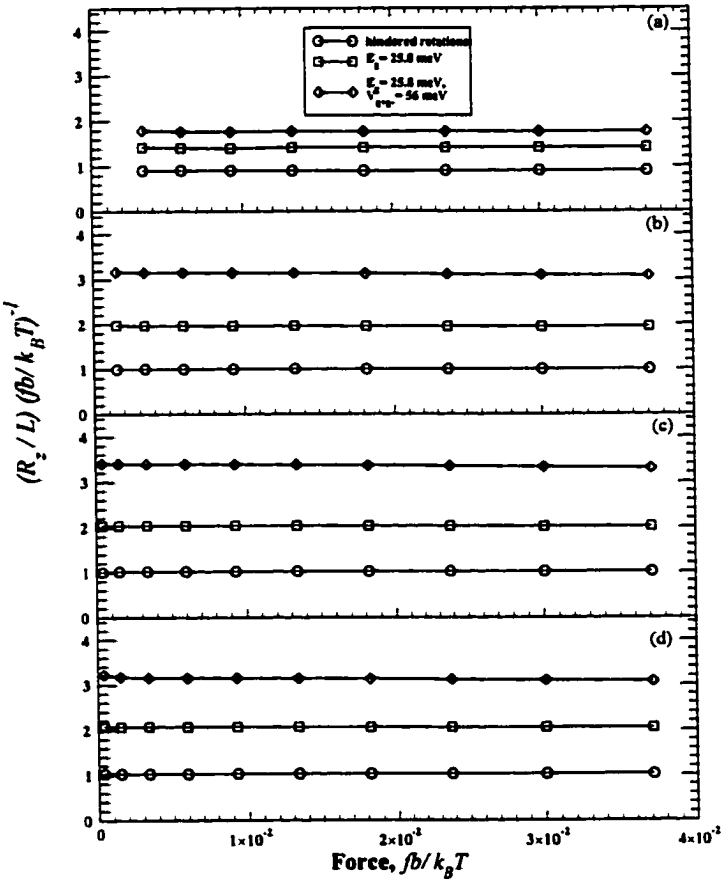

Figure 5.21: Slope of force-extension curves for RIS in the small-force regime. From top to bottom the four panels correspond in this order to $N = 10, 50, 100, 200$. The energy set for each curve is shown in the legend, common for all panels.

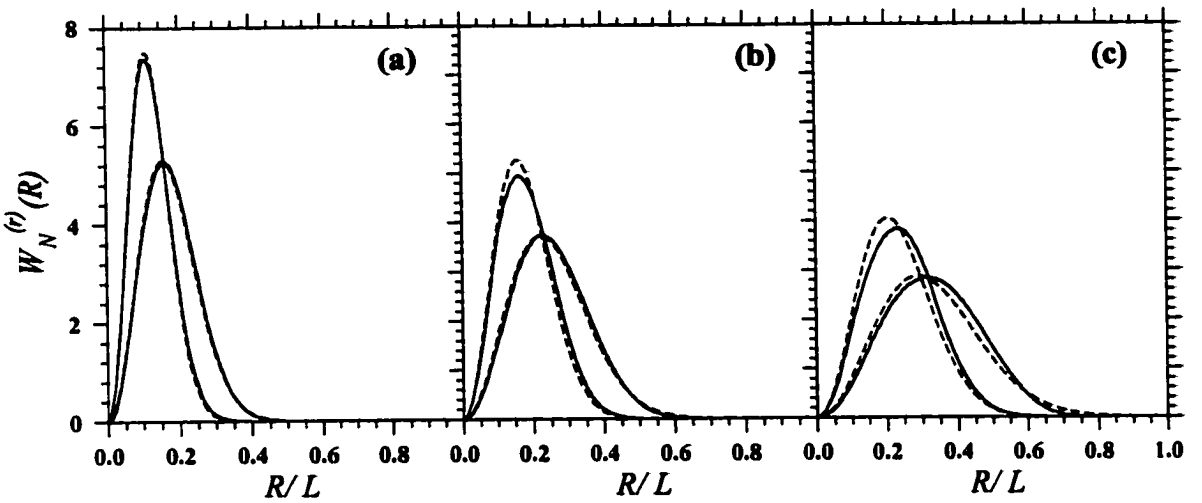

Figure 5.22: Comparison of the end distance distribution of the RIS model obtained by TM (solid lines) with Gaussian curves (dashed lines) for $N = 100$ (lower maxima in each panel) and $N = 200$ (higher maxima). From left to right panels are in this order for:(a) no energy parameters; (b) only gauche energy difference; (c) self energies and interactions included.

the curve for $N = 100$ has a lower maxima and a larger width. The Gaussian fits give excellent agreement for the curves in panel (a), good in (b), and present visible deviations from the curves in (c). This is attributable to the fact that the introduction of interactions, besides making the chain stiffer, render the spatial distribution to be non-trivial—impossible to characterize by a single quantity like the Kuhn length—even for relatively long chains.

In Figure 5.23 we show the dependence of the characteristic ratio on the temperature for alkanes of different lengths in a broad range of temperatures. The virtual overlap of the curves for $N > 400$ entitles us to regard this length as a substitute for the infinite chain limit. Our calculations for the longer chains shown in this figure agree very well with the results obtained in the canonical ensemble (see Figures 5.7 and 5.10). At $T = 300K$, we recover the value of $C_\infty = 9.1$, also obtained in Figure 5.7, this time with a higher accuracy, better than 1%. At $T = 400K$, the value of 7.1 can be read on the curve for $N = 400$, in excellent agreement with the results in Figure 5.10.

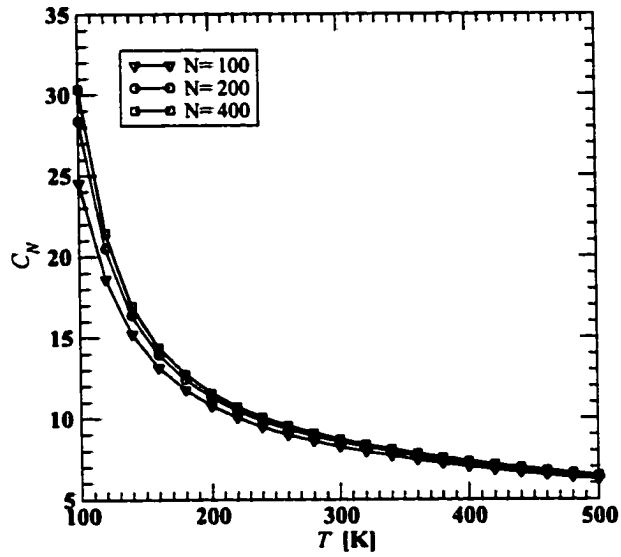

Figure 5.23: The characteristic ratio of n-alkanes versus temperature for different chain lengths specified in the legend.

5.3 N-Alkane Chains with "Continuous" Rotational Potential

With the advent of large scale quantum chemistry computations, one can now obtain detailed information on the electronic structure of short polymer molecules. This information can be used for larger molecules or systems of molecules. For instance, we can extract the information we need from short molecules like n-butane and n-pentane and use it for the statistical study of longer n-alkane chains. Such data are available for n-butane[55].

While the shape of the potential is roughly as given in Figure 1.2, Smith et al.[55] found the rotational potential in n-butane to be of the form

$$E_\varphi(\varphi) = \sum_{k=1,8} \frac{E_k}{2}(1 + \cos k\varphi)\,, \tag{5.34}$$

with the leading coefficients $E_1 = 1.19, E_3 = 3.41 Kcal/mol$. For simplicity, we neglect the remaining coefficients, which are an order of magnitude smaller. The potential depends only on one dihedral angle and accounts for interactions between the pendant groups of monomers separated by three covalent bonds. It does not include

interactions between atoms further apart along the backbone, like the "pentane effect", which as shown in the previous section play an important role in the statistical properties of long alkane chains.

Such longer-ranged intrachain interactions can be taken into account within a force-field technique[2, 21, 23] for instance by using a Lennard-Jones potential

$$V_{ij}(r) = \frac{A_{ij}}{r^{12}} - \frac{C_{ij}}{r^6}, \tag{5.35}$$

where i and j denote a pair of atoms, r is the distance between them, A_{ij} and C_{ij} are constants specific to the atomic species under consideration. For alkanes, the interactions can take place between the following possible pairs: $(C,C), (C,H), (H,H)$. It was shown (see for instance ref. [21, 23]) that the interactions in the first pair in this list are significantly greater than in the following pairs, so much so that we can neglect the last two. For interactions between two C atoms the constants in the expression of the rotational potential taken from ref. [23] are $A_{ij} = 908 \times 10^3$, $C_{ij} = 363$ in units such that V_{ij} is in $Kcal/mol$ if r is in units of Å.

Although in principle possible to incorporate in the TM treatment of n-alkanes, the Lennard-Jones interactions will not be considered in the present formulation. They bring a further complication — the necessity to account for distances between monomers four and more bonds apart along the chain. In the present scheme we restrict our attention to incorporating the bond rotational potential only. Accordingly, we will keep this in mind when comparing the following results with the ones in the previous section.

The TM method that we used to perform the configurational statistics of this model is identical in its formulation with the method used for the RIS model, described in the previous section, with the sole difference that the dihedral angle for each bond, instead of having just three possible values, is allowed to assume a large number of values, mimicking a continuous potential $E_\varphi(\varphi)$. Within this procedure, we were able to sample the potential curve by an array of M_α rotational states with $M_\alpha = 10, 20, 30$. We estimate that for $M_\alpha = 20$ the discretization effects are greatly diminished for our model — the continuous rotational potential limit is approached. Due to the increased computational cost when using large mesh parameters, we were able to obtain only a few selected results for those, which nonetheless are valuable

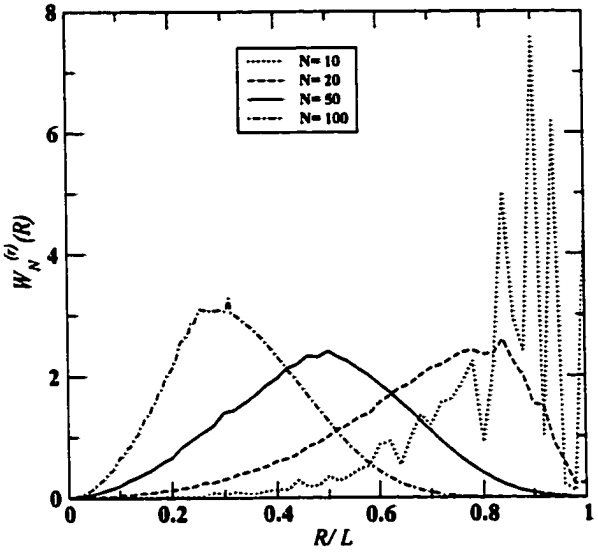

Figure 5.24: End to end distribution functions for alkanes with continuous rotational potential for different lengths.

and will be displayed below.

Below we present a compilation of results obtained in the Helmholtz and Gibbs ensembles. In Figure 5.24 we plot the end to end distributions for n-alkanes with increasing lengths. The rotational mesh parameter used here is $M_\alpha = 10$. Note that the chain with $N = 10$ bonds has a very irregular distribution and as we increase the chain length this becomes smoother. There are significant differences between these curves and the corresponding ones in the RIS model.

Calculation of some of the results presented in this section were feasible only for a rather small value of the rotational mesh parameter (a few tens) and therefore will carry some discretization effects. The role of the rotational mesh parameter in the force-extension curve is shown in Figure 5.25 for just two relatively small chain lengths. The results for $M_\alpha = 30$ are not shown here, but were found to virtually overlap those for $M_\alpha = 20$, which signals the decay of the discretization effects.

Next, we turn to calculating the force-extension curves for alkanes with increasing lengths, presented in Figure 5.26. As expected from previous findings, one can notice that beyond a certain chain length these curves will practically overlap — the long

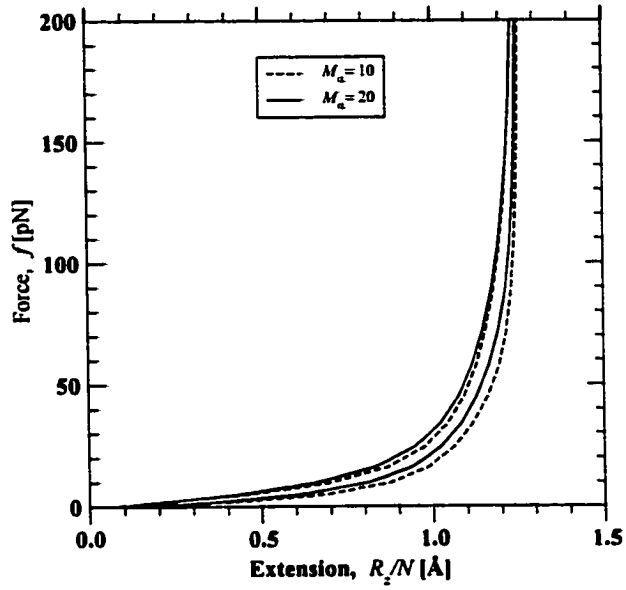

Figure 5.25: Influence of the mesh parameter (in the legend) for the rotational potential on the force-extension curve for two chain lengths: $N = 10$ (two left-hand curves) and $N = 20$ (two right-hand curves).

chain limit is reached. We will analyze in more detail the various regimes of the mechanical equation of state in the subsequent discussion. For now it is relevant to compare the stretching curves for long alkanes in their various models presented in this work. We do this in Figure 5.27. It is important to observe that the maximal length is not reached for the continuous potential model for the same magnitude of forces as for the RIS model. In other words, this model is stiffer than the RIS, an aspect which will be emphasized later in this section.

The small-force regime is studied by plotting the quantity $(R_Z/L)(fb/k_BT)^{-1}$ versus the force (fb/k_BT) in Figure 5.28, for the same array of chain lengths $N = 10, 20, 50, 100$. We note the constancy of the slope for this range of forces which indicates that the chain obeys the same law as the Gaussian chain in eq. 1.16.

We use this fact to extract the Kuhn length and via eq. 1.12, the characteristic ratio at various temperatures as seen in Figures 5.30 and 5.29. The effects of the rotational mesh parameter on the characteristic ratio are shown in Figure 5.29, where we plotted this quantity as a function of the temperature for $M_\alpha = 10, 20, 30$. The

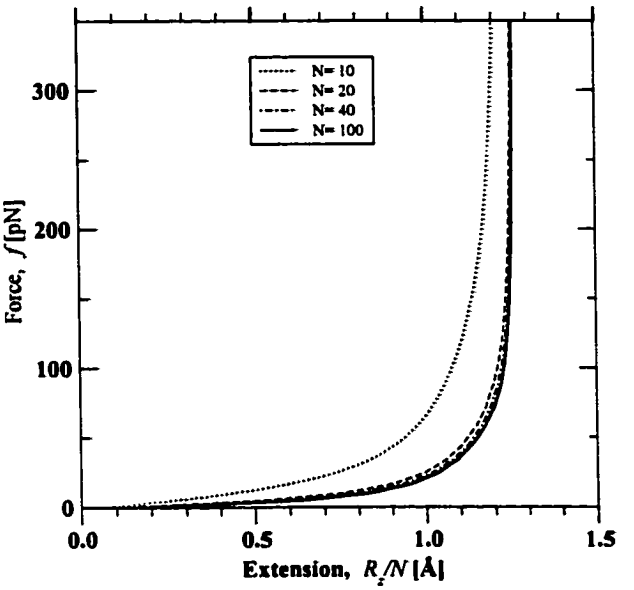

Figure 5.26: Scaling analysis of the force-extension curve with respect to the chain length for $n-$alkanes with continuous rotational potential.

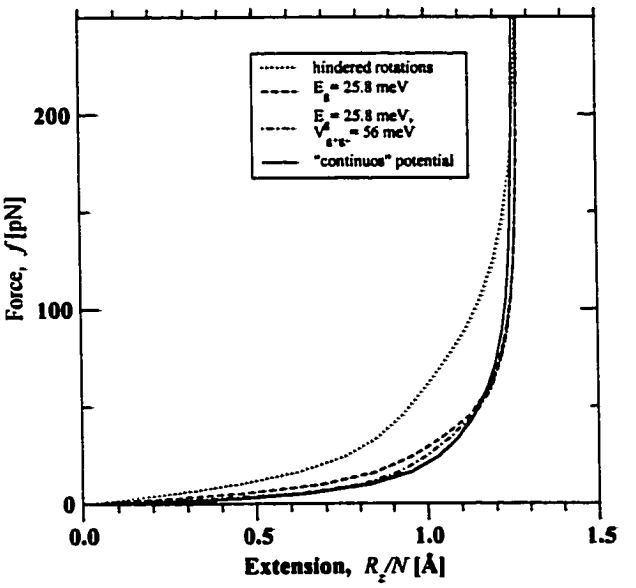

Figure 5.27: Force-extension curves for long alkane chains ($N > 200$) in the various models with parameters specified in the legend.

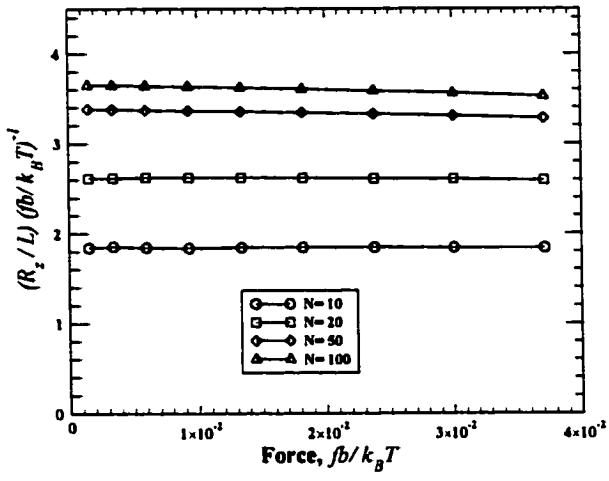

Figure 5.28: Slopes of the force-extension curve as a function of the force in the small force regime for alkanes with chain lengths indicated in the caption.

chain length was chosen to be relatively long ($N = 50$) with respect to the persistence length of the model. We note that there are still some very pronounced discretization effects for $M_\alpha = 10$, while for $M_\alpha = 20$ and 30 we see a convergence of results indicating that the discretization effects are greatly diminished.

A scaling analysis of the characteristic ratio with respect to the chain length is performed in Figure 5.30. Due to long computational time taken by this analysis, only the mesh parameter $M_\alpha = 10$ was used. We would like to comment that for the chain with continuous rotational potential C_N exhibits a more pronounced dependence on the temperature than the corresponding RIS model. The experimental value of $C_\infty = 6.7 \pm 0.3$[27, 28, 29, 30] is not recovered as in the RIS model (after corrections that compensate for discretization effects, we obtain 4.5 ± 0.5). This underestimation is mainly due to the fact that we neglected the interactions between monomers four and more bonds apart along the chain. As we saw in the previous section, Figure 5.7, the presence of the interactions (e.g. V_{g+g-}) leads to a stiffening of the chain and therefore to a pronounced increase of the characteristic ratio.

Figure 5.31 shows the modified form of the force-extension curve $(1 - R_Z/L)^{-1}$ versus fb/k_BT in the limit of long chains ($L \gg l_P$).We can now make a quantitative

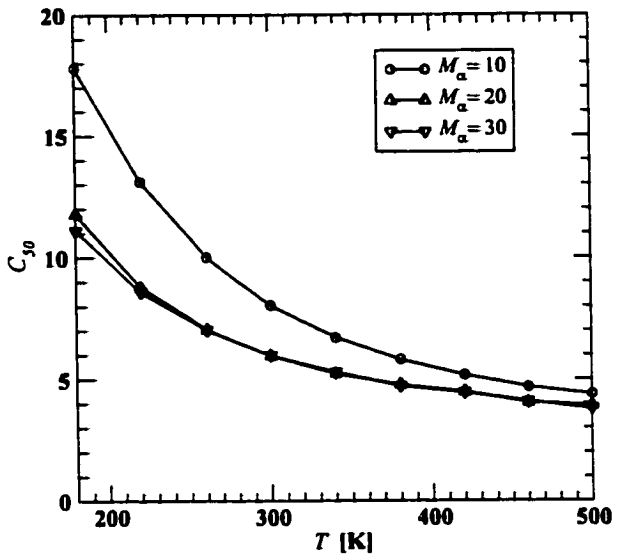

Figure 5.29: Scaling analysis of the dependence of the characteristic ratio of n-alkanes on the temperature with the mesh parameter M_α, whose values are indicated in the legend. The chain length is $N = 50$.

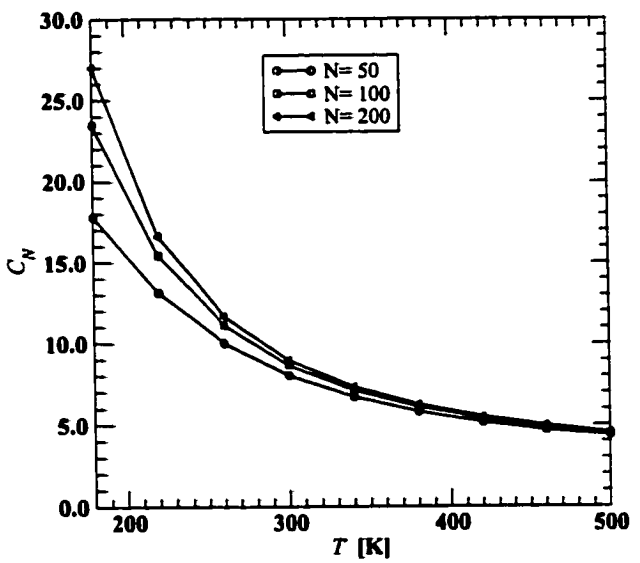

Figure 5.30: The characteristic ratio of alkanes versus temperature for three different chain lengths specified in the legend. Mesh parameter $M_\alpha = 10$.

comparison between this model and the RIS, FJC and FRC models. In the large-force regime, in contrast with the RIS, but with some similarity also to the FRC, the chain with continuous rotational potential exhibits a behavior similar to the FJC model in that

$$\frac{R_z}{L} = 1 - \left(\frac{cfb}{k_B T}\right)^{-1}, \tag{5.36}$$

where c is a coefficient whose particular value is specific to a given model. In other words, the curves plotted here become parallel in the region of large forces. In Chapter 4, we saw that for the FRC the value of this coefficient is $c = 2$. For n-alkanes, we estimate with the help of the curves in Figure 5.31 that this coefficient is about 20 for $M_\alpha = 10$ and 10 for $M_\alpha = 20$. In contrast, the RIS model exhibits in this regime a behavior of the form

$$\frac{R_z}{L} = 1 - \left(\frac{cfb}{k_B T}\right)^{\nu}, \tag{5.37}$$

with $\nu = -3$ and $c = 1$, as seen in eq. 5.33. We should comment that the softness of the RIS model in this regime relative to the FRC and FJC, reflected in a higher magnitude of the exponent ν is a non-physical effect, due to the small number of rotational states allowed in the model. Thus, we conjecture that in real polymers one could fit the large-force behavior to eq. 5.36, rather than to the corresponding result for the RIS model.

5.4 Conclusion

In this chapter we went a step further towards the study of real polymers by incorporating the effects of the bond rotational potential. We proceeded gradually, by first accounting only for the hindered rotations within the RIS approximation and then introducing energy parameters associated with the three possible bond states. Then we introduced more rotational states that accurately sample the continuum of the rotational potential curve. For this last model, we neglected the intrachain interactions between monomers more than four bonds apart.

We adapted the TM method to study this model in both Helmholtz and Gibbs ensembles. We tested the accuracy of the method and found it to be satisfactory for all purposes needed here. Some shortcomings are present for the TM in the

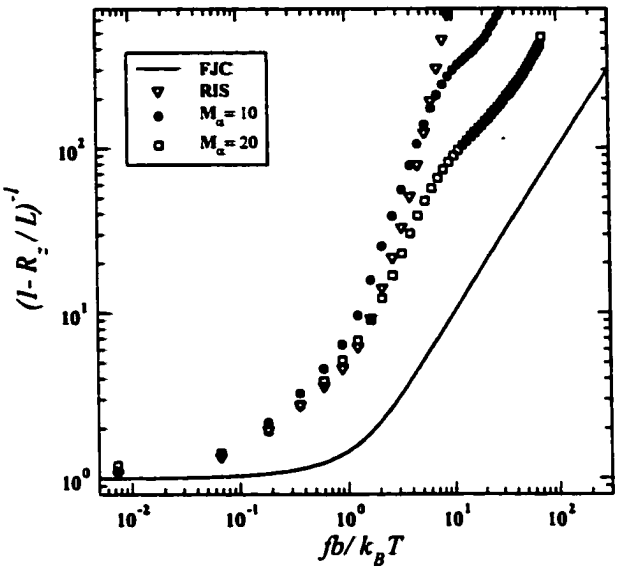

Figure 5.31: Plot of the modified force-extension curve in logarithmic axes for rotational potentials with parameter M_α specified in the legend for long chains. Also shown for comparison are the corresponding curves for RIS and FJC models.

Helmholtz ensemble, emerging from the size of the matrices involved in computations, that require much time and computer memory, especially for the study of very long chains. For the continuous potential model, we concentrated more on the Gibbs ensemble, given that the feasibility of the method is not restricted there so much by the finiteness of computational resources as for the Helmholtz ensemble.

We studied the influence of the model parameters in the statistical properties such as the characteristic ratio, radius of gyration, static structure factors, radial distribution, temperature coefficients, force-extension curve and the persistence length of the molecule. Close agreement was obtained with findings in other experimental and theoretical investigations. Overall our method performs well and gives insightful information in the statistical properties of polymers.

CHAPTER 6

INTERACTING CHAIN MODEL FOR POLY(ETHYLENE GLYCOL)

Poly(ethylene glycol) consists of a sequence of ethylene glycol, **EG,** subunits where **EG** denotes the group $(-O-CH_2-CH_2-)$. The theoretical study of a single poly(ethylene glycol) chain presents an additional challenge when compared to the molecular models approached in previous chapters. The impediment resides in that this molecule features two different types of bonds along its backbone, $C-C$ and $C-O$. Furthermore, the intrachain interactions have seemingly a longer range than those in simpler chains, like n-alkanes. For instance, there is clear evidence[12, 13] that two adjacent **EG** subunits strongly interact when in opposite *gauche* states. This adds considerable difficulty to the solving of the configurational statistics for this molecule.

Two approaches to this problem have been developed. One is to perform quantum chemical calculations on small PEG chains and use them to construct force fields for use in Molecular Dynamics simulations. This avenue has been pursued, among many others, by Smith and coworkers[56, 57] to study the structure and dynamics of PEG melts and by Bandyopadhyay[58] et al. for PEG in water. These studies are limited to relatively short chains, up to 12 **EG** subunits.

In another approach to the polymer problem that dates back half a century[2] one sets up a simple model whose solution is amenable to statistical mechanics. Because we are mainly interested in the stretching behavior of single molecules the latter approach is more appealing and will be pursued in this chapter. By treating the molecule as an RIS chain[2, 7], one can employ the statistical weight matrix method proposed by Eyring[31] to calculate mean square moments (end-to-end distance, radius of gyration) and related quantities for this chain. However, other quantities, such as end vector distribution functions and force-extension curves, are not obtainable by this method.

Stimulated by advances in single molecule experiments, the theoretical front also registered considerable progress. Recently, the stretching of PEG molecules[12, 13] was studied starting from ab initio quantum mechanical calculations on short segments (up to four subunits) of PEG and the results were found to be consistent with the experiment. The statistical mechanics analysis of macromolecules in an AFM[14] was carried out for PEG chains with lengths ranging from 3 to 21 **EG** subunits. The methods used there have the merit of providing exact results, but they are difficult to apply to the long chain limit, which is the condition in the experimental study[6]. This chapter is dedicated to extending the statistical mechanical treatment to long PEG molecules, with focus on the mechanical equation of state and related properties.

Whereas the standard RIS model treats the individual bonds as subunits, we will argue in this chapter that an Interacting Chain Model (ICM) can be set up in which the **EG** subunits of PEG themselves are treated as the repeat subunits. This is based on the findings from ab initio calculations that the $C-O$ bonds are predominantly in the trans configuration while for the $C-C$ bonds we must account for a rotational potential with three minima, *trans, gauche* + and *gauche* −. This reduces the number of accessible conformers significantly but, in contrast to the standard RIS model, allows us to include (*i*) variable subunit lengths, (*ii*) more rotational states (up to seven in this work) and (*iii*) longer ranged interactions along the chain. Most of the content of this chapter is based on the work coauthored in reference [24]. Our programme is as follows:

1. We will use the results of ab initio quantum chemical calculations for the energetically lowest conformers of short chains of up to 4 (EG) subunits to extract the geometrical information such as bond lengths, bond angles and dihedral angles needed for the ICM approximation, see Section *6.1.*

2. From the ab initio calculations for short chains we can also extract the self energies of the **EG** subunits and the interaction energies between pairs of adjacent **EG** subunits needed for the 3-state ICM for molecules of any length, see Section *6.2.* We will also generalize the RIS approximation to include further rotational states in addition to those at the potential minima of each **EG** conformer, see Section *6.3.*

3. Turning to the statistics of long polymer chains we will consider both the Helmholtz and Gibbs ensembles, but we will argue in favor of the latter. An exact evaluation is possible for PEG molecules with up to about $N \approx 20$ subunits in the 3-state model by constructing all 3^N conformers explicitly.

4. To obtain the statistics of long chains we develop the transfer matrix method in the Gibbs ensemble, i.e. in the presence of an external force. This will allow us to calculate all macroscopic properties of long chains such as the force-extension curve (the mechanical equation of state of a long molecule), the chain end distribution functions, probabilities of rotational states and the persistence length, see Section *6.4*.

In Section *6.5* we will present numerical results. For short chains of up to 21 subunits we will compare the results obtained by the transfer matrix method with those obtained by the exact evaluation of the Gibbs partition function. We analyze the effect of the variation of geometrical and energy parameters in the model, as well as the effect of chain length on our final results. We show that the infinite chain length limit is reached beyond 200 subunits. Chain end distribution functions, probabilities of rotational states and the persistence length are calculated. Additional rotational states beyond those of the potential minima used in the RIS approximation as described in Section *6.3*, can be included for a more accurate description. Finally we show that the force-extension curve, calculated with the 7-state ICM, reproduces the experimental results very well.

6.1 Ab Initio Results for Short Chains of Poly(ethylene glycol)

In a recent paper[17] extensive ab initio calculations were reported for $(\mathbf{EG})_n$ with $n = 2, 3, 4$ and its interaction with water, using density functional theory with nonlocal gradient corrections. By necessity, one is restricted in such calculations to a tractable number of conformers which, however, must be chosen such that they are representative of those states accessible at room temperature. It was shown in the previous study that most low energy conformers have the $C - O$ bonds in the trans configuration and the $C - C$ bonds in trans and clockwise and anticlockwise gauche configurations, resulting in three states of the **EG** subunit, (tg^+t), (tg^-t) and (ttt),

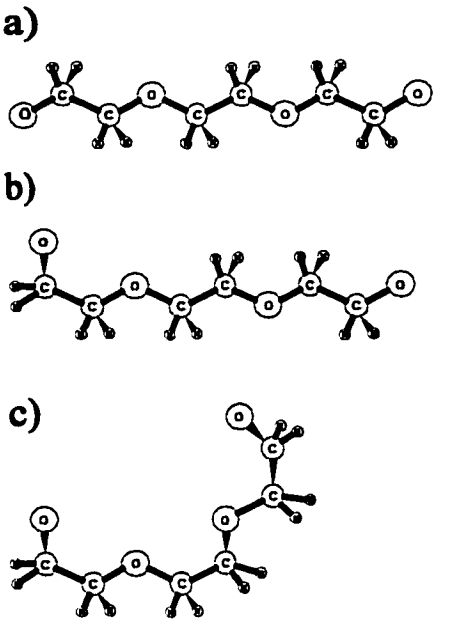

Figure 6.1: Stereochemical diagrams of three conformers of $(EG)_3$ segments, $(t|t|t)$ in panel (a), $(g^-|t|t)$ in panel (b) and $(g^-|g^+|g^+)$ in panel (c).

to be placed on N positions along the chain of $\mathbf{(EG)}_N$, for a total of 3^N combinations or conformers of the molecule. For a simpler notation we will drop the reference to the trans configuration of the $C-O$ bonds so that, as examples the all-trans and helical conformers of $\mathbf{(EG)}_3$ are denoted by $(t|t|t) = (ttt - ttt - ttt)$ and $(g^+|g^+|g^+)$ $= (tg^+t - tg^+t - tg^+t)$, respectively. In Figure 6.1, we depict for better visualization, the stereochemical configurations of three representative conformers of $\mathbf{(EG)}_3$. Of the 27 such conformers of $\mathbf{(EG)}_3$ only 10 are energetically different because, as an example, the energies $E(g^+|g^+|g^+) = E(g^-|g^-|g^-)$ are the same.

In Table 6.1 we list the ground state energies for the ten energetically different, conformers of $\mathbf{(EG)}_3$. The energies are relative to that of the helical conformer, e.g. $E(t|t|t) = E_t(t|t|t) - E_t(g^+|g^+|g^+)$, because it is only their relative stability that determines which conformers are likely to be present in a given environment.

All conformers except those with neighboring $(g^+|g^-)$ pairs have about equal energy, with the helical $(g^+|g^+|g^+)$ conformer the most stable (by a margin), in agreement with experiment and previous theoretical work on the density driven transition

$(\mathbf{EG})_3$	E[kJ/mol]	O_1–O_4	C_1–C_8	O_1-O_3	O_2-O_4	D[Debye]
$(t\|t\|t)$	0.68	10.70	13.07	7.12	7.12	0.0
$(t\|t\|g)$	0.55	9.78	12.23	6.38	7.12	1.41
$(t\|g\|t)$	0.15	9.58	11.11	6.40	6.39	0.17
$(g^+\|t\|g^+)$	0.74	8.82	11.39	6.38	6.38	1.70
$(g^+\|t\|g^-)$	0.48	9.26	11.79	6.38	6.39	0.11
$(g^+\|g^+\|t)$	0.08	8.92	10.60	5.83	6.37	1.45
$(g^+\|g^+\|g^+)$	0.0	8.61	10.44	5.79	5.81	0.95
$(g^+\|g^-\|t)$	1.92	7.99	9.34	5.21	6.39	1.33
$(g^+\|g^+\|g^-)$	2.01	7.19	8.73	5.71	5.06	1.37
$(g^+\|g^-\|g^+)$	4.46	6.24	7.32	5.18	5.17	1.27

Table 6.1: Energies of the inequivalent groups of conformers of $(EG)_3$ relative to the helical conformers. Also listed are the lengths, given either as the distance between terminal oxygen or carbon atoms, and the distances between pairs of next nearest oxygen atoms, in Ångstroms. The last column lists the total dipole moments[12].

from the helical to the all-trans conformers[18] and on the effect of high electrostatic fields on $(\mathbf{EG})_3$ and $(\mathbf{EG})_6$[19, 20]. However, those conformers with neighboring gauche **EG** units with opposite dihedral rotational angles, i.e. g^+ next to g^- , are energetically very unfavorable. The reason[17] is that, although the distances between subsequent oxygen atoms along the chain remains almost the same (2.96 Å for $(g^+|g^+|g^+)$, 2.97 Å for $(g^+|g^+|g^-)$, and 2.99 Å for $(g^+|g^-|g^+)$), the distance between at least one pair of next nearest neighbor oxygens is reduced considerably from a value of 5.81 Å for $(g^+|g^+|g^+)$ to only 5.17 Å between the second and fourth oxygens in $(g^+|g^+|g^-)$, whereas for $(g^+|g^-|g^+)$ such a reduction is observed for the distances between the first and the third, and between the second and the fourth oxygen atoms. This leads to an enhanced repulsion between these (partially charged) oxygens, enhanced also by the fact that the hydrogen atoms on the carbons are turned towards the other side of the molecule. A similar argument applies to the $(g^+|g^-|t)$ conformer in which the distance between the second and fourth oxygens is reduced to 5.21 Å from 5.83 Å in $(g^+|g^+|t)$. It is astounding how close in energy the $(g^+|g^-|t)$ and $(g^+|g^+|g^-)$ conformers are, 1.92 and 2.01 kJ/mol, respectively! Indeed, this net loss in energy for changing a neighboring pair of $(g^+|g^+)$ **EG** subunits to $(g^+|g^-)$ subunits is very close, within less than 5 %, to the energy difference between the $(g^+|g^+)$ and the $(g^+|g^-)$ conformers of $(\mathbf{EG})_2$, and also between the $(g^+|g^+|g^+|g^+)$ and $(g^+|g^+|g^+|g^-)$

conformers of $(\mathbf{EG})_4$. Thus as long as conformers of different lengths in a given sequence differ only by the last subunit, their energy differences are independent of the length of the molecule. However, if a different subunit is built into the middle of the molecule such as for the $(g^+|g^-|g^+)$ conformer of $(\mathbf{EG})_3$, there is a synergetic effect that is obviously absent in $(\mathbf{EG})_2$ but again is more or less the same in $(\mathbf{EG})_3$ and $(\mathbf{EG})_4$.

6.2 Derivation of the 3-State ICM

We can use the results of the ab initio calculations for short polymer molecules to construct a 3-state ICM with nearest neighbor interactions valid for any length of the polymer. By necessity, one loses some details, both structurally and energetically, but it turns out that this loss is by far compensated by the possibility of being able to deal with large molecules.

In the 3-state ICM of PEG we allow individual **EG** subunits to be in three independent conformations, (ttt), (tg^+t), and (tg^-t). We define occupation number vectors, $\mathbf{n}_i$, whose transpose take values $\mathbf{n}_i^T = (100)$, (010) and (001) if the i-th **EG** subunit along the chain is (ttt), (tg^+t) or (tg^-t), respectively. We also define a vector of self-energies $\mathbf{E} = (E_t, E_{g^+}, E_{g^-})$ and a matrix of nearest neighbor interaction energies

$$\mathbb{V}_2 = \begin{pmatrix} V_{tt} & V_{tg} & V_{tg} \\ V_{tg} & V_{gg} & V_{g^+g^-} \\ V_{tg} & V_{g^+g^-} & V_{gg} \end{pmatrix}. \tag{6.1}$$

We then write the total potential energy of a chain of N **EG** subunits as

$$U_N(\mathbf{n}_1, \mathbf{n}_2, .., \mathbf{n}_N) = E_s + \sum_{i=1}^{N} \mathbf{E} \cdot \mathbf{n}_i + \sum_{i=1}^{N-1} \mathbf{n}_i^T \cdot \mathbb{V}_2 \cdot \mathbf{n}_{i+1}. \tag{6.2}$$

E_s is the energy of the two terminating groups, either methoxy or hydroxy, at each end of the chain. The degeneracies among conformers imply restrictions on the model parameters. For instance, the fact that helical conformers with all clockwise or all anticlockwise rotations around the $C-C$ bonds are degenerate implies that $E_{g^+} = E_{g^-} = E_g$ and $V_{g^+g^+} = V_{g^-g^-} = V_{gg}$. Also, all conformers are degenerate in

energy that do not have a g^+ and a g^- subunit next to each other, such as, for $(\mathbf{EG})_3$,

$$\begin{aligned} E(t|g^+|t) &= E(t|g^-|t), \\ E(t|t|g^+) &= E(t|t|g^-). \end{aligned} \tag{6.3}$$

so that $V_{tg^+} = V_{tg^-} = V_{tg}$. This latter symmetry in the ICM with nearest neighbor interactions only, implies degeneracies that are not present in the ab initio calculations. For instance for $(\mathbf{EG})_3$ we find five relationships between the model energies of the conformers, namely

$$(0.48)E^{(nn)}_{g^+tg^-} = E^{(nn)}_{g^+tg^+}(0.74) \tag{6.4}$$

$$(0.36)2E^{(nn)}_{ttg} - E^{(nn)}_{g^+tg^+} = E^{(nn)}_{ttt}(0.68) \tag{6.5}$$

$$(-0.44)2E^{(nn)}_{g^+g^+g^-} - E^{(nn)}_{g^+g^-g^+} = E^{(nn)}_{g^+g^+g^+}(0.0) \tag{6.6}$$

$$(0.01)2E^{(nn)}_{tg^+g^+} - E^{(nn)}_{tgt} = E^{(nn)}_{g^+g^+g^+}(0.0) \tag{6.7}$$

$$(3.69)2E^{(nn)}_{tg^-g^+} - E^{(nn)}_{tgt} = E^{(nn)}_{g^+g^-g^+}(4.46). \tag{6.8}$$

The numbers in brackets are energies (in *kJ/mol)* from the ab initio calculations and show that keeping only nearest neighbor interactions is a satisfactory approximation. However, it must be stressed that these five relations imply that we have only five independent conformers from which we can determine the six parameters of the chain model. This by itself is not surprising because we need only relative energies, and we will choose the self energy of the helical conformer as the energy zero.

The self energies and the nearest neighbor interactions are determined from the ab initio calculations of short $(\mathrm{EG})_n$ chains. Ideally, the length of the chain must be chosen such that adding another **EG** subunit will yield more or less identical results from the ICM and from the ab initio calculations. As we outlined in the introduction we have only ab initio results for $(\mathbf{EG})_n$ for $n = 2, 3, 4$. It turns out that using the 27 conformers of $(\mathbf{EG})_3$ gives excellent results.

In Table 6.2 we list the contributions of the self energies and nearest neighbor interactions to the group of 10 energetically different conformers of $(\mathbf{EG})_3$ and four

$(EG)_n$ conformer	E_s	E_t	E_g	V_{tt}	V_{gg}	V_{tg}	$V_{g^+g^-}$
$(t\|t\|t)$	1	3		2			
$(t\|t\|g)$	1	2	1	1		1	
$(t\|g\|t)$	1	2	1			2	
$(t\|g^+\|g^+)$	1	1	2		1	1	
$(t\|g^-\|g^+)$	1	1	2			1	1
$(g^+\|t\|g^+)$	1	1	2			2	
$(g^+\|t\|g^-)$	1	1	2			2	
$(g^+\|g^+\|g^-)$	1		3		1		1
$(g^+\|g^-\|g^+)$	1		3				2
$(g^+\|g^+\|g^+)$	1		3		2		
$(t\|t\|t\|t)$	1	4		3			
$(t\|t\|t\|g)$	1	3	1	2		1	
$(g^+\|g^+\|g^+\|g^+)$	1		4		3		
$(g^+\|g^+\|g^+\|g^-)$	1		4		2		1

Table 6.2: Contributions of the self energies and nearest neighbor interactions to the conformers of $(EG)_3$ and $(EG)_4$.

conformers of $\mathbf{(EG)_4}$. The entries in this table are exactly the coefficients that each energy parameter must be multiplied by in order to obtain the conformational potential energy of each conformer in the first column, as prescribed by eq. 6.2.

As we discussed above, there are only five independent conformers left to determine the five model parameters (relative to $E_g = 0$) in the chain model with nearest neighbor interactions, and there is no further rule to select those five conformers, i.e. to reject the remaining five. We have approached this problem as follows. In Table 6.3 we compile three sets of values to reveal the importance of each parameter in discussion: set 1 neglects all energy and interactions; in set 2 we have included only the "pentane effect", the g^+g^- interaction; and in set 3 we have done a least squares fit of the five model parameters to all ten conformers of $\mathbf{(EG)_3}$. We also find that parameters in set 3 reproduce the energies of the four conformers of $\mathbf{(EG)_4}$ to better than ten percent.

So far we have only considered the energetics of the interacting chain model determining nearest neighbor interaction parameters from ab initio calculations of short polymer molecules. Because polymer chains are not linear but one-dimensional structures in three-dimensional space it is of equal importance to specify the geometrical

Parameter	Set1[meV]	Set2[meV]	Set3[meV]
$E_t - E_g$	0.0	0.0	-5.60
V_{tt}	0.0	0.0	11.70
V_{tg}	0.0	0.0	-0.15
V_{gg}	0.0	0.0	5.80
V_{g+g-}	0.0	20.0	22.14

Table 6.3: Self energies and nearest neighbor interactions. Set1: no energy parameters. Set2: a simple parametrization, which includes only the "pentane effect". Set3: least squares fit to all ten conformers of $(EG)_3$.

characteristics, i.e. bond lengths, bond angles and dihedral angles. Again, we do this for the **EG** subunits as a whole rather than for the individual $C-C$ and $C-O$ bonds within a **EG** subunit.

We proceed by listing the subunit lengths of the g and t subunits in all the conformers of $\mathbf{(EG)_3}$ and then take averages. Similarly we look at all the bond angles between $(g|g)$, $(g|t)$, $(g^+|g^-)$ and $(t|t)$ neighboring pairs in all the conformers and again determine their averages. Lastly, we determine the dihedral angles in all the conformers of $\mathbf{(EG)_3}$. In Table 6.4 we list these parameters.

The fact that the variation in the bond lengths and bond angles within the group of all conformers of $\mathbf{(EG)_3}$ is so small, justifies, a posteriori, our attempt to characterize the **EG** subunits themselves rather than the covalent bonds. Together with the energies listed in Table 6.3, these geometric factors in Table 6.4 specify the ICM for PEG completely. But before we proceed to the statistical mechanics we generalize the RIS approximation to include more rotational states.

6.3 Generalization of the Interacting Chain Model

In real polymers, the spectrum of rotational states is not discrete. The dihedral angles φ of each subunit can assume, with appropriate statistical weights, any value between 0 and 2π. The weights must reflect the fact that the rotational potential is not flat, as assumed in the freely rotating chain approximation, but typically has a parabolic shape around a minimum with finite barriers to the next conformer as can be seen in Figure 6.2. In the 3-state ICM, as outlined above, only the minima of the potential energy curves of $\mathbf{(EG)_3}$ were used, implying fixed dihedral angles for

Sequence	Subunit length [Å]	Bond angle[°]	Dihedral angle[°]
g	2.93±0.15		
t	3.61		
$(g\|g)$		26.0±1.0	
$(g^+\|g^-)$		60.3±0.6	
$(g\|t)$		28.4±1.6	
$(t\|t)$		20.2±0.1	
$(g^+\|g^+\|g^+)$			102.4
$(g^+\|g^+\|g^-)$			34.4
$(g^+\|g^+\|t)$			15.5
$(g^+\|g^-\|g^+)$			35.45
$(g^+\|g^-\|t)$			55.16
$(g^+\|t\|g^-)$			-173.92
$(g^+\|t\|g^+)$			-12.29
$(t\|g^\pm\|t)$			$\mp$85.66
$(t\|t\|g^\pm)$			±75.61
$(t\|t\|t)$			180.0

Table 6.4: Geometrical parameters of EG units as determined from ab initio calculations[12].

the 10 conformers as given in Table 6.4. As we will see when presenting numerical results, this gives a qualitative fit to the measured force-extension curve. However, a straightforward generalization of the RIS approximation to include more rotational states will give quantitative agreement with experiment. In principle we are in a position to include a continuum of such rotational states because we have the complete potential energy curves for the relevant conformers of $\mathbf{(EG)_3}$ as a function of chain length, see Figure 6.2[12]. This is equivalent to having the energy as a function of dihedral angle as long as bond lengths and bond angles remain unchanged, which is the case for all but the all-trans configuration. However, to retain the simplicity of an ICM with a discrete number of conformers we add only a small number of additional rotational states.

To incorporate further rotational states in our model, we must know their self-energies and mutual interactions between neighbors along the chain (as in Table 6.3), as well as their geometrical parameters (specified in Table 6.4). This is a non-trivial task, considering the ambiguities we have already encountered in extracting energetic and geometrical parameters for the **EG** subunits when only the energy minima of the

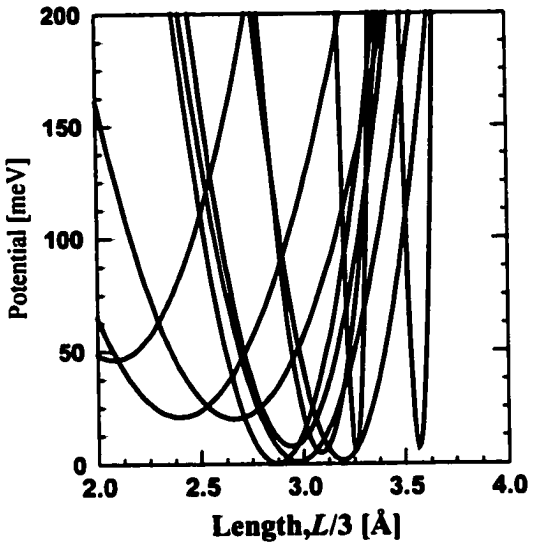

Figure 6.2: Potential energy curves of the ten energetically different $(EG)_3$ conformers versus their lengths from left to right according to their minima: $(g^+|g^-|g^+)$, $(g^+|g^+|g^-)$,$(g^+|g^-|t)$, $(g^+|g^+|g^+)$, $(g^+|g^+|t)$, $(g^+|t|g^+)$, $(g^+|t|g^-)$, $(t|g^+|t)$, $(g^+|t|t)$, $(t|t|t)$[13, 12].

potential energy curves are included in the model.

While the geometrical parameters of **EG** subunits within each possible conformer of $(\mathbf{EG})_3$ appearing in Figure 6.2 could be easily obtained for any length of these conformers, extracting the corresponding potential curves for the rotation states of a **EG** subunit from that data is again an overdetermined problem. We can still optimize the quasi-solution, but we expect that the more states of **EG** we include, the poorer the optimization will be.

For example, suppose that the $(\mathbf{EG})_3$ molecule can assume a small number of additional states. A simple choice is to take two further points, one on each side of the minima. Furthermore, we assume that within these new conformers, each **EG** subunit stretches out or is compressed in the same way as each conformer of $(\mathbf{EG})_3$. In that case, we have to include a total of four additional rotation states of an **EG** subunit. These are: stretched g^+, g^- and compressed g^+, g^-, which we denote $g_s^{\pm}$ respectively $g_c^{\pm}$. Because for the *trans* subunit the dihedral angle is optimal for any length, the variation in the $(t|t|t)$ conformer in Figure 6.2 is entirely due to $(t|t)$ bond angle bending. We have ignored this degree of freedom because it requires

forces far outside the experimental range. Due to the approximate symmetry of g^+ and g^- states, the variation of rotation angles corresponding to these states upon stretching/compression is roughly equal and opposite. Thus the generalization of the RIS approximation takes the number of rotational states from 3 to 7 states generating 7^3 conformers of $(\mathbf{EG})_3$ to approximate the continuum (as a function of length or dihedral angle) of the 3^3 conformers represented in Figure 6.2. Within our assumption, there is a unique correspondence between the length variation $\pm\Delta L$ of a given $(\mathbf{EG})_3$ conformer about its potential minimum, and the variation $\pm\Delta\phi$ of dihedral angles of the $C-C$ bonds inside the gauche **EG** subunits of that conformer. Thus the additional states $g_s^\pm$ and $g_c^\pm$ are characterized by the same variation $\pm\Delta\phi$ which becomes a parameter of our 7-state model.

If we try to extract the model parameters by means of a system of linear equations, analogous to the one in eq. (6.2), we will get a total of 30 algebraic linear equations (3 for each conformer in Figure 6.2) with 5 unknowns. To reduce the redundancy we assume that the interactions between neighbors along the chain will take the values in Table 6.3 for the rotational states at the potential minima, for instance $V_{g_s^+ g_c^-} = V_{g^+ g^-}$ etc. For the determination of the self-energies of $g_s^\pm$ and $g_c^\pm$ we simply increased the energy of $g^\pm$ by the same amount E' which we treat as an adjustable parameter. This concludes the construction of the 7-state ICM.

6.4 Transfer Matrix for the Gibbs Ensemble

Next the transfer matrix method will be implemented for the statistical treatment of long PEG chains. We assume that the chain is placed in a $\theta-$solvent so that the volume interactions and the monomer-solvent interactions mutually cancel out. In this situation, the only factors to be considered are the self energies of chain subunits, the nearest-neighbor interactions and the action of the external force.

The Green function for this problem satisfies the integral equation 2.4, where the transfer matrix, $\mathbf{T}(\Gamma_i, \Gamma_{i+1})$ reads

$$\mathbf{T}(\Gamma_i, \Gamma_{i+1}) = \mathbf{C}(\Gamma_i, \Gamma_{i+1}) \exp[(f s_{i+1} \cos\theta_{i+1} - E_{\alpha_{i+1}} - E_{\beta_{i+1}} - V_{\alpha_{i+1}\beta_i} - V_{\alpha_{i+1}\beta_{i+1}})/k_B T]. \tag{6.9}$$

Unlike previously approached models, this time the notation Γ_i designates the coor-

dinates of a sequence of six covalent bonds—two **EG** monomers—which we regard as a *virtual bond* of our chain. This is required in order to incorporate the nearest neighbor interactions in our analysis. The initial condition (the probability distribution function for the first virtual bond) reads

$$G_1^f(\Gamma_1) \propto \exp\left(\frac{fs_1\cos\theta_1 - E_{\alpha_1} - E_{\beta_1} - V_{\alpha_1\beta_1}}{k_BT}\right)\sin\theta_1 \tag{6.10}$$

6.4.1 Calculating the Connectivity Operator

There is a close similarity between the algorithm used in the study of alkanes in the previous chapter and the one that will follow here for the study of PEG. Like there, in order to find the connectivity operator **C** in eq. 6.9 we have to account for the geometrical restrictions of the bond lengths, rotational angles and bond angles characteristic for the RIS model.

As for alkanes, Figure 5.15 serves as a good representation for the vector geometry of a PEG segment in an external force. When looking at this diagram, we must bear in mind that within our PEG model there is an important difference from the case of alkanes: the vectors $\mathbf{a}_i, \mathbf{b}_i, \mathbf{a}_{i+1}, \mathbf{b}_{i+1}$ shown there correspond to entire **EG** monomers and not bond vectors. Each of these vectors has its ends at the locations of consecutive oxygen atoms in the molecule. Consequently, their lengths vary with the state assumed by that monomer. Furthermore, the bond angles depend on the states of a pair of adjacent monomers and the rotational angles depend on the states of a trio of consecutive monomers. This further complicates the treatment of this model and requires appropriate modification of the method used in the previous chapter.

We will take the vectors $\mathbf{s}_i = \mathbf{a}_i + \mathbf{b}_i$ as the basis for implementing the Transfer Matrix method. Note that this time, the index i numbers a pair of subunits (and thus runs from 1 to $N/2$, assuming N even) and not only a single monomer. The most convenient choice for describing the orientation of $\mathbf{s}_i$ is the coordinate set given by $\Gamma_i = \{\theta_i, \psi_i, \alpha_i, \beta_i\}$, which consists of:

- θ_i, the angle formed by the subunit vector $\mathbf{s}_i$ with the force $\mathbf{f}$, with range $[0, \pi]$;
- ψ_i the dihedral angle formed by the planes $(\mathbf{a}_i, \mathbf{s}_i)$ and $(\mathbf{s}_i, \mathbf{f})$, with range $[-\pi, \pi)$;

- α_i the rotational state corresponding to subunit vector $\mathbf{a}_i$ (i.e. one of the t, g^+, g^- states);
- β_i the rotational state corresponding to subunit vector $\mathbf{b}_i$ (i.e. one of the t, g^+, g^- states);

To compute $\mathbf{C}$, one has to find, from geometrical considerations, the orientation of the $\mathbf{s}_{i+1}$ vector when the orientation of $\mathbf{s}_i$ and the rotation states of the vectors $\mathbf{a}_i, \mathbf{b}_i, \mathbf{a}_{i+1}, \mathbf{b}_{i+1}$ are known. With the choice of the coordinate set above, the connectivity operator becomes

$$\mathbf{C}(\Gamma_i, \Gamma_{i+1}) = \delta[\theta_{i+1} - g_\theta(\Gamma_i, \Gamma_{i+1})]\delta[\psi_{i+1} - g_\psi(\Gamma_i, \Gamma_{i+1})], \tag{6.11}$$

where the functions $g_\theta(\Gamma_i, \Gamma_{i+1})$ and $g_\psi(\Gamma_i, \Gamma_{i+1})$ are yet to be determined. Similarly with the procedure in the previous chapter, we refer back to eq. 5.4, where we denote $\mathbf{t}(\varphi, \gamma)$ as the rotation matrix with dihedral angle φ and bond angle γ. Next, we calculate the vectors $\mathbf{a}_i, \mathbf{b}_i, \mathbf{a}_{i+1}, \mathbf{b}_{i+1}, \mathbf{s}_i, \mathbf{s}_{i+1}$ in a common frame chosen as $Ox_0y_0z_0$ in Figure 5.15, for which we employ the rotation matrices in the list below:

- $\mathbf{t}_0 \equiv \mathbf{t}(\psi_i, \gamma'_{\alpha_i\beta_i})$, corresponding to vector $\mathbf{s}_i$;
- $\mathbf{t}_1 \equiv \mathbf{t}(\pi, \gamma_{\alpha_i\beta_i})$, corresponding to vector $\mathbf{a}_i$;
- $\mathbf{t}_2 \equiv \mathbf{t}(\varphi_{\alpha_i\beta_i\alpha_{i+1}}, \gamma_{\beta_i\alpha_{i+1}})$, corresponding to vector $\mathbf{b}_i$;
- $\mathbf{t}_3 \equiv \mathbf{t}(\varphi_{\beta_i\alpha_{i+1}\beta_{i+1}}, \gamma_{\alpha_{i+1}\beta_{i+1}})$, corresponding to vector $\mathbf{a}_{i+1}$.

Note that here we have a significantly larger number of parameters: $\gamma_{\alpha_i\beta_i}$ the bond angles characterizing the $(\alpha_i|\beta_i)$ pair; $\varphi_{\alpha_i\beta_i\alpha_{i+1}}$ the dihedral angles characterizing the $(\alpha_i|\beta_i|\alpha_{i+1})$ trio as evaluated in Table 6.4; $\gamma'_{\alpha_i\beta_i} = \sin^{-1}(\sin\gamma_{\alpha_i\beta_i}\,|\mathbf{a}_i| \,/\, |\mathbf{s}_i|)$. With the help of these matrices we get

$$\hat{\mathbf{f}} = \begin{bmatrix} 0 \\ \sin\theta_i \\ \cos\theta_i \end{bmatrix}, \tag{6.12}$$

$$\mathbf{a}_{i+1} = \mathbf{t}_0\mathbf{t}_1\mathbf{t}_2 \begin{bmatrix} 0 \\ 0 \\ |\mathbf{a}_{i+1}| \end{bmatrix}, \tag{6.13}$$

$$\mathbf{b}_{i+1} = \mathbf{t}_0\mathbf{t}_1\mathbf{t}_2\mathbf{t}_3 \begin{bmatrix} 0 \\ 0 \\ |\mathbf{b}_{i+1}| \end{bmatrix}. \tag{6.14}$$

As a result we have

$$g_\theta(\Gamma_i, \Gamma_{i+1}) = \cos^{-1}\left[\frac{\mathbf{s}_{i+1}\cdot\hat{\mathbf{f}}}{|\mathbf{s}_{i+1}|}\right], \tag{6.15}$$

$$\cos\left[g_\psi(\Gamma_i, \Gamma_{i+1})\right] = \frac{\hat{\mathbf{f}}\times\mathbf{s}_{i+1}}{\left|\hat{\mathbf{f}}\times\mathbf{s}_{i+1}\right|}\cdot\frac{\mathbf{s}_{i+1}\times\mathbf{a}_{i+1}}{|\mathbf{s}_{i+1}\times\mathbf{a}_{i+1}|}, \tag{6.16}$$

$$\left|\sin\left[g_\psi(\Gamma_i, \Gamma_{i+1})\right]\right| = \left|\frac{\hat{\mathbf{f}}\times\mathbf{s}_{i+1}}{\left|\hat{\mathbf{f}}\times\mathbf{s}_{i+1}\right|}\times\frac{\mathbf{s}_{i+1}\times\mathbf{a}_{i+1}}{|\mathbf{s}_{i+1}\times\mathbf{a}_{i+1}|}\right|, \tag{6.17}$$

which concludes our task of finding the connectivity operator.

6.5 Results

To evaluate the canonical partition function, $Z_N(\mathbf{R}, T)$ in eq. 1.20, we note that for $(\mathbf{EG})_N$ there are 3^N conformers in the 3-state model, which we denote by the set of dihedral angles of all bonds $\{\varphi_1, \varphi_2, ..., \varphi_N\}$. We proceed by first calculating the end-to-end vectors $\mathbf{r}_N(\{\varphi_1, \varphi_2, ..., \varphi_N\})$, by eq. 5.7, and energies $U_N(\{\varphi_1, \varphi_2, ..., \varphi_N\})$, by eq. 6.2, for all the conformers and store them in an array from which they are recalled when performing the summation in eq. 1.20.

The exact evaluation of the partition function can be done on our computer for short molecules, up to 10 monomers, within a few minutes of processor time. To speed up the enumeration of all conformers, we take the initial building blocks as large as possible (e.g. $(\mathbf{EG})_3$ in our case) and double the chain length successively, storing their energies and lengths in each step, up to $(\mathbf{EG})_{12}$. To obtain the conformers of $(\mathbf{EG})_{21}$, we start from the conformers of $(\mathbf{EG})_{12}$ and $(\mathbf{EG})_9$ and join them appropriately. This procedure turns out to be much more efficient than the straightforward approach of directly joining n **EG** subunit blocks. The exact account of all chain conformers is a time consuming approach and becomes impractical for chain lengths

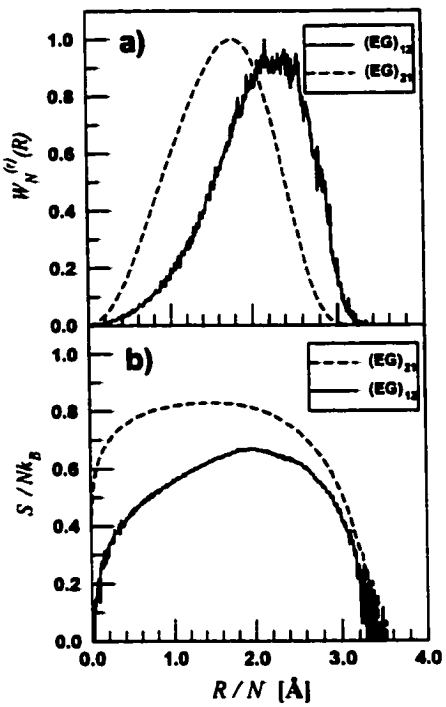

Figure 6.3: End-to-end distribution function (a) and entropy S (b) for $(\mathbf{EG})_{12}$ and $(\mathbf{EG})_{21}$ molecules as functions of length, R, calculated by exact enumeration of all conformers.

larger than $N \approx 20$ (computation time exceeds 10 hours for $N = 21$).

In the transfer matrix calculations we first checked their accuracy by increasing the number of mesh points, M_θ and M_ψ. We found that a mesh with $M_\theta = M_\psi = 40$ (used for the 7-state model) yields an accuracy of $\pm 0.5\%$ or better, while $M_\theta = M_\psi = 100$ (used in the 3-state model) yields an accuracy of better than $\pm 0.2\%$. Such computations took up to 10 hours on our computer for chains 200 **EG** subunits length in the 3-state model, and 48 hours for the 7-state model.

In what follows, we shall present and discuss the results for various thermodynamic and statistical quantities of short and long PEG molecules obtained in the 3-state and 7-state models. All results shown are for $T = 300K$ and for parameter sets 1, 2 and 3. The force-extension curves below obtained by TM are computed exclusively by eq. 2.13.

To begin with we show in Figure 6.3 results for short chains, $(\mathbf{EG})_{12}$ and $(\mathbf{EG})_{21}$, using the exact account of all conformers technique. In panel (a) we show the end-to-

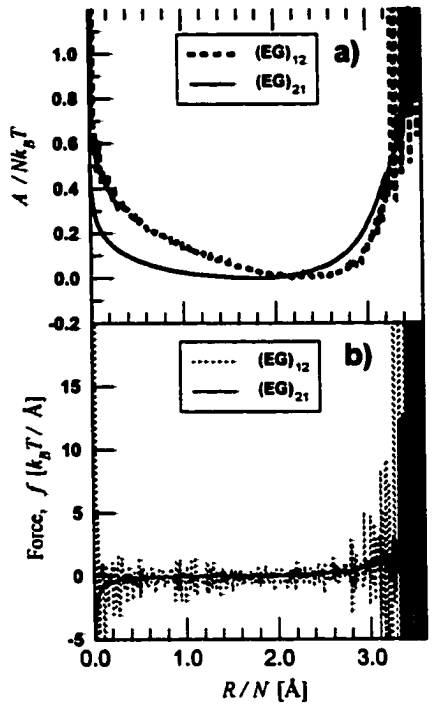

Figure 6.4: Helmholtz free energy A (a) and the average contractile force f (b) of $(\mathbf{EG})_{12}$ and $(\mathbf{EG})_{21}$.

end distribution function calculated from eq. 2.26 as a function of normalized length R/N. The maximum occurs at the most probable length of the chain for which the contractile force, as a derivative of the free energy, is zero. The width is a measure of the length fluctuations which are considerable for such short chains. In panel (b) we show the entropy versus length which is zero for the most unlikely conformations of zero and maximal end-to-end lengths of the chain.

The irregular appearance of the $(\mathbf{EG})_{12}$ curves has its origin in the discrete nature of the end-to-end length spectrum of an ICM molecule, which for this molecule consists of 3^{12} discrete points or conformers with rapidly varying degeneracies. For longer chains, such as $(\mathbf{EG})_{21}$, the irregularities are smoothed out because of the exponential increase in the number of conformers as a function of chain length. From the canonical partition functions in Figure 6.3(a) we can also obtain the Helmholtz free energies, Figure 6.4(a) and, by differentiation, the force-extension curves, i.e. the mechanical equation of state.

Figure 6.5 presents the comparison of the force-extension curves, calculated by the exact and TM methods for the 3-state model of PEG chains $(\mathbf{EG})_{12}$ and $(\mathbf{EG})_{21}$ in panels (a) and (b), respectively. For simplicity, we have selected as model parameters only set 3 and set 2 in Table 6.3, while the exact calculation uses the interaction parameters in set 3 only. The agreement between the two methods is very good.

The curves differ slightly in the intermediate force region. This is attributable to the fact that in the exact enumeration procedure, we used $(\mathbf{EG})_3$ segments as elementary blocks to build up all the conformers of $(\mathbf{EG})_{12}$ and $(\mathbf{EG})_{21}$, while in the TM procedure, we employed **EG** subunits as the elementary blocks. In the exact enumeration, one thus has, as input, the correct ab initio energies of 27 conformers of $(\mathbf{EG})_3$, which leaves as the single source of error the nearest neighbor interaction parameters necessary to join the elementary blocks. (It is unfortunately very difficult to implement the TM method starting with $(\mathbf{EG})_3$ as building subunits due to the very large dimensions of the **T** operator involved in such a computation). Panel (c) shows the length dependence of the force-extension curve for the 3-state chain with parameter set 2. The long chain limit is reached for chains with more than 200 **EG** subunits; the curve will practically remain unchanged (at least within our accuracy limits).

Next we examine the generalization of the 3-state to the 7-state ICM. In Figure 6.6 we show in panels (a) and (b) the force extension curves for $(\mathbf{EG})_{50}$ and $(\mathbf{EG})_{200}$. We choose two values for E', k_BT and $2k_BT$, and vary $\Delta\phi$ between 10^o and 40^o. At small and large forces, all models produce the same force-extension curves, indicating that the persistence lengths for all models are approximately equal. In the low force regime the chain extension is driven mainly by a decrease in its entropy, with no perceptible effects of its internal energy: the stretching is purely entropic. In the large force regime the entropy is essentially zero because all subunits are in the trans configuration and stretching is accompanied by large increases in energy, so that again 3-state and 7-state models give the same results. In contrast, in the intermediate force regime the chain entropy continues to decrease, but its energy increases. Therefore we expect the details of the molecular structure (geometrical and energy parameters) to play a role in the shape of the force-extension curve. Introducing two more subunit conformations for each gauche conformation that are only slightly different in energy ($E' = k_BT$) and not much of a change in the dihedral angle ($\Delta\phi = 10^o$) has a

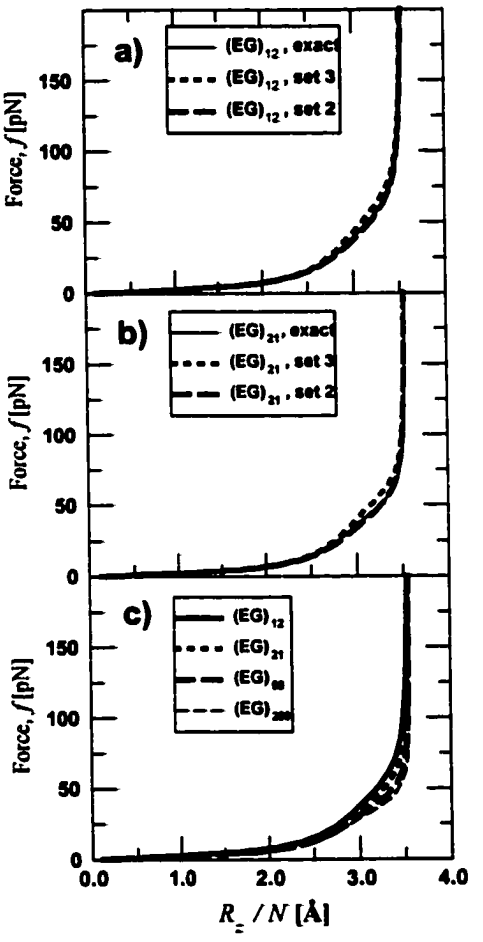

Figure 6.5: Comparison of force-extension curves for the 3-state model obtained by the exact enumeration of all conformers and by the transfer matrix method: $(\mathbf{EG})_{12}$ in panel (a) and $(\mathbf{EG})_{21}$ in panel (b). The force-extension curves for increasing chain lengths up to the asymptotic limit in panel (c). Set 3 and set 2 in the legend are given in Table 6.3. For simplicity, in panel (c), only results for set 2 are displayed.

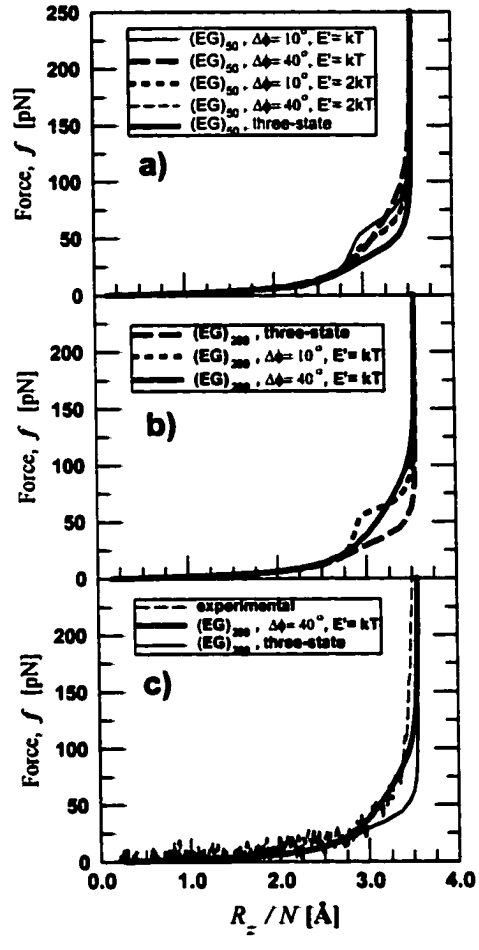

Figure 6.6: Force-extension curves for PEG molecules with 50 and 200 subunits as obtained by the transfer matrix method with parameter set 2: the 3-state and 7-state models for $(\mathbf{EG})_{50}$ with selected $\Delta\phi$ and E' parameters in panel (a), for $(\mathbf{EG})_{200}$ in panel (b); comparison of the three- and 7-state models for $(\mathbf{EG})_{200}$ with the experimental stretching curve for PEG[6] in panel (c).

significant effect by increasing the force necessary to stretch the chain. This is the result of two counteracting effects, namely an increase in the entropy over the 3-state model which would lower the force which is overcompensated by the fact that the newly available states have a higher energy. However, this increase in force in the intermediate regime can be reduced again by increasing the energy cost to $E' = 2k_BT$ and reducing the entropy gain by changing $\Delta\phi$ to 40^o. Such qualitative changes in the force-extension curves can obviously be used to distinguish between chains with different structure and energy on the basis of their stretching curves.

In panel (c) of Figure 6.6 we compare our results for the 3-state and a 7-state model for $N = 200$ with the experimental curve[6] (which was measured for chains of lengths between a few hundred and a few thousand subunits). The agreement is extremely good for all but very high degrees of stretching. The deviation of the TM result from the experimental curve in the region of $f > 100pN$ can be explained on the basis of our previous findings. We have already seen that with the transition from 3 to 7 rotational states the characterization of the stretching behavior is improved. We expect the agreement to improve as we further increase the number of allowed rotational states in an attempt to approach the continuous limit for this degree of freedom (as we noted in previous chapters for the FRC and alkanes).

In Figure 6.7 we plotted the probabilities (average fractions) of g and t states as well as those of all possible pairs in a molecule versus normalized chain length. For small and medium extensions below half the full contour length these probabilities vary slowly with the g and t populations becoming equal close to two thirds of the maximum extension, corresponding to an applied force of $f \approx 14pN$. This is a measure of the supramolecular reorganization[12] of **EG** subunits for forces of this magnitude. The least energetically favorable pair of states, $(g^+|g^-)$, is less probable by an order of magnitude compared to the most preponderant $(t|g)$ pair throughout the entire stretching regime. Note a slight increase of the $(t|g)$ pair probability for extensions up to 2/3 which reflects the evolution of the t state probability in panel a). The following rapid decrease is due to the fact that the g state population subsides with increasing force.

The small force regime behavior is captured in Figure 6.8, where we plot the slopes of the force-extension curves for a variety of chain lengths and parameter sets. As for the other models studied in this work, these slopes are found to be constant for

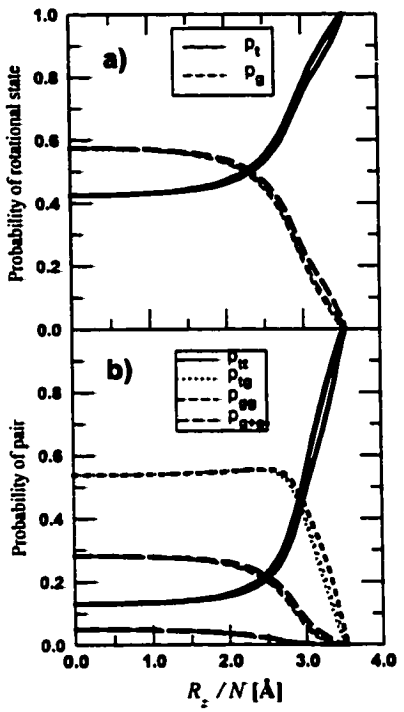

Figure 6.7: Probabilities of rotational states (a), and of pairs of rotational states (b) versus chain extension in PEG molecules with 12, 21 and 200 subunits (plotted in this order respectively in increasingly thick lines), as obtained in the 3-state model with parameter set 3.

small forces, $fb/kT \ll b/l_P$. Another trend is that, as we increase the chain length, the slopes for a given parameter set become practically independent of N. For the longest chain shown here, $(\mathbf{EG})_{200}$, the slopes are approximately equal to $\frac{a}{3}$, see eq. 1.16, where a is the Kuhn length for this model.

Since the contour length of a $(\mathbf{EG})_N$ molecule is $L = Nb_t \cos(\gamma_{tt}/2)$ the characteristic ratio can be expressed (see eq. 1.12) for long PEG chains as

$$C_\infty = \frac{La}{N\overline{b^2}} = \frac{b_t \cos(\gamma_{tt}/2)\, a}{\overline{b^2}}. \tag{6.18}$$

Using the data in Table 6.4 we determined a mean square bond length $\overline{b^2} = 10.07\text{Å}^2$ and the characteristic ratio

$$C_\infty = 0.353a, \tag{6.19}$$

if a is expressed in units of Å.

The Kuhn length of PEG was extracted from the slopes of the force-extension curves in the small-force regime via eq. 1.16, and found to be $a = 19.06$Å, which is close to the average contour length of 6 **EG** monomers and considerably longer than the 7Å used in the phenomenological model based on the extended Langevin function[6]. This finding explains why a freely jointed chain with this bond length gives a good fit to the force-extension curves[13] and it also implies that the persistence length of PEG is about 9.5Å, close to the average contour length of a $(\mathbf{EG})_3$ segment. We also found that the characteristic ratio for this model exhibits a very weak dependence on the temperature and is overestimated by a factor of 2 from the experimental value for long chains $C_\infty = 4$[2], which may be due to the fact that in this ICM we restricted the $C - O$ bonds to be always in the *trans* conformer.

In Figure 6.9 we show the force-extension curve in the modified form $(1 - R_z/L)^{-1}$ versus fb/k_BT for a long PEG molecule in the 3-state model as compared to other previously studied models. We note an abrupt change in the slope of this curve at about $fb/k_BT \simeq l_P/b_t$.To facilitate identifying a scaling expression for the large-force regime we plotted on the same graph a straight line (dashed thick line)

$$(1 - R_z/L)^{-1} \propto (fb/k_BT)^5 \tag{6.20}$$

In comparing this result to the behavior of previous models, eq. 4.26, 5.33, we see that the functional form of the stretching curve is given by an expression like eq. 5.37, where the exponent $\nu = -5$ indicates that the PEG chain is even softer in this regime than other models shown in Figure 6.9. Like the RIS for n-alkanes, the model for PEG exhibits a rather non-physical behavior for forces of this magnitude.

6.6 Conclusion

We have constructed n-state interacting chain models (with n =3 or 7) with nearest neighbor interactions. For PEG we extract the energetic and geometric parameters of the models from ab initio quantum mechanical calculations on short segments - up to four repeat units. This allows us to extend exact statistical mechanical calculations on short molecules to chains of any length. The models are essentially parameter-free.

One of the main objectives of this chapter is to extend the statistical mechanics

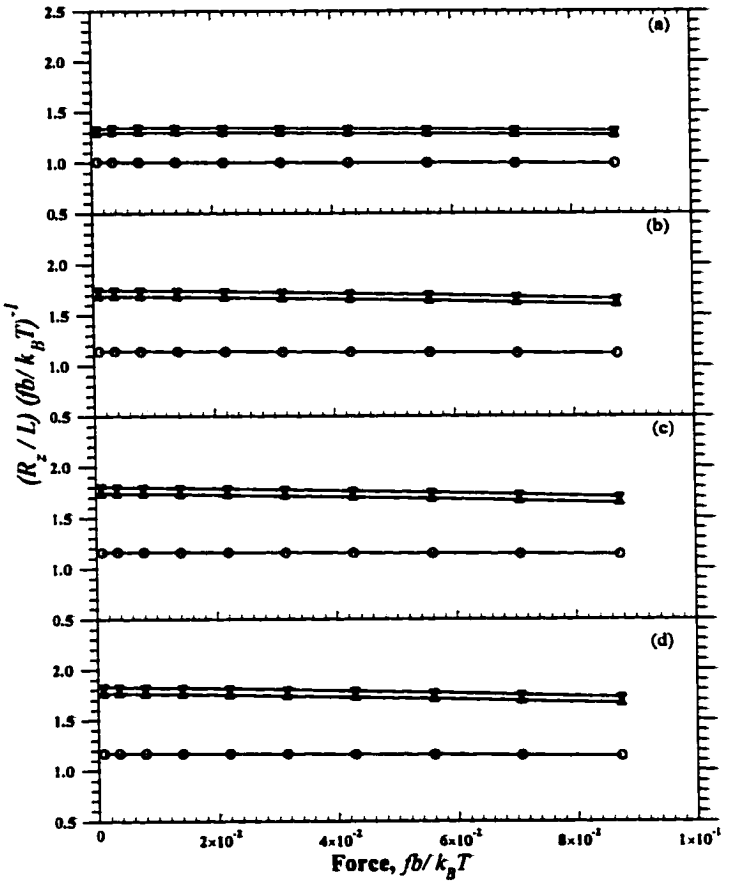

Figure 6.8: Small-force regime study of the PEG stretching. The different panels show results for (a) $N = 10$, (b) $N = 50$, (c) $N = 100$, (d) $N = 200$. For all panel the symbols correspond to different parameter sets: circle–set1, triangle down–set2, triangle up–set3.

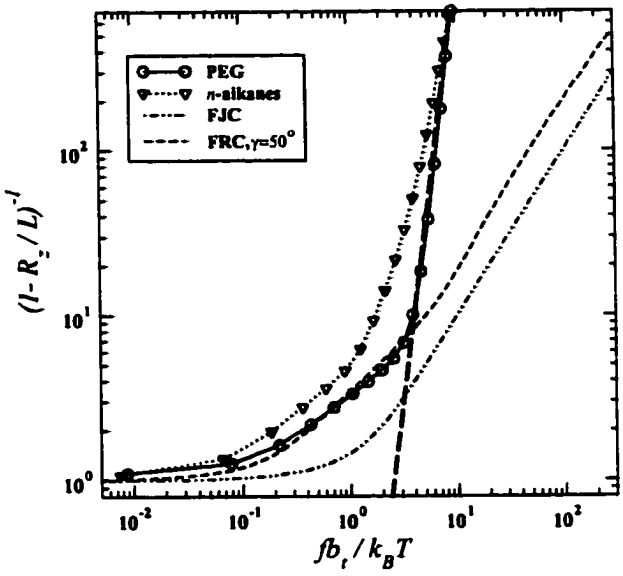

Figure 6.9: Double logarithmic plot of the modified form of the force-extension curve for long chains. The curves for PEG and n-alkanes are for $N = 200$.

analysis from short to long polymer molecules. For chains up to $N = 21$ subunits we construct, in the 3-state model, all 3^N conformers exactly. For longer chains we develop the transfer matrix method in the Gibbs ensemble in the presence of an external force. The results of the two methods have been compared with each other and with experimental data. We have identified the contributions to the stretching behavior of the geometrical structure parameters (the subunit lengths, the dihedral and bond angles), the energy parameters (the interactions between subunits and their self-energies).

We analyzed the modification of the force-extension curves with the change in chain length (short chain effects). Within our accuracy limits (better than $\pm 0.2\%$), the long chain asymptotics are reached for chains with more than 200 subunits. The geometrical parameters (Table 6.4) of the ICM models are of major relevance: changing dihedral and/or bond angles leads to significant changes of the force-extension curve in the intermediate force regime, where the stretching is both entropic and energetic. It is therefore imperative to have available ab initio data on the molecular structure.

Chain end distribution functions, probabilities of rotational states and the persistence length are calculated. We show that additional rotational states beyond those of the potential minima used in the Rotational-Isomeric-State approximation must be included for an accurate description.

We summarize the physical picture emerging from our theory. Stretching a PEG molecule by an external force proceeds in three stages: (*i*) initially trios of neighboring **EG** subunits will change from those with small dihedral angles to those with larger dihedral angles; this is mostly driven by entropy. (*ii*) Pairs of neighboring **EG** subunits will change to those with the larger bond angles, i.e. initially eliminating the $(g^-|g^+)$ pairs; both entropy and energy affect this regime. (*iii*) Lastly, the helical **EG** subunits will change to the longer trans subunits. Because these transformations proceed over intermediate activation barriers, individual **EG** subunits, pairs and trios will be stretched away from their lowest energy configurations. This stage is driven solely by energy.

CHAPTER 7

CONCLUSION

The transfer matrix method has been successfully applied to the configurational statistics of the following models of polymer molecules:

- freely jointed chain;
- freely rotating chain;
- rotational isomeric state approximation;
- model with continuous rotational potential for n-alkanes;
- interacting chain model with variable bond lengths, bond angles and rotational angles for PEG.

From a modelling point of view, pursuing the above is accompanied by a gradual incorporation of the intrachain constrictions and interactions. Starting with the FJC, where only the bond length is fixed, we can make a next step to the FRC, where the directional character of the covalent bonds is reflected by a fixed bond angle. The next logical step was to mimic the rotational potential of covalent bonds, first by the RIS approximation and then by introducing a large number of rotational angles that accurately sample the full potential curve. In addition to that, the nearest neighbor interactions, when introduced in our model, are shown to play an important role in the spatial configuration of a polymer.

The transfer matrix method was adapted for all models to carry out the statistical mechanics within Gibbs and Helmholtz ensembles, whichever proved feasible for our purposes. The TM method proved to be very flexible and yielded many new and insightful results. For the FJC the Green function in the Helmholtz ensemble is a function of a spatial coordinate only. The bond orientation is irrelevant, since there is no correlation between the direction of adjacent bonds. Adaptation of the TM

method to the FRC under the same ensemble required introducing one more angular coordinate as argument of the Green function accounting for the bond orientation. The procedure becomes more involved for the most complex models approached in this work, where the dihedral angles come into play. The Green function argument must include the spatial coordinate and a few angular coordinates, necessary to describe the position of a set of two or more covalent bonds.

We investigated by this method the following statistical quantities: end distribution functions, characteristic ratio, mean square radius of gyration, static structure factor, radial distribution function, force-extension curve. Wherever possible, we compared our results with others, both theoretical and experimental in literature. Overall, the TM calculations proved to be very accurate for all these quantities.

Scaling relations for various regimes of the force-extension curve for the models under consideration were derived. A remarkable fact is that the stretching behavior of the continuous rotational potential model and the FRC both present similarities with the FJC model in the large-force regime, while the RIS model and the ICM for PEG do not, proving to be much softer. As discussed in the final parts of Chapter 4, a FRC with small bond angle exhibits a crossover from the semiflexible model to a discrete chain behavior similar but not identical to the FJC.

It becomes increasingly difficult to account for interactions further than the nearest neighbor ones. Therefore, for PEG we choose to treat the chain not as a sequence of covalent links, but as one of chemical monomers, EG, consisting of three covalent bonds. This is done at the cost of having to deal with variable virtual bond lengths, virtual bond angles and dihedral angles.

We have seen that, for the most complicated models approached in this work, in order to make the statistical treatment feasible, we have to judiciously choose the most relevant degrees of freedom, while other degrees of freedom must be ignored. We illustrated this strategy for alkanes and PEG chains.

The polymers were considered to be in $\theta-$condition, which justifies the neglect of the excluded volume interaction canceled by the action of the solvent[1]. Designed for systems with nearest neighbor interactions, the TM method in the present formulation cannot directly account for excluded volume interactions. Nonetheless, it is possible to design a scheme which investigates such interactions by a self-consistent mean-field theory. In this scheme, the volume interactions are turned on gradually and the Green

function accounting for their presence is repeatedly calculated until self consistency is reached.

Owing to its efficiency in resolving the effects of the external fields, the TM technique can be further employed to investigate the properties of single molecules subject to such fields. For instance, a simple application would be to calculate the free energy of confining a molecule into a nanotube as a function of the radius of confinement. This can be done for simple models, like the FJC and the FRC, by a slight adaptation of the algorithm used in this work for determining end distribution functions in the canonical ensemble with the modification that one more spatial coordinate must be included as an argument of the Green function.

In a similar manner, one could also devise an implementation of the TM method as a single chain thoretical approach to polymer brushes — polymer chains grafted onto a surface. In this theory, one could do a self-consistent study of a "central" single molecule placed in the field created by the surrounding polymers. Alternatively, one can extract via TM the properties (e.g. free energies, average dimensions) of a chain in the presence of a potential wall mimicking the interactions with the neighboring grafted molecules and use that information to resolve a well defined statistical mechanical formalism for the whole system of chains. These ideas, together with the prospect of applying the transfer matrix method to the dynamics of polymer chains constitute, we hope, good seminal material for future projects.

In principle, one can use the TM method to study polymers with any primary structures. To list a few cases of interest in recent literature we mention branched polymers, copolymers and biopolymers. Since the TM technique can be adapted to handle model systems with any type of short-ranged interactions, we can also employ it to study secondary structures of biopolymers, in particular hydrogen-bonded structures, such as $\alpha-$helices, $\beta-$sheets and double helices. For instance, the helix-coil transition in DNA can be investigated by such an approach[1].

As a final word on the method transfer matrix applied to single polymer chains we would like to emphasize its efficiency as a computational method. It can deal with chain-like systems that possess a tremendous amount of conformers, for instance in the RIS model, for a chain with N bonds there are 3^N conformers—a number that sharply rises. Remarkably enough, the computational cost of the TM increases linearly with the size of the system, thus surpassing this difficulty. Besides, the accuracy of the

method can be very precisely determined and rendered as high as desired, the only constraining factor being the memory size of the computer. These and many others are the reasons for which we deem this method remarkable and worth pursuing in our theoretical quest.

BIBLIOGRAPHY

[1] Grosberg A. Yu., Khokhlov A. R. *Statistical Physics of Macromolecules* (American Institute of Physics Press, New York, **1994**).

[2] Flory P.J. *Statistical Mechanics of Chain Molecules*, Hanser Verlag: München, **1989**.

[3] Volkenstein M.V. *Configurational Statistics of Polymeric Chains*, Interscience: NewYork, **1963**.

[4] Doi M., Edwards S.F. *The Theory of Polymer Dynamics*, Oxford University Press, New York, **1994**.

[5] Landau and Lifshitz, *Theory of Elasticity* (Pergamon Press, Oxford, 1986).

[6] Oesterhelt F., Rief M., Gaub H. E. *New J. Phys.* **1999**, *1*, 6.1-6.11.

[7] Boyd R.H., Phillips P. J. *The Science of Polymer Molecules*, Cambridge University Press, **1996**.

[8] Hill T.L. *Thermodynamics of Small Systems*, Dover Publications Inc., New York, **1994**.

[9] Hansen J.P., McDonald I.R. *Theory of Simple Liquids*, Academic Press Inc., London, **1986**.

[10] Israelachvili J. *Intermolecular & Surface Forces*, Academic Press Inc., San Diego, **1991**.

[11] Yamakawa H. *Modern Theory of Polymer Solutions*, Harper&Row Publishers, New York, **1971**.

[12] Kreuzer H.J., Wang R.L.C., M Grunze, *New J. Phys.***1999**, *1*, 21.1-21.16.

[13] Kreuzer H.J., Grunze M. *Europhys. Lett.* **2001**, *55*(5), 640-646.

[14] Kreuzer H.J., Payne S.H., Livadaru L. *Biophysical Journal* **2001**, *80*(6), 2505-2514.

[15] Abe Y., Flory P. J. *J.Chem.Phys.* **1970**, *52*(6), 2814.

[16] Yoon D.Y., Flory P.J. *J. Chem. Phys.* **1974**, *61*, 5366.

[17] Wang R.L.C., Kreuzer, H.J., Grunze, M. *Phys. Chem. Chem. Phys.* ***2000***, *2*, 3613.

[18] Pertsin A.J., Grunze, M., Garbuzova, I.A. *J. Phys. Chem. B* **1998**, *102*, 4918.

[19] Wang R.L.C., Kreuzer, H.J., Grunze, M., Pertsin, A.J. *Phys. Chem. Chem. Phys.*, **2000**, *2*, 1721.

[20] Pertsin A.J., Grunze M., Kreuzer H.J., Wang R.L.C. *Phys. Chem. Chem. Phys.*, **2000**, *2*, 1729.

[21] Welsh W.J., "Force field techiques and their use in estimating the conformational

stability of polymers" in *Computational Modeling of Polymers* (ed. J. Bicerano), Marcel Dekker Inc., New York, **1992**.

[22] Binder K., "Monte Carlo and Molecular Dynamics simulations of amorphous polymers" in *Computational Modeling of Polymers* (ed. J. Bicerano), Marcel Dekker Inc., New York, **1992**.

[23] Welsh W.J., Debolt and Mark J. E., *Macromolecules*, **1986**, 19, 2978.

[24] Livadaru L., Netz R.R., Kreuzer H.J., "Interacting Chain Model for Poly(ethylene glycol) from First Principles – Stretching of a Single Molecule using the Transfer Matrix Approach", submitted to *Macromolecules* (February 2002).

[25] Livadaru L., Netz R.R., Kreuzer H.J., "Stretching Response of Discrete Semi-flexible Polymers" submitted to *Macromolecules* (April 2002).

[26] Ciferri A., Hoeve C.A., Flory P.J., *J. Am. Chem. Soc.* **1961**, *83*, 1015.

[27] Flory P.J., Ciferri A., Chiang R. *J. Am. Chem. Soc.* **1961**, *83*, 1023.

[28] Chiang R., *J. Phys. Chem.*, **1966**, *70*, 2348.

[29] Stacy C.J., Arnett R.L., *J. Phys. Chem.*, **1965**, *69*, 3109.

[30] Nakajima A., Hamada F., Hayashi S., *J. Polymer Sci. C*, **1966**, *15*, 285.

[31] Eyring E, *Phys. Rev.*, **1932**, *39*, 746.

[32] Porod G., *J. Polymer Sci.*, **1953**, *10*, 157.

[33] Clausen-Schaumann H., Seitz M., Krautbauer R., Gaub H.E. *Curr. Opin. Chem. Biol.* **2000**, *4*, 524.

[34] Smith S.B., Finzi L., Bustamente C. *Science* **1992**, *258*, 1122.

[35] Bustamente C., Marko J.F., Siggia E.D. *Science* **1994**, *265*, 1600.

[36] Vogolodskii A. *Macromolecules* **1994**, *27*, 5623.

[37] Odijk T. *Macromolecules* **1995**, *28*, 7016.

[38] Marko J.F., Siggia E.D. *Macromolecules* **1995**, *28*, 8759.

[39] Ha B.Y., Thirumalai D. *J. Chem. Phys.* **1997**, *106*, 4243.

[40] Rief M., Clausen-Schaumann H., Gaub, H.E. *Nature Struct. Biol.* **1999**, *6*, 346.

[41] Rief M., Gautel M., Oesterhelt F., Fernandez J.M., Gaub H.E. *Science* **1997**, *276*, 1109.

[42] Rief M., Oesterhelt F., Heymann B., Gaub H.E. *Science* **1997**, *275*, 1295.

[43] Oesterhelt F., Rief M., Gaub H.E. *New J. Phys.* **1999**, *1*, 6.

[44] Ortiz C., Hadziioannou G. *Macromolecules* **1999**, *32*, 780.

[45] Hugel T., Grosholz M., Clausen-Schaumann H., Pfau A., Gaub H., Seitz M. *Macromolecules* **2001**, *34*, 1039.

[46] Kovac J., Crabb C.C. *Macromolecules* **1982**, *15*, 537.

[47] Fixman M., Kovac J. *J. Chem. Phys.* **1973**, *58*, 1564.

[48] Odijk T. *Macromolecules*, **1983**, *16*, 1340, **1984**, *17*, 502.

[49] Kostrowicki J., Scheraga H. A. *Computational Polymer Science* **1995**, *5*, 47.

[50] Vogel H., Nilsson L., Rigler R., Voges K.-P., Jung, G. *Proc. Natl. Acad. Sci USA* **1988**, *85*, 5067.

[51] Gittes F., Mickey B., Nettleton J., Howard J. *J. Cell Biol.* **1993**, *120*, 923.

[52] Ott A., Magnasco M., Simon A., Libchaber A. *Phys. Rev. E* **1993**, *48*, R1642.

[53] Netz R.R.*Macromolecules* **2001**, *34*, 7522.

[54] Kreuzer H.J., Wang R.L.C., Grunze M. *New J. Phys.* **1999**, *1*, 1.21.

[55] Smith G.D., Jafee R.L. *J. Chem. Phys.* **1996**, 100, 18718-19724.

[56] Smith G.D., Yoon D.Y., Jafee R.L., Colby R.H., Krishnamoorti R, Fetters L.J. *Macromolecules* **1996**, 29, 3462-3469.

[57] Smith G.D., Yoon D.Y., Wade C.G., O'Leary D., Chen A., Jafee R.L. *J. Chem. Phys.* **1997**, 106 (9), 3798-3805.

[58] Bandyopadhyay S., Tarek M., Lynch M.L., Klein M.L. *Langmuir* **2000**, 16, 942-946.

[59] Heymann B., Grubmuler H. *Chem. Phys. Lett.* **1999**, *307*, 425-432.

[60] Kramers H.A., Wannier G. *Phys. Rev.* **1941**, *60*, 252.

[61] Birshtein T.M., Ptitsyn O.B. *Zh. Teknn. Fiz.* **1959**, *29*, 523.

[62] Birshtein T.M., Ptitsyn O.B. *Conformations of Macromolecules*, Vol. 22 in *High Polymers*, New York: Interscience, **1966**.

[63] Nagai K.J. *J. Chem. Phys.* **1959**, *30*, 964.

[64] Lifson S. *J. Chem. Phys.* **1959**, *31*, 1169.

[65] Honeycutt J. D., *Comput. Theor. Polym. Sci.* **1998**, *8*(1-2), 1-8.

[66] Taylor D.J.R., Stepto R.F.T., Bleackley M., Ward I.M. *Phys. Chem. Chem. Phys.***1999**, *1*, 2065-2070.

[67] Cail J.I., Stepto R.F.T., Taylor D.J.R., Jones R.A., Ward I.M. *Phys. Chem. Chem. Phys.* **2000**, *2*, 4361-4367.

[68] Cifra P., Bleha T., *J. Chem. Soc. Faraday Trans.* **1995**, *91*(16), 2465-2471.

[69] Raplod R. F., Mattice W. L., *J. Chem. Soc. Faraday Trans.* **1995**, *91*(16), 2435-2441.

[70] Doruker P., Rapold R. F., Mattice W. L., *J. Chem. Phys.* **1996**, *104*(21),8742-8749.

[71] Haliloglu T., Mattice W. L. *J. Chem. Phys.* **1998**, *108*(16), 6989-6995.

[72] McCoy J.D., Honnell K.G. , Curro J.G., Schweizer K.S., Honeycutt J.D. *Macromolecules* **1992**, *25* (19), 4905-4910.

[73] Yoon D.Y., Flory P.J. *Macromolecules* **1976**, *9*, 294.

[74] Uhlherr A. *Macromolecules* **2000**, *33*, 1351-1360.

[75] Abe A., Furuya H., Mitra M.K., Hiejima T. *Comput. Theor. Polym. Sci.* **1998**, *8*(1-2) Part 2, 253-258.

[76] Stepto R.F.T., Taylor D.J.R. *Comput. Theor. Polym. Sci.* **1996**, *6*(1-2), 49-60.

[77] Bowen H.J, Sutton L.E., *Tables of Interatomic Distances and Configurations in Molecules and Ions*, The Chemical Society , London, **1965**.

[78] Vacatello M., Yoon D. Y. *Macromolecules* **1992**, *25*, 2501-2508.

[79] Tiller A.R. *Polymer* **1994**, *35*(21), 4511-4520.

[80] Buchner S., Heuer A., Spiess H.W. *Macromolec. Theor. & Simul.* **1998**, *7*(6), 665-674.

[81] Williams A.D., Flory P.J. *J. Polym. Sci.* **1967**, Part A-2, *5*,417.

APPENDICES

A. Fortran Code for Calculation of the Force-Extension Curve of the FRC

```
***  Code calculates the force-extension curve for the FRC [May 2000]
***  Variable declarations:
 implicit none
 integer i, N,ip, it, ip1, i1,j, jf, ig, iig
 integer it1, it2, iz1, iz2, ith, Mt, Nf
 parameter (Mt= 1000)              !  the angular mesh parameter
 integer gamma_table(100)
 integer ITH2table(0:Mt,0:2*Mt)
 real*8 kT, b, pi, cg, sg, gamma, phi, phi1, Lmax
 real*8 sumP, cth, Pmax, L, t1, t2, th, df, gm_deg
 real*8 cs1, cs2, th1, th2, sn2, fb1, z, z1,Rzmax
 real*8 , slope(0:100), Rz(0:100), fb(0:100)
 real*8 Pnew(0:Mt), Pold(0:Mt)
 real*8 Pnew1(0:Mt), Pold1(0:Mt)
 real*8 cst(0:Mt), snt(0:Mt), csp(0:2*Mt)
 real*8 expfb(0:Mt), expfb1(0:Mt)
 real*8 TH2table(0:Mt,0:2*Mt), CSTH2table(0:Mt,0:2*Mt)


*** Commands of the main program begin
 N= 100             !  the chain length
 Nf= 20             !  number of force points
```

```
 pi= 2.0* dasin(1d0)
 b= 1.0d0 !  the bond length
 df= 1d-10          !  ''infinitesimal'' variation in force
*** Tables of SIN and COS functions
 do ip= 0, 2*Mt
     phi= pi* real(ip)/ real(Mt)
     csp(ip)= dcos(phi)
 end do      !  ip
 do ith= 0, Mt
     th= pi* real(ith)/ real(Mt)
     cst(ith)= dcos(th)
     snt(ith)= dsin(th)
 end do     !  ith
*** Table of selected bond angle values

 do iig= 1, 9
     gamma_table(iig)= iig* 10
 end do      !  iig


*** Gamma loop begins:
** Table of functions of gamma:
 do iig= 1, 9
    ig= gamma_table(iig)
     gamma= ig*pi/ 180.0
     cg= dcos(gamma)
     sg= dsin(gamma)
     Rzmax= dcos(gamma/ 2.0)      !  contour length per bond
*** Calculation of the connectivity matrix:
     do it1= 0, Mt
         do ip= 0, 2*Mt
             CSTH2table(it1,ip)= cg* cst(it1)+ sg* snt(it1)* csp(ip)
             TH2table(it1,ip)= dacos(CSTH2table(it1,ip))
```

```
            ITH2table(it1,ip)= nint(Mt* TH2table(it1,ip)/ pi)
        end do !  ip
    end do !  it1
*** Force loop:
    do jf= 1, Nf !  force loop
        fb(jf)= real(jf)**4/ 800.0 !  this is fb in [kT] units
        fb1= fb(jf)+ df
        Z= 0.0d0
        Z1= 0.0d0
!  zeroing the Gibbs partition function for f and f+df
        sumP= 0.0
** Table of exponential functions
        do it2= 0, Mt
            expfb(it2)= dexp(fb(jf)* cst(it2))
            expfb1(it2)= dexp(fb1* cst(it2))
        end do !  it2
** Initialization of Green function P
        do it2= 0, Mt
            Pold(it2)= expfb(it2)* snt(it2)
            Pold1(it2)= expfb1(it2)* snt(it2)
        end do !  it2
** Iteration of Green function proceeds
        do j= 2, N
            do it2= 0, Mt
                Pnew(it2)= 0.0
                Pnew1(it2)= 0.0
            end do !  it2
            SumP= 0.0
            do it1= 0, Mt
                do ip= 0, 2*Mt
                    it2= ITH2table(it1,ip)
!  here we use the connectivity matrix
                    Pnew(it2)= Pnew(it2)+ Pold(it1)
```

```
                    Pnew1(it2)= Pnew1(it2)+ Pold1(it1)
                end do !  (ip)
            end do !  (it1)
            do it2= 0, Mt
                Pnew(it2)= Pnew(it2)* expfb(it2)
                Pnew1(it2)= Pnew1(it2)* expfb1(it2)
                SumP= SumP+ Pnew(it2)
            end do !  (it2)
            do it2= 0, Mt
                Pold(it2)= Pnew(it2)/ SumP
                Pold1(it2)= Pnew1(it2)/ SumP
            end do !  it2
        end do !  (j)
        do it2= 0,Mt
            Z= Z+ Pnew(it2)
!  the Gibbs partition function
            Z1= Z1+ Pnew1(it2)
        end do !  it2
        Rz(jf)= (1.0/real(N))*(dlog(Z1)- dlog(Z))/df
!  the chain extension as the numerical derivative of log(Z)
        write (6,*) f, Rz(jf) !write output as a 2 column table
    end do !  force loop ends
    write (6,*) ''#'','' gamma= '', ig
    write (6,*)
end do !  gamma loop ends
write (6,*) ''#'','' Mt='',Mt,'', N='',N
close (6)
end program
```

B. Structure Factor of a Rod-like Polymer

Based on the definition of the static structure factor, eq. 1.35a, one can show that, for a rod-like chain with N bonds of equal length b, the structure factor can be re-written as

$$S(\mathbf{k}) = \frac{1}{4\pi N}\int \mathrm{d}\mathbf{u}\int \mathrm{d}\mathbf{b}_1\mathrm{d}\mathbf{b}_2...\mathrm{d}\mathbf{b}_N p(\mathbf{b}_1,\mathbf{u})\,p(\mathbf{b}_2,\mathbf{u})...p(\mathbf{b}_N,\mathbf{u}) \quad \text{(B.1a)}$$
$$\times\left\{N+\sum_{n<m=0,N}\left[\mathrm{e}^{i\mathbf{k}\cdot(\mathbf{r}_n-\mathbf{r}_m)}+\mathrm{e}^{-i\mathbf{k}\cdot(\mathbf{r}_n-\mathbf{r}_m)}\right]\right\},$$

where $\mathbf{b}_n$ $(n=1,N)$ denote the bond vectors, the unit-vector $\mathbf{u}$ gives the overall orientation of the chain, and $p(\mathbf{b}_n,\mathbf{u})=\delta(\mathbf{b}_n-b\mathbf{u})$ is the probability distribution of a bond vector $\mathbf{b}_n$ and orientation $\mathbf{u}$. The above expression can be further simplified expanding the curl bracket and performing the integration as

$$S(\mathbf{k}) = 1+\frac{1}{4\pi N}\sum_{n<m=0,N}\int \mathrm{d}\mathbf{u}\left[\prod_{k=n+1,m}\int \mathrm{d}\mathbf{b}_k\delta(\mathbf{b}_k-b\mathbf{u})\,\mathrm{e}^{i\mathbf{k}\cdot\mathbf{r}_k}\right. \quad \text{(B.2)}$$
$$\left.+\prod_{k=n+1,m}\int \mathrm{d}\mathbf{b}_k\delta(\mathbf{b}_k-b\mathbf{u})\,\mathrm{e}^{-i\mathbf{k}\cdot\mathbf{r}_k}\right]. \quad \text{(B.3)}$$

Since the integral

$$\int \mathrm{d}\mathbf{b}_k\delta(\mathbf{b}_k-b\mathbf{u})\,\mathrm{e}^{i\mathbf{k}\cdot\mathbf{r}_k}=\mathrm{e}^{ib\mathbf{k}\cdot\mathbf{u}}, \quad \text{(B.4)}$$

we have

$$S(\mathbf{k})=1+\frac{1}{4\pi N}\sum_{n<m=0,N}\int \mathrm{d}\mathbf{u}\left[\mathrm{e}^{i(m-n)b\mathbf{k}\cdot\mathbf{u}}+\mathrm{e}^{-i(m-n)b\mathbf{k}\cdot\mathbf{u}}\right], \quad \text{(B.5)}$$

and further

$$S(\mathbf{k}) = 1+\frac{1}{2\pi N}\int_0^N \mathrm{d}n\int_{n+1}^N \mathrm{d}m\int \mathrm{d}\mathbf{u}\cos\left[(m-n)\,b\mathbf{k}\cdot\mathbf{u}\right] \quad \text{(B.6)}$$
$$= 1+\frac{1}{2\pi N}\int \mathrm{d}\mathbf{u}\int_0^N \mathrm{d}n\left[\frac{\sin\left[(N-n)b\mathbf{k}\cdot\mathbf{u}\right]}{b\mathbf{k}\cdot\mathbf{u}}-\frac{\sin(b\mathbf{k}\cdot\mathbf{u})}{b\mathbf{k}\cdot\mathbf{u}}\right] \quad \text{(B.7)}$$
$$= 1+\frac{1}{2\pi N}\int \mathrm{d}\mathbf{u}\left[\frac{1-\cos(Nb\mathbf{k}\cdot\mathbf{u})}{(b\mathbf{k}\cdot\mathbf{u})^2}-\frac{N\sin(b\mathbf{k}\cdot\mathbf{u})}{b\mathbf{k}\cdot\mathbf{u}}\right] \quad \text{(B.8)}$$

Finally, performing the integration over **u**, we obtain

$$S(\mathbf{k}) = N \int_0^1 \mathrm{d}x \left\{ \frac{1}{N} - \frac{2\sin(bkx)}{Nbkx} + \frac{2\left[1-\cos\left(Nbkx\right)\right]}{\left(Nbkx\right)^2} \right\}. \tag{B.9}$$

Assuming large N, we can neglect the first two terms under the integral above and we are left with

$$S(\mathbf{k}) \simeq N \int_0^1 dx \left[\frac{\sin(Nkbx/2)}{(Nkbx/2)} \right]^2, \tag{B.10}$$

expression which was employed in Chapter 3 of this work.